IOP Institute of Physics
Semiconductor Physics Group

IOP Institute of Physics
Quantum Electronics and Photonics Group

Semiconductor and Integrated Optoelectronics

Cardiff, Wales

27th – 29th March 2018

Programme and Abstracts

Conference Locations (see map opposite)

Tues 27th March
Location: Queens Buildings site CF24 3AA (North and South Buildings)
Address: Queen's Buildings, 5 The Parade, Newport Road, CF24 3AA

Parking: NCP parking is available in the Knox Road car park (we cannot reimburse costs)

Registration location: North Building foyer.
Session 1 location: room N3-28 (third floor – 3 flights of stairs, turn left)
Poster session & Reception location: WX3.07 & 3.14

Wed 28th and Thurs 29th March
Sessions location: Law Building CF10 3AT, Room 0.22
Refreshments location: Aberdare Hall CF10 3UP

Address: Law Building, Museum Avenue (entrance on either side of building - Park Place) CF10 3AT. Room 0.22 closest room to the entrance.

Parking: On-street pay and display on Museum Avenue (we cannot reimburse costs)

Banquet location: Cardiff Castle, Cardiff CF10 3RB

See map opposite – arrows indicate approximate position of entrances

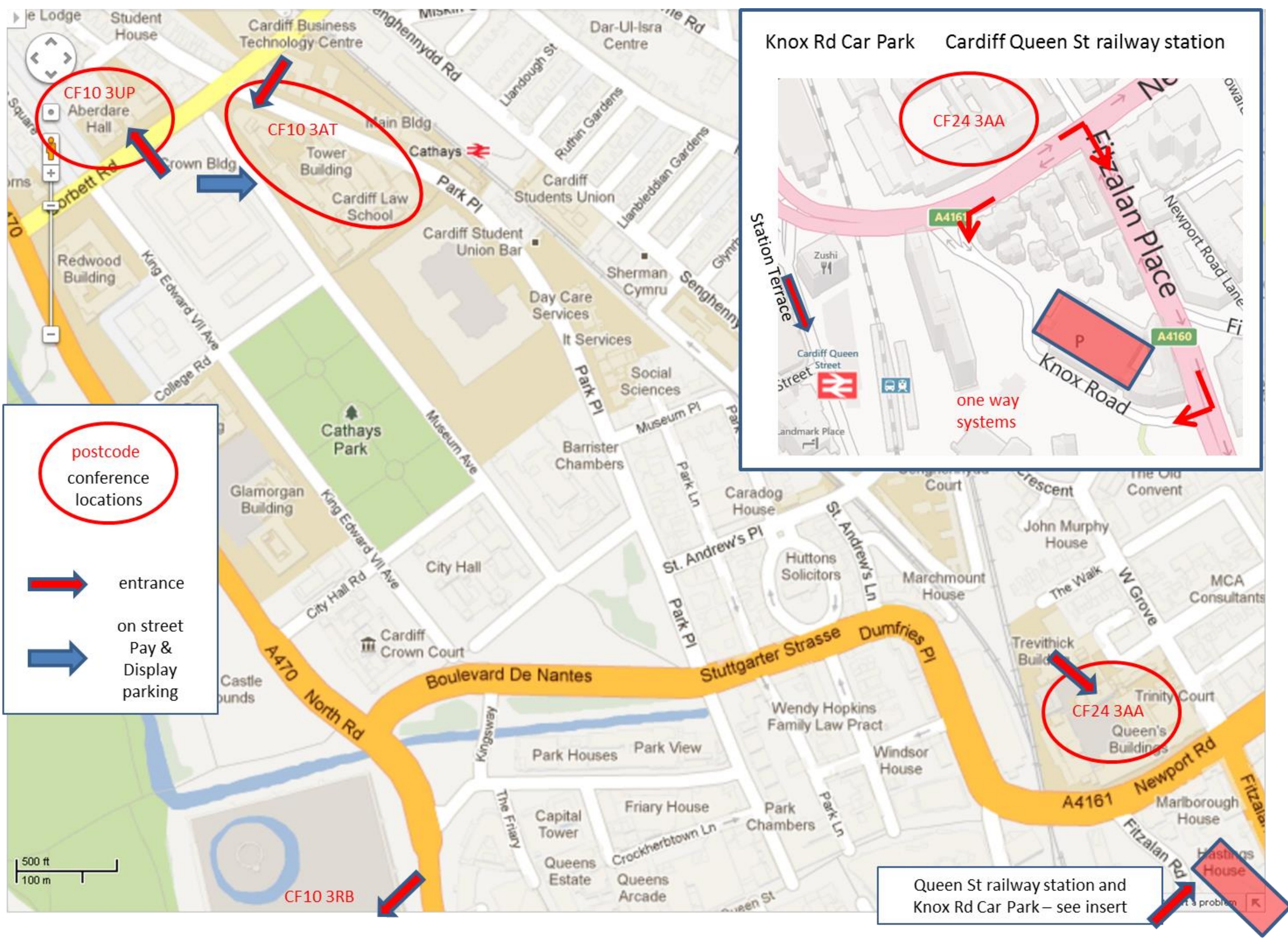
Knox Rd Car Park
Cardiff Queen St railway station
CF24 3AA
Fitzalan Place
Newport Road Lane
Station Terrace
A4161
A4160
Knox Road
P
one way
systems
Cardiff Queen
Street
Zushi
CF10 3UP
Aberdare
Hall
CF10 3AT
Tower
Building
Cardiff Law
School
Main Bldg
Cathays
Student
House
Cardiff Business
Technology Centre
Dar-Ul-Isra
Centre
Senghennydd Rd
Llandough St
Ruthin Gardens
Llanbleddian Gardens
Cardiff
Students Union
Cardiff Student
Union Bar
Sherman
Cymru
Day Care
Services
It Services
Social
Sciences
Park Pl
Redwood
Building
King Edward VII Ave
College Rd
Cathays
Park
Museum Ave
Barrister
Chambers
Museum Pl
Park Ln
Caradog
House
Glamorgan
Building
City Hall
City Hall Rd
Cardiff
Crown Court
St. Andrew's Pl
Huttons
Solicitors
St. Andrew's Ln
Marchmount
House
John Murphy
House
The Walk
W Grove
MCA
Consultants
The Old
Convent
Trevithick
CF24 3AA
Trinity Court
Queen's
Buildings
A470
North Rd
Boulevard De Nantes
Stuttgarter Strasse
Dumfries Pl
Kingsway
Park Houses
Park View
Wendy Hopkins
Family Law Pract
Windsor
House
A4161
Newport Rd
Marlborough
House
Fitzalan Rd
Hastings
House
The Friary
Capital
Tower
Friary House
Crockherbtown Ln
Park
Chambers
Queens
Estate
Queens
Arcade
CF10 3RB
500 ft
100 m
postcode
conference
locations
entrance
on street
Pay &
Display
parking
Queen St railway station and
Knox Rd Car Park – see insert

Welcome Message

SIOE '18

Croeso i Gaerdydd a chroeso unwaith eto i SIOE

It gives me great pleasure to welcome you to the 32nd SIOE conference in Cardiff.

We begin on Tuesday afternoon with two invited talks from our Guest speakers – the first on the development of nanowire lasers that can be integrated on Silicon. The second focusses on the physics and optics that can be performed using epsilon-near-zero materials and nano-antennas. These are kindly given by leading international experts Dr Gregor Koblmüller (Semiconductor Nanostructures and Quantum Systems Group lead by Prof Jonathan Finley at TU Munich) and Dr Sebastian Schulz (University of St Andrews). We continue with a session on "Detectors", which highlights some of the different approaches and the new materials being developed. We finish Tuesday with a reception and Poster session allowing you to interact and discuss some interesting posters, and socialise with your colleagues. This reception is sponsored by IET Publishing, who will also be facilitating the special issue of IET Optoelectronics associated with the conference. The guest editors' role will be taken this year by **Dr Sudha Mokkapati.** Sudha will be available to discuss potential papers with authors wishing to expand their conference presentation for this special issue.

On Wednesday morning **we change location** and switch topic to two sessions focussed on "light sources and lasers". In the afternoon we move onto integration, starting with individual contributed talks using a variety of approaches and material systems, before an interactive discussion session including a debate on the best approaches to integration, at which we welcome contributions from everyone. After a full day we can relax in the 19th Century Library of Cardiff Castle with some music and refreshments, followed by dinner in the banqueting hall.

On Thursday morning we return to materials development for both integration and for particular applications. These sessions really reinforce the message that optoelectronic devices and subsystems are incorporating a larger and more diverse range of materials to achieve ever increasing functionality.

In putting together this programme I have relied on help from a large number of people in Cardiff but particular mention goes to Dr Sarah Taylor, who organised the conference, Drs Sudha Mokkapati, Daryl Beggs and Juan Pereiro who formed the program committee and Drs Sam Shutts and Lewis Kastein. I would also like to thank Cardiff University for sponsorship, IET Publishing for sponsoring the Poster Reception and the IOP Semiconductor Physics Group and IOP Quantum Electronics and Photonics Group for financial assistance. Finally I would like to thank IOP Wales for contributing to the musical introduction to the banquet.

I'm also pleased to be able to remind you to pick up our souvenir glass at the poster session and reception as a memento of the meeting.

Prof. Peter Smowton, School of Physics and Astronomy, Cardiff University

Contents

Conference Locations page 2

Welcome Message page 4

Programme page 5

Tuesday 27th March

Registration North Building Foyer; 13:00 onwards
Welcome address North Building N3.28; 13:40 – 13:45
Session 1: Guest Speakers North Building N3.28; 13:45 – 15:45
15:45 Refreshment Break Room N3.23 (Opposite N3.28)
Session 2: Photodetectors North Building N3.28; 16:15 – 17:45
Session 3: Posters & IET Publishing Reception (including drinks and buffet)
West Extension Building WX3.07/WX3.14; 18:00 – 20:00

Wednesday 28th March

Session 4: Light Sources & Lasers I Law Building 0.22; 08:45 – 10:45
10:45 Refreshment Break, Aberdare Hall
Session 5: Light Sources & Lasers II Law Building 0.22; 11:15 – 12:45
12:45 Lunch, Aberdare Hall
Session 6: Integration Strategies and Approaches Law Building 0.22; 13:45 – 15:30
15:30 Refreshment Break, Aberdare Hall
Session 7: Discussion/Forum Law Building 0.22; 16:00 – 16:45
Conference Banquet, Cardiff Castle: Music (Library) followed by dinner; 18:00 onwards

Thursday 29th March

Session 8: Materials Development I Room 0.22, Law Building; 08:45 - 10:30
10:30 Refreshment Break, Aberdare Hall
Session 9: Materials Development II Room 0.22, Law Building; 11:00 - 12:00
12:00 Lunch, Aberdare Hall
Conference Close

Abstracts page 20

IET Call for Papers page 76

Programme, Tuesday 27th March

Registration

North Building Foyer; 13:00 onwards

Welcome address, Prof Peter Smowton (Cardiff University)

North Building N3.28; 13:40 – 13:45

Session 1: Guest Speakers

North Building N3.28; 13:45 – 15:45

13:45 *Invited* **Monolithically integrated nanowire lasers on Si and SOI photonic platform**

G. Koblmueller, T. Stettner, J. Bissinger, D. Ruhstorfer, B. Mayer, and J. J. Finley.

Technical University Munich

14:45 *Invited* **Optical response of nanoantennas on epsilon-near-zero substrates**

Sebastian A. Schulz[1-4], M. Zahirul Alam[1], Jeremy Upham[1], Israel De Leon[1,5] and Robert W. Boyd[1,6]

[1]Department of Physics, University of Ottawa, Ottawa, Canada; [2]Centre for Advanced Photonics & Process Analysis, Cork Institute of Technology, Cork, Ireland; [3]Tyndall National Institute, Cork, Ireland; [4]SUPA, School of Physics and Astronomy, University of St Andrews, St Andrews, UK; [5]School of Engineering and Science, Tecnologico de Monterrey, Monterrey, Mexico

15:45 to 16:15 Refreshment Break Room N3.23 (Opposite N3.28)

Session 2: Photodetectors

North Building N3.28; 16:30 – 17:45

16:15 A18_37 **Growth of Type-II InAs/GaSb superlattice**

Marie Delmas[1], Yaksh Rawal[1], Baolai Liang[2], Diana Huffaker[1,2].

[1]School of Physics and Astronomy, Cardiff University, the Parade, Cardiff, CF24 3AA, UK; [2]California NanoSystem Institute, University of California, Los Angeles, CA90095, USA.

16:30 A18_43 **Modification of hole ionization coefficients in GaAsBi based avalanche photodiodes**

X. Yi, Y. Liu, Z. Zhou, F. Harun, R. D. Richards*, C.H. Tan and J. P. R. David*.

Advanced Detector Centre, Department of Electronic & Electrical Engineering, University of Sheffield, Sheffield, South Yorkshire, S1 3JD, UK.

16:45 A18_35 **Modelling Timing Jitter in Silicon Single Photon Avalanche Diodes**

J. Petticrew, S. Dimler, and J. S. Ng*.

Department of Electronic & Electrical Engineering, University of Sheffield, Sheffield, UK.

17:00 A18_32 **InGaAs-InP HBT-PIN Based Optoelectronic Integrated Circuit for over 10Gb/s Optical Systems**

S. G. Muttlak*, J. Sexton and M. Missous.
School of Electrical and Electronic Engineering, University of Manchester, UK.

17:15 A18_03 **Physical Modelling of InGaAs-InAlAs APD and PIN Photodetectors for > 25Gb/s Data Rate Applications**

O. S. Abdulwahid[1], Saad Muttlak[1], J. Sexton[1], I. Kostakis[2], K.W. Ian[2] and M. Missous[1].
[1]School of Electrical and Electronic Engineering, the University of Manchester, United Kingdom; [2]Integrated Compound Semiconductors, Manchester, United Kingdom.

17:30 A18_02 **Temperature and temporal stability of avalanche gain for $Al_{0.85}$ $Ga_{0.15}$ $As_{0.56}$ $Sb_{0.44}$ avalanche photodiodes**

S. Abdullah, C.H.Tan*, L. Pinel and J.S. Ng.

Session 3: Posters & IET Publishing Reception (including drinks and buffet)

West Extension Building WX3.07/WX3.14; 18:00 – 20:00

A18_06 **Modelling of single-mode GaAs-based 1x2 MMI and Y-branch splitters**

T. Albiladi*, D. Beggs, E. Le Boulbar Z. Li and P. M. Smowton.
School of Physics and Astronomy, Cardiff University, Queen's Building, The Parade, Cardiff, Wales, UK, CF24 3AA.

A18_08 **Optical properties of drug-resistant human osteosarcoma cells - the potential for microfluidic-based Lab-on-Chip analysis**

Basmah Almagwashi[1], Marie Wiltshire[2], Rachel Errington[2], and Peter Smowton[1].
[1]School of Physics and Astronomy, Cardiff University, 5 The Parade, Cardiff, CF24 3AA, UK; [2]School of Medicine, Division of Cancer Genetics, Heath Park, Cardiff University, Cardiff, CF14 4XN, UK.

A18_15 **InP Nanowire Solar Cells with Carrier-Selective Layers**

M. Fleet* and S. Mokkapati.
School of Physics and Astronomy, North Queen's Building, Cardiff University, The Parade, Cardiff, UK, CF24 3AA.

A18_26 **Computing Resonant Modes of PCSELs using the Transfer Matrix Method**

G. Li, J. Sarma*, R. A. Hogg. *Visiting Researcher
School of Engineering, University of Glasgow, Glasgow, G12 8TL, UK.

A18_41 **Multi-beam Laser Interference Patterning of Semiconductors**

Y. R. Wang*, C. Y. Jin, and M. Hopkinson.
Department of Electronic and Electrical Engineering, University of Sheffield, Sheffield S3 7HQ, UK.

A18_30 **Silicon mid-infrared photodetectors**

M. A. Lourenço[1,2] and K. P. Homewood[1,2,3].
[1]Materials Research Institute and School of Physics and Astronomy, Queen Mary University of London, Mile End Road, E1 4NS London, UK; [2]Advanced Technology Institute, Faculty of Engineering and Physical Sciences, University of Surrey,

Guildford, Surrey GU2 7XH, UK; [3]School of Materials Science & Engineering, Hubei University, Wuhan 430062, P. R. China.

A18_12 Growth mechanisms in InAs/GaAs QDs with and without Bi surfactant

X. Y. Chen, Y. Gu*, Y. J. Ma, B. Du, J. Zhang, Y. H. Shi, W. Y. Ji, Y. G. Zhang.

State Key Laboratory of Functional Materials for Informatics, Shanghai Institute of Microsystem and Information Technology, Chinese Academy of Sciences, Shanghai 200050, China.

Programme, Wednesday 28th March

Session 4: Light Sources & Lasers I

Law Building 0.22; 08:45 – 10:45

8:45 A18_42 **Simulation and Depth Profiling of Telecoms Vertical-Cavity Surface-Emitting Lasers Using Cross-Sections and X-Ray Photoelectron Spectroscopy**

T. J. Wilson[1]*, P. D. Hodgson[1], A. J. Robson[1,2], J. Counsell[3] and M. Hayne[1,2].

[1]Department of Physics, Lancaster University, Lancaster, LA1 4YB, UK; [2]Lancaster Material Analysis, Lancaster University, Lancaster, LA1 4YB, UK; [3]Kratos Analytical Ltd, Trafford Wharf Rd, Wharfside, Manchester, M17 1GP.

9:00 A18_14 **Effect of feedback phase on the stability of semiconductor nanolasers**

Yuanlong Fan[1], K. Alan Shore[1], Pu Li[2,3] and Yanhua Hong[1].

[1]School of Electronic Engineering, Bangor University, Wales, LL57 1UT, United Kingdom; [2]Key Laboratory of Advanced Transducers & Intelligent Control System, Ministry of Education, Taiyuan University of Technology, Taiyuan, 030024, China; [3]Institute of Optoelectronic Engineering, College of Physics & Optoelectronics, Taiyuan University of Technology, Taiyuan, 030024, China.

9:15 A18_05 **Nanolaser optimization through statistical optoelectronic analysis**

Juan Arturo Alanis[1], Tim Burgess[2], Mykhaylo Lysevych[2], Dhruv Saxena[2], Sudha Mokkapati[3], Xiaoyan Tang[1], Kun Peng[2], Lan Fu[2], Hark Hoe Tan[2], Chennupati Jagadish[2] and Patrick Parkinson[1].*

[1]The Photon Science Institute and School of Physics and Astronomy, University of Manchester, UK; [2]Electronic Materials Engineering, The Australian National University, Canberra, Australia; [3]School of Physics and Astronomy and Institute for Compound Semiconductors, Cardiff University, UK.

9:30 A18_21 **Linewidth Reduction of Photonic Microwave in Optically Injected VCSELs Using Optical Feedback**

Songkun Ji[1], Chenpeng Xue[1,2], Angel Valle[4], Paul Spencer[1], Hongqiang Li[4] and Yanhua Hong[1].

[1]School of Electronic Engineering, Bangor University, Wales, LL57 1UT, UK; [2]School of Communication and Information Engineering, University of Electronic Science and Technology of China, Chengdu 611731, China; [3]Instituto de Física de Cantabria (CSIC-Univ. de Cantabria), Avda. Los Castros s/n, E39005 Santander, Spain; [4]Tianjin Key Laboratory of Optoelectronic Detection Technology and Systems, School of Electronics and Information Engineering, Tianjin Polytechnic University, Tianjin 300387, China.

9:45 A18_20 **The effects of P-doping on 1.3µm quantum dot lasers grown on GaAs and Si substrates**

L. Jarvis[1]*, S. Shutts[1], P. M. Smowton[1], M. Tang[2], J. Wu[2], and H. Liu[2].

[1]School of Physics and Astronomy, Cardiff University, The Parade, Cardiff, CF24 3AA; [2]Department of Electronic and Electrical Engineering, University College London, Torrington Place, WC1E 7JE.

10:00 A18_07 **Resonant pulse amplification based on mode-locked semiconductor lasers**

M. A. Alloush[1*], R. H. Pilny[1], C. Brenner[1], A. Klehr[2], A. Knigge[2], G. Trankle[2], M. R. Hofmann[1].

[1]Lehrstuhl fur Photonik und Terahertztechnologie, Ruhr-Universitat Bochum, Bochum, Germany; [2]Ferdinand-Braun-Institut, Leibniz Institut fur Hochstfrequenztechnik, Berlin, Germany.

10:15 A18_04 **Semiconductor Quantum Well Lasers with a Temperature Insensitive Threshold Current**

A. R. Adams[1]*, I. P. Marko[1], J. Mukherjee[1], S. J. Sweeney[1], A. Gocalinska[2], E. Pelucchi[2] and B. Corbett[2].
[1]Advanced Technology Institute and Department of Physics, University of Surrey, Guildford GU2 7XH, UK; [2]Tyndall National Inst., University of Cork, Lee Maltings, Dyke Parade, Cork, Ireland.

10:30 A18_13 **Effects of Auger Recombination on the Temperature and Wavelength Dependence of Type I Mid Infrared Lasers**

Timothy Eales[1], Igor P. Marko[1], Barnabas A. Ikyo[1], Alf R. Adams[1], Shamsul Arafin[2], Stephan Sprengel[2], M.-C. Amann[2], Leon Shterengas[3], and Stephen J. Sweeney[1]*.
[1]Advanced Technology Institute, University of Surrey, Guildford GU2 7XH, United Kingdom; [2]Walter Schottky Institut, Technische Universität München, Am Coulombwall 3, 85748 Garching, Germany; [3]Department of Electrical and Computer Engineering, State University of New York at Stony Brook, New York 11794, USA.

10:45 – 11:15 Refreshment Break, Aberdare Hall

Session 5: Light Sources & Lasers II

Law Building 0.22; 11:15 – 12:45

11:15 A18_33 **Terahertz Generation in Nonlinear Gain Coupled Distributed Feedback Mid-Infrared Quantum Cascade Lasers**

W. Oberhausen*, F. Demmerle, D. Burghart, A. Wolf, G. Boehm, H. Schmeiduch, M. C. Amann.
Walter Schottky Institut, Technische Universitaet Muenchen, 85748 Garching, Germany.

11:30 A18_10 **Theory of strain-balanced In(N)AsSb/AlInAs metamorphic quantum wells for mid-infrared applications**

Reza Arkani[1, 2], Christopher A. Broderick[1, 2], Eva Repiso[3], Peter J. Carrington[4], Anthony Krier[3], and Eoin P. O'Reilly[1, 2].
[1]Tyndall National Institute, Lee Maltings, Dyke Parade, Cork, T12 R5CP, Ireland; [2]Department of Physics, University College Cork, Cork, T12 YN60, Ireland; [3]Department of Physics, Lancaster University, Lancaster, LA1 4YB, United Kingdom; [4]Department of Engineering, Lancaster University, Lancaster, LA1 4YW, United Kingdom.

11:45 A18_09 **Mid infrared (3-5 µm) InAsSb resonant cavity light emitting diode (RCLED)**

F.A. Al-Saymari*, A.P. Craig, Y. J. Noori, Q. Lu, A.R.J. Marshall & A. Krier.
Department of Physics, Lancaster University, United Kingdom.

12:00 A18_18 **Tamm plasmons and confined Tamm plasmons coupled to telecom wavelengths quantum dots**

Edmund Harbord[1], Matthew Parker[2], Petros Androsanvitaneas[1], Andrew Young[1], Edmund Clarke[3], John Rarity[1], Ruth Oulton[1,2].
[1]Department of Electrical and Electronic Engineering, University of Bristol, Merchant Venturers Building, Woodland Road, Bristol, BS8 1UB, UK; [2]HH Wills Physics Laboratory, University of Bristol, Tyndall Avenue, Bristol, BS8 1TL, UK; [3]EPSRC National Centre for III-V Technologies, University of Sheffield, Mappin Street, Sheffield, S1 3JD, UK.

12:15 A18_16 **The Generation of an Optical Frequency Comb using a Photonic Crystal Cavity**

H. Francis*, S. Chen, C.H. Ho, K.J. Che, M. Hopkinson and C.Y. Jin.
Department of Electronic and Electrical Engineering, University of Sheffield.

12:30 A18_25 **Epitaxy of InAs/InP QD structures for single photon emitters & lasers operating at 1.5-2 µm**

A.B. Krysa[1]*, J. Skiba-Szymanska[2], T. Müller[2], J. Huwer[2], M. Anderson[2,3], B. Harrison[1], R.M. Stevenson[2], D.A. Ritchie[3], A.J. Shields[2].

[1]EPSRC National Epitaxy Facility, Department of Electrical and Electronic Engineering, University of Sheffield, Mappin Street, Sheffield, S1 3JD, UK; [2]Toshiba Research Europe Limited, 208 Science Park, Milton Road, Cambridge, CB4 0GZ, UK; [3]Cavendish Laboratory, University of Cambridge, JJ Thomson Avenue, Cambridge, CB3 0HE, UK.

12:45 – 13:45 Lunch, Aberdare Hall

Session 6: Integration Strategies & Approaches

Law Building 0.22; 13:45 – 15:30

13:45 A18_29 **CORNERSTONE: Silicon photonics device prototyping capability**

C. G. Littlejohns[1], S. Stankovic[1], D. T. Tran[1], X. Yan[1], H. Du[1], G. Sharp[2], M. Sorel[2], R. Webb[3], J. England[3], H. M. H. Chong[1], F. Y. Gardes[1], D. J. Thomson[1], G. Z. Mashanovich[1], G. T. Reed[1].

[1]Optoelectronics Research Centre, University of Southampton, Southampton, SO17 1BJ, UK; [2]University of Glasgow, Glasgow, G12 8LP, UK; [3]Ion Beam Centre, University of Surrey, Guildford, GU2 7XH, UK.

14:00 A18_39 **Investigation of the Expansion in InP layer bonded to Si and its Effects on the Performance of the Photonic Crystal Lasers with the Buried Heterostructure**

A. Sakanas*, Y. Yu, E. Semenova, L. Ottaviano, H. K. Sahoo, J. Mørk, and K. Yvind.

DTU Fotonik, Technical University of Denmark, Ørsteds Plads 345A, 2800 Kongens Lyngby, Denmark.

14:15 A18_01 **Suspended Nanocrystalline Diamond-on-Air Waveguide Platform for Chip-Scale Infrared Photonics.**

A. R. Abdou[1], P. Panduranga[1], J. Richter[2], O. A. Williams[3], J. Witzens[2], and M. P. Nezhad[1].

[1]School of Electronic Engineering, Bangor University, LL57 1UT, United Kingdom; [2]Institute of Integrated Photonics, RWTH Aachen University, Sommerfeldstrasse 24, D-52074, Aachen, Germany; [3]School of Physics and Astronomy, Cardiff University, Queen's Buildings, The Parade, Cardiff, CF24 3AA, United Kingdom.

14:30 A18_17 **Multiplexed Integrated Source in III-V Materials**

Geraint Gough[1], Daryl M Beggs[2], Jorge Barreto[1].

[1]Centre for NSQI, University of Bristol, Tyndall Avenue, Avon, Bristol, BS8 1FD, UK; [2]School of Physics and Astronomy, Cardiff University, 5 The Parade, Cardiff, CF24 3AA, UK.

14:45 A18_24 **III-V Nanowire Heterostructures on Silicon-on-Insulator for Silicon Photonics Applications**

Hyunseok Kim, Ting-Yuan Chang, Wook-Jae Lee, and Diana L. Huffaker.

15:00 A18_44 **Hybrid polymer-based Er-doped waveguide amplifiers**

Marcin Ziarko[1], Nikos Bamiedakis[1], Eric Kumi-Barimah[2], Gin Jose[2], Richard Penty[1], Ian H. White[1].

[1]Centre for Photonic Systems, Department of Engineering, University of Cambridge, 9 JJ Thomson Ave, Cambridge CB3 0FA, UK; [2]Institute for Materials Research, School of Chemical and Process Engineering, University of Leeds, Leeds LS2 9JT, UK.

15:15 A18_34 **Electrical Control of Critical Coupling in Graphene Chiral Metamaterials**

Sang Soon Oh[1], Teun-Teun Kim[2], Hyeon-Don Kim[3], Hyun Sung Park[3], Ortwin Hess[4], Bumki Min[3], Shuang Zhang[5].

[1]School of Physics and Astronomy, Cardiff University, Cardiff CF24 3AA, United Kingdom; [2]Center for Integrated Nanostructure Physics, Institute for Basic Science, Suwon 16419, Republic of Korea; [3]Department of Mechanical Engineering, Korea Advanced Institute of Science and Technology, Daejeon 34141, Republic of Korea; [4]Blackett Laboratory, Department of Physics, Imperial College London, South Kensington Campus, London SW7 2AZ, UK; [5]School of Physics and Astronomy, University of Birmingham, Birmingham B15 2TT, UK.

15:30 – 16:00 Refreshment Break, Aberdare Hall

Session 7: Forum / Discussion Group

Law Building 0.22; 16:00 – 16:45

16:00 Discussion/forum **Approaches for Integrated Optoelectronics**

Chair: Peter Smowton

Cardiff University

Conference Banquet

Cardiff Castle: Music (Library) followed by dinner; 18:00 onwards

Programme, Thursday 29th March

Session 8: Materials Development I

Room 0.22, Law Building; 08:45 - 10:30

8:45 A18_28 **Novel Few-layer $MoS_{2(1-x)}Se_{2x}$ Phototransistors**

Xiao Li[1], Hao Xu[1]*, Wei Liu[1,2], Juntong Zhu[3], Guifu Zou[3], Jiang Wu[1], Huiyun Liu[1]. *hao.xu.15@ucl.ac.uk

[1]Department of Electronic and Electrical Engineering, University College London, Torrington Place, London WC1E 7JE, UK; [2]London Centre for Nanotechnology, University College London, London WC1H 0AH, UK; [3]College of Physics, Optoelectronics and Energy and Collaborative Innovation Centre of Suzhou Nano Science and Technology, Soochow University, Suzhou 215006, China.

9:00 A18_36 **Restraining Effect of Film Thickness on the Behavior of Amplified Spontaneous Emission from Methylammonium Lead Iodide Perovskite**

Saif Qaid[1], M. Naziruddin Khan[2], Abdulaziz Alqasem[1], Mahmoud Hezam[2], Abdullah Aldwayyan[1,2].

[1]Photonics Lab., Physics and Astronomy Department, King Saud University, Riyadh, Saudi Arabia; [2]King Abdullah Institute for Nanotechnology, King Saud University, Riyadh, Saudi Arabia.

9:15 A18_27 **Low threading dislocation density GaAs growth on CMOS-compatible Si (001) by MOCVD for integration of quantum dot lasers**

Qiang Li*, Zhao Yan, Kei May Lau.

Department of Electronic and Computer Engineering, Hong Kong University of Science and Technology, Clear Water Bay, Kowloon, Hong Kong.

9:30 A18_22 **Investigation of strain and morphology of non-polar GaN overgrown on different patterned templates**

L. Jiu, Y. Gong, and T. Wang.

Department of Electronic and Electrical Engineering, University of Sheffield, United Kingdom.

9:45 A18_23 **Measurement of the transport parameters of AlGaInAs for use in Quantum Well Laser Structures**

Christopher Kemp[1]*, Igor Marko[1], Ian Lealman[2], Graham Berry[2], Michael Robertson[2], Steven K. Clowes[1] and Stephen J. Sweeney[1].

[1]Advanced Technology Institute and Department of Physics, University of Surrey, Guildford, Surrey GU2 7XH, United Kingdom; [2]Huawei Technologies R&D (UK), Adastral Park, Martlesham Heath, Martlesham, Ipswich, Suffolk, IP5 3RE, United Kingdom.

10:00 A18_11 **InAs/GaAs Quantum Dot Solar Cells with QDs in Base Region**

S. Chan[*1], D. Kim[1], M. Tang[1], J. Wu[1], and H. Liu[1]

[1] Department of Electronic and Electrical Engineering, University College London, Torrington Place, London WC1E 7JE, United Kingdom.

10:15 A18_45 **Efficiency Enhancement of Plasmonic Solar Cells**

Riyadh Mansoor

Faculty of Engineering, ALMuthanna University, Iraq

10:30 – 11:00 Refreshment Break, Aberdare Hall

Session 9: Materials Development II

Location: Room 0.22, Law Building; 11:00 - 12:00

11:00 A18_19 **GaAsBi MQW device performance at solar concentrator temperatures**

F Harun, R D Richards*, A Ray, and J P R David.
University of Sheffield, Sheffield, South Yorkshire, S1 3JD, UK.

11:15 A18_31 **Strain-Compensated $GaAs_{1-y}P_y/GaAs_{1-x}Bi_x$ Quantum Wells for Laser and Solar Cell Application**

Luke J. Mawst[1]*, Honghyuk Kim[1], Kangho Kim[2], Jaejin Lee[2], Thomas F. Kuech[3].
[1]Department of Electrical and Computer Engineering, University of Wisconsin-Madison, Madison, WI 53706; Department of Electronic Engineering, Ajou University, Republic of Korea; [3]Department of Chemical and Biological Engineering, University of Wisconsin-Madison, Madison, WI 53706.

11:30 A18_40 **Uniquely designed micro-striped GaN-on-Si as a highly energy efficient photoelectrode**

Z. A. Syed# Y. Hou#, X. Yu, S. Shen, M. Athanasiou, J. Bai and T. Wang*.
Department of Electronic and Electrical Engineering, University of Sheffield, Sheffield, S1 3JD.

11:45 A18_38 **1305nm $MoTe_2$-on-Silicon Light Source**

Lewis Reeves*, Yue Wang[1], Juntao Li[2], Thomas F. Krauss[1].
[1]University of York, York, UK; [2]School of Physics, Sun Yat-Sen University, Guangzhou, 510275, China.

12:00 Lunch, Aberdare Hall

Conference Close

Abstract List

Numerical order

A18_01 **Suspended Nanocrystalline Diamond-on-Air Waveguide Platform for Chip-Scale Infrared Photonics.**

A. R. Abdou[1], P. Panduranga[1], J. Richter[2], O. A. Williams[3], J. Witzens[2], and M. P. Nezhad[1].

[1]School of Electronic Engineering, Bangor University, LL57 1UT, United Kingdom; [2]Institute of Integrated Photonics, RWTH Aachen University, Sommerfeldstrasse 24, D-52074, Aachen, Germany; [3]School of Physics and Astronomy, Cardiff University, Queen's Buildings, The Parade, Cardiff, CF24 3AA, United Kingdom.

A18_02 **Temperature and temporal stability of avalanche gain for $Al_{0.85}$ $Ga_{0.15}$ $As_{0.56}$ $Sb_{0.44}$ avalanche photodiodes**

S. Abdullah, C.H.Tan*, L. Pinel and J.S. Ng.

A18_03 **Physical Modelling of InGaAs-InAlAs APD and PIN Photodetectors for > 25Gb/s Data Rate Applications**

O. S. Abdulwahid[1], Saad Muttlak[1], J. Sexton[1], I. Kostakis[2], K.W. Ian[2] and M. Missous[1].

[1]School of Electrical and Electronic Engineering, the University of Manchester, United Kingdom; [2]Integrated Compound Semiconductors, Manchester, United Kingdom.

A18_04 **Semiconductor Quantum Well Lasers with a Temperature Insensitive Threshold Current**

A. R. Adams[1]*, I. P. Marko[1], J. Mukherjee[1], S. J. Sweeney[1], A. Gocalinska[2], E. Pelucchi[2] and B. Corbett[2].

[1]Advanced Technology Institute and Department of Physics, University of Surrey, Guildford GU2 7XH, UK; [2]Tyndall National Inst., University of Cork, Lee Maltings, Dyke Parade, Cork, Ireland.

A18_05 **Nanolaser optimization through statistical optoelectronic analysis**

Juan Arturo Alanis1, Tim Burgess2, Mykhaylo Lysevych2, Dhruv Saxena2, Sudha Mokkapati3, Xiaoyan Tang1, Kun Peng2, Lan Fu2, Hark Hoe Tan2, Chennupati Jagadish2 and Patrick Parkinson1.*

1The Photon Science Institute and School of Physics and Astronomy, University of Manchester, UK; 2Electronic Materials Engineering, The Australian National University, Canberra, Australia; 3School of Physics and Astronomy and Institute for Compound Semiconductors, Cardiff University, UK.

A18_06 **Modelling of single-mode GaAs-based 1x2 MMI and Y-branch splitters**

T. Albiladi*, D. Beggs, E. Le Boulbar Z. Li and P. M. Smowton.

School of Physics and Astronomy, Cardiff University, Queen's Building, The Parade, Cardiff, Wales, UK, CF24 3AA.

A18_07 **Resonant pulse amplification based on mode-locked semiconductor lasers**

M. A. Alloush[1*], R. H. Pilny[1], C. Brenner[1], A. Klehr[2], A. Knigge[2], G. Trankle[2], M. R. Hofmann[1].

[1]Lehrstuhl fur Photonik und Terahertztechnologie, Ruhr-Universitat Bochum, Bochum, Germany; [2]Ferdinand-Braun-Institut, Leibniz Institut fur Hochstfrequenztechnik, Berlin, Germany.

A18_08 **Optical properties of drug-resistant human osteosarcoma cells - the potential for microfluidic-based Lab-on-Chip analysis**

Basmah Almagwashi[1], Marie Wiltshire[2], Rachel Errington[2], and Peter Smowton[1].

[1]School of Physics and Astronomy, Cardiff University, 5 The Parade, Cardiff, CF24 3AA, UK; [2]School of Medicine, Division of Cancer Genetics, Heath Park, Cardiff University, Cardiff, CF14 4XN, UK.

A18_09 **Mid infrared (3-5 µm) InAsSb resonant cavity light emitting diode (RCLED)**

F.A. Al-Saymari*, A.P. Craig, Y. J. Noori, Q. Lu, A.R.J. Marshall & A. Krier.

Department of Physics, Lancaster University, United Kingdom.

A18_10 Theory of strain-balanced In(N)AsSb/AlInAs metamorphic quantum wells for mid-infrared applications

Reza Arkani[1, 2], Christopher A. Broderick[1, 2], Eva Repiso[3], Peter J. Carrington[4], Anthony Krier[3], and Eoin P. O'Reilly[1, 2].

[1]Tyndall National Institute, Lee Maltings, Dyke Parade, Cork, T12 R5CP, Ireland; [2]Department of Physics, University College Cork, Cork, T12 YN60, Ireland; [3]Department of Physics, Lancaster University, Lancaster, LA1 4YB, United Kingdom; [4]Department of Engineering, Lancaster University, Lancaster, LA1 4YW, United Kingdom.

A18_11 InAs/GaAs Quantum Dot Solar Cells with QDs in Base Region

S. Chan* [1], D. Kim[1], M. Tang[1], J. Wu[1], and H. Liu[1]

[1] Department of Electronic and Electrical Engineering, University College London, Torrington Place, London WC1E 7JE, United Kingdom.

A18_12 Growth mechanisms in InAs/GaAs QDs with and without Bi surfactant

X. Y. Chen, Y. Gu*, Y. J. Ma, B. Du, J. Zhang, Y. H. Shi, W. Y. Ji, Y. G. Zhang.

State Key Laboratory of Functional Materials for Informatics, Shanghai Institute of Microsystem and Information Technology, Chinese Academy of Sciences, Shanghai 200050, China.

A18_13 Effects of Auger Recombination on the Temperature and Wavelength Dependence of Type I Mid Infrared Lasers

Timothy Eales[1], Igor P. Marko[1], Barnabas A. Ikyo[1], Alf R. Adams[1], Shamsul Arafin[2], Stephan Sprengel[2], M.-C. Amann[2], Leon Shterengas[3], and Stephen J. Sweeney[1]*.

[1]Advanced Technology Institute, University of Surrey, Guildford GU2 7XH, United Kingdom; [2]Walter Schottky Institut, Technische Universität München, Am Coulombwall 3, 85748 Garching, Germany; [3]Department of Electrical and Computer Engineering, State University of New York at Stony Brook, New York 11794, USA.

A18_14 Effect of feedback phase on the stability of semiconductor nanolasers

Yuanlong Fan[1], K. Alan Shore[1], Pu Li[2,3] and Yanhua Hong[1].

[1]School of Electronic Engineering, Bangor University, Wales, LL57 1UT, United Kingdom; [2]Key Laboratory of Advanced Transducers & Intelligent Control System, Ministry of Education, Taiyuan University of Technology, Taiyuan, 030024, China; [3]Institute of Optoelectronic Engineering, College of Physics & Optoelectronics, Taiyuan University of Technology, Taiyuan, 030024, China.

A18_15 InP Nanowire Solar Cells with Carrier-Selective Layers

M. Fleet* and S. Mokkapati.

School of Physics and Astronomy, North Queen's Building, Cardiff University, The Parade, Cardiff, UK, CF24 3AA.

A18_16 The Generation of an Optical Frequency Comb using a Photonic Crystal Cavity

H. Francis*, S. Chen, C.H. Ho, K.J. Che, M. Hopkinson and C.Y. Jin.

Department of Electronic and Electrical Engineering, University of Sheffield.

A18_17 Multiplexed Integrated Source in III-V Materials

Geraint Gough[1], Daryl M Beggs[2], Jorge Barreto[1].

[1]Centre for NSQI, University of Bristol, Tyndall Avenue, Avon, Bristol, BS8 1FD, UK; [2]School of Physics and Astronomy, Cardiff University, 5 The Parade, Cardiff, CF24 3AA, UK.

A18_18 Tamm plasmons and confined Tamm plasmons coupled to telecom wavelengths quantum dots

Edmund Harbord[1], Matthew Parker[2], Petros Androsanvitaneas[1], Andrew Young[1], Edmund Clarke[3], John Rarity[1], Ruth Oulton[1,2].

[1]Department of Electrical and Electronic Engineering, University of Bristol, Merchant Venturers Building, Woodland Road, Bristol, BS8 1UB, UK; [2]HH Wills Physics Laboratory, University of Bristol, Tyndall Avenue, Bristol, BS8 1TL, UK; [3]EPSRC National Centre for III-V Technologies, University of Sheffield, Mappin Street, Sheffield, S1 3JD, UK.

A18_19 GaAsBi MQW device performance at solar concentrator temperatures

F Harun, R D Richards*, A Ray, and J P R David.
University of Sheffield, Sheffield, South Yorkshire, S1 3JD, UK.

A18_20 The effects of P-doping on 1.3µm quantum dot lasers grown on GaAs and Si substrates

L. Jarvis[1]*, S. Shutts[1], P. M. Smowton[1], M. Tang[2], J. Wu[2], and H. Liu[2].
[1]School of Physics and Astronomy, Cardiff University, The Parade, Cardiff, CF24 3AA; [2]Department of Electronic and Electrical Engineering, University College London, Torrington Place, WC1E 7JE.

A18_21 Linewidth Reduction of Photonic Microwave in Optically Injected VCSELs Using Optical Feedback

Songkun Ji[1], Chenpeng Xue[1,2], Angel Valle[4], Paul Spencer[1], Hongqiang Li[4] and Yanhua Hong[1].
[1]School of Electronic Engineering, Bangor University, Wales, LL57 1UT, UK; [2]School of Communication and Information Engineering, University of Electronic Science and Technology of China, Chengdu 611731, China; [3]Instituto de Física de Cantabria (CSIC-Univ. de Cantabria), Avda. Los Castros s/n, E39005 Santander, Spain; [4]Tianjin Key Laboratory of Optoelectronic Detection Technology and Systems, School of Electronics and Information Engineering, Tianjin Polytechnic University, Tianjin 300387, China.

A18_22 Investigation of strain and morphology of non-polar GaN overgrown on different patterned templates

L. Jiu, Y. Gong, and T. Wang.
Department of Electronic and Electrical Engineering, University of Sheffield, United Kingdom.

A18_23 Measurement of the transport parameters of AlGaInAs for use in Quantum Well Laser Structures

Christopher Kemp[1]*, Igor Marko[1], Ian Lealman[2], Graham Berry[2], Michael Robertson[2], Steven K. Clowes[1] and Stephen J. Sweeney[1].
[1]Advanced Technology Institute and Department of Physics, University of Surrey, Guildford, Surrey GU2 7XH, United Kingdom; [2]Huawei Technologies R&D (UK), Adastral Park, Martlesham Heath, Martlesham, Ipswich, Suffolk, IP5 3RE, United Kingdom.

A18_24 III-V Nanowire Heterostructures on Silicon-on-Insulator for Silicon Photonics Applications

Hyunseok Kim, Ting-Yuan Chang, Wook-Jae Lee, and Diana L. Huffaker.

A18_25 Epitaxy of InAs/InP QD structures for single photon emitters & lasers operating at 1.5-2 µm

A.B. Krysa[1]*, J. Skiba-Szymanska[2], T. Müller[2], J. Huwer[2], M. Anderson[2,3], B. Harrison[1], R.M. Stevenson[2], D.A. Ritchie[3], A.J. Shields[2].
[1]EPSRC National Epitaxy Facility, Department of Electrical and Electronic Engineering, University of Sheffield, Mappin Street, Sheffield, S1 3JD, UK; [2]Toshiba Research Europe Limited, 208 Science Park, Milton Road, Cambridge, CB4 0GZ, UK; [3]Cavendish Laboratory, University of Cambridge, JJ Thomson Avenue, Cambridge, CB3 0HE, UK.

A18_26 Computing Resonant Modes of PCSELs using the Transfer Matrix Method

G. Li, J. Sarma*, R. A. Hogg. *Visiting Researcher
School of Engineering, University of Glasgow, Glasgow, G12 8TL, UK.

A18_27 Low threading dislocation density GaAs growth on CMOS-compatible Si (001) by MOCVD for integration of quantum dot lasers

Qiang Li*, Zhao Yan, Kei May Lau.
Department of Electronic and Computer Engineering, Hong Kong University of Science and Technology, Clear Water Bay, Kowloon, Hong Kong.

A18_28 Novel Few-layer $MoS_{2(1-x)}Se_{2x}$ Phototransistors

Xiao Li[1], Hao Xu[1]*, Wei Liu[1, 2], Juntong Zhu[3], Guifu Zou[3], Jiang Wu[1], Huiyun Liu[1]. *hao.xu.15@ucl.ac.uk
[1]Department of Electronic and Electrical Engineering, University College London, Torrington Place, London WC1E 7JE, UK; [2]London Centre for Nanotechnology, University College London, London WC1H 0AH, UK; [3]College of Physics, Optoelectronics and Energy and Collaborative Innovation Centre of Suzhou Nano Science and Technology, Soochow University, Suzhou 215006, China.

A18_29 CORNERSTONE: Silicon photonics device prototyping capability

C. G. Littlejohns[1], S. Stankovic[1], D. T. Tran[1], X. Yan[1], H. Du[1], G. Sharp[2], M. Sorel[2], R. Webb[3], J. England[3], H. M. H. Chong[1], F. Y. Gardes[1], D. J. Thomson[1], G. Z. Mashanovich[1], G. T. Reed[1].
[1]Optoelectronics Research Centre, University of Southampton, Southampton, SO17 1BJ, UK; [2]University of Glasgow, Glasgow, G12 8LP, UK; [3]Ion Beam Centre, University of Surrey, Guildford, GU2 7XH, UK.

A18_30 Silicon mid-infrared photodetectors

M. A. Lourenço[1,2] and K. P. Homewood[1,2,3].
[1]Materials Research Institute and School of Physics and Astronomy, Queen Mary University of London, Mile End Road, E1 4NS London, UK; [2]Advanced Technology Institute, Faculty of Engineering and Physical Sciences, University of Surrey, Guildford, Surrey GU2 7XH, UK; [3]School of Materials Science & Engineering, Hubei University, Wuhan 430062, P. R. China.

A18_31 Strain-Compensated $GaAs_{1-y}P_y/GaAs_{1-x}Bi_x$ Quantum Wells for Laser and Solar Cell Application

Luke J. Mawst[1]*, Honghyuk Kim[1], Kangho Kim[2], Jaejin Lee[2], Thomas F. Kuech[3].
[1]Department of Electrical and Computer Engineering, University of Wisconsin-Madison, Madison, WI 53706; Department of Electronic Engineering, Ajou University, Republic of Korea; [3]Department of Chemical and Biological Engineering, University of Wisconsin-Madison, Madison, WI 53706.

A18_32 InGaAs-InP HBT-PIN Based Optoelectronic Integrated Circuit for over 10Gb/s Optical Systems

S. G. Muttlak*, J. Sexton and M. Missous.
School of Electrical and Electronic Engineering, University of Manchester, UK.

A18_33 Terahertz Generation in Nonlinear Gain Coupled Distributed Feedback Mid-Infrared Quantum Cascade Lasers

W. Oberhausen*, F. Demmerle, D. Burghart, A. Wolf, G. Boehm, H. Schmeiduch, M. C. Amann.
Walter Schottky Institut, Technische Universitaet Muenchen, 85748 Garching, Germany.

A18_34 Electrical Control of Critical Coupling in Graphene Chiral Metamaterials

Sang Soon Oh[1], Teun-Teun Kim[2], Hyeon-Don Kim[3], Hyun Sung Park[3], Ortwin Hess[4], Bumki Min[3], Shuang Zhang[5].
[1]School of Physics and Astronomy, Cardiff University, Cardiff CF24 3AA, United Kingdom; [2]Center for Integrated Nanostructure Physics, Institute for Basic Science, Suwon 16419, Republic of Korea; [3]Department of Mechanical Engineering, Korea Advanced Institute of Science and Technology, Daejeon 34141, Republic of Korea; [4]Blackett Laboratory, Department of Physics, Imperial College London, South Kensington Campus, London SW7 2AZ, UK; [5]School of Physics and Astronomy, University of Birmingham, Birmingham B15 2TT, UK.

A18_35 Modelling Timing Jitter in Silicon Single Photon Avalanche Diodes

J. Petticrew, S. Dimler, and J. S. Ng*.
Department of Electronic & Electrical Engineering, University of Sheffield, Sheffield, UK.

A18_36 Restraining Effect of Film Thickness on the Behavior of Amplified Spontaneous Emission from Methylammonium Lead Iodide Perovskite

Saif Qaid[1], M. Naziruddin Khan[2], Abdulaziz Alqasem[1], Mahmoud Hezam[2], Abdullah Aldwayyan[1,2].
[1]Photonics Lab., Physics and Astronomy Department, King Saud University, Riyadh, Saudi Arabia; [2]King Abdullah Institute for Nanotechnology, King Saud University, Riyadh, Saudi Arabia.

A18_37 Growth of Type-II InAs/GaSb superlattice

Yaksh Rawal[1], Marie Delmas[1], Baolai Liang[2], Diana Huffaker[1,2].

[1]School of Physics and Astronomy, Cardiff University, the Parade, Cardiff, CF24 3AA, UK; [2]California NanoSystem Institute, University of California, Los Angeles, CA90095, USA.

A18_38 1305nm $MoTe_2$-on-Silicon Light Source

Lewis Reeves*, Yue Wang[1], Juntao Li[2], Thomas F. Krauss[1].

[1]University of York, York, UK; [2]School of Physics, Sun Yat-Sen University, Guangzhou, 510275, China.

A18_39 Investigation of the Expansion in InP layer bonded to Si and its Effects on the Performance of the Photonic Crystal Lasers with the Buried Heterostructure

A. Sakanas*, Y. Yu, E. Semenova, L. Ottaviano, H. K. Sahoo, J. Mørk, and K. Yvind.

DTU Fotonik, Technical University of Denmark, Ørsteds Plads 345A, 2800 Kongens Lyngby, Denmark.

A18_40 Uniquely designed micro-striped GaN-on-Si as a highly energy efficient photoelectrode

Z. A. Syed# Y. Hou#, X. Yu, S. Shen, M. Athanasiou, J. Bai and T. Wang*.

Department of Electronic and Electrical Engineering, University of Sheffield, Sheffield, S1 3JD.

A18_41 Multi-beam Laser Interference Patterning of Semiconductors

Y. R. Wang*, C. Y. Jin, and M. Hopkinson.

Department of Electronic and Electrical Engineering, University of Sheffield, Sheffield S3 7HQ, UK.

A18_42 Simulation and Depth Profiling of Telecoms Vertical-Cavity Surface-Emitting Lasers Using Cross-Sections and X-Ray Photoelectron Spectroscopy

T. J. Wilson[1]*, P. D. Hodgson[1], A. J. Robson[1,2], J. Counsell[3] and M. Hayne[1,2].

[1]Department of Physics, Lancaster University, Lancaster, LA1 4YB, UK; [2]Lancaster Material Analysis, Lancaster University, Lancaster, LA1 4YB, UK; [3]Kratos Analytical Ltd, Trafford Wharf Rd, Wharfside, Manchester, M17 1GP.

A18_43 Modification of hole ionization coefficients in GaAsBi based avalanche photodiodes

X. Yi, Y. Liu, Z. Zhou, F. Harun, R. D. Richards*, C.H. Tan and J. P. R. David*.

Advanced Detector Centre, Department of Electronic & Electrical Engineering, University of Sheffield, Sheffield, South Yorkshire, S1 3JD, UK.

A18_44 Hybrid polymer-based Er-doped waveguide amplifiers

Marcin Ziarko[1], Nikos Bamiedakis[1], Eric Kumi-Barimah[2], Gin Jose[2], Richard Penty[1], Ian H. White[1].

[1]Centre for Photonic Systems, Department of Engineering, University of Cambridge, 9 JJ Thomson Ave, Cambridge CB3 0FA, UK; [2]Institute for Materials Research, School of Chemical and Process Engineering, University of Leeds, Leeds LS2 9JT, UK.

A18_45 Efficiency Enhancement of Plasmonic Solar Cells

Riyadh Mansoor

Faculty of Engineering, ALMuthanna University, Iraq.

Abstracts

Session 1: Guest Speakers

Invited Optical response of nanoantennas on epsilon-near-zero substrates

Sebastian A. Schulz[1-4], M. Zahirul Alam[1], Jeremy Upham[1], Israel De Leon[1,5] and Robert W. Boyd[1,6]
1. Department of Physics, University of Ottawa, Ottawa, Canada; 2. Centre for Advanced Photonics & Process Analysis, Cork Institute of Technology, Cork, Ireland; 3. Tyndall National Institute, Cork, Ireland; 4. SUPA, School of Physics and Astronomy, University of St Andrews, St Andrews, UK; 5. School of Engineering and Science, Tecnologico de Monterrey, Monterrey, Mexico.

Epsilon-near-zero (ENZ) materials have a spectral region where the real part of the permittivity crosses through zero. In the vicinity of this crossing the real part of the permittivity is between 1 and -1, leading to unusual optical effects [1], such as optical propagation through arbitrary shaped waveguide sections [2] or extreme nonlinear responses [3,4]. Yet, the ENZ materials also affect the behaviour of nearby optical components, for example optical emitters [5]. Following from this work we investigate the behaviour of a metamaterial consisting of a plasmonic resonator array (27nm thick gold antennas) coupled to a thin ENZ film. The ENZ film consists of a 27nm thick ITO layer, with an epsilon-zero crossing at 1430nm, as shown in fig.1.
We demonstrate that the modes of the plasmonic antennas couple to the thin-film modes of the ENZ layer, resulting in a strong splitting of the coupled resonances and offering a broad band optical response, spanning over 200nm in bandwidth, see fig.2 [6].
In the nonlinear regime the coupling of the antenna and ENZ thin film modes further enhances the already strong nonlinear response of the ITO layer [7]. The metamaterial exhibits an ultra-strong nonlinear response, with the nonlinear refractive index change of $|\Delta n>2|$ (see fig 3), over a broad spectral range (>200nm) on an ultra-fast timescale (<1ps on-off time).
We believe that metamaterials consisting of resonator arrays coupled to ENZ films offer a new avenue to achieve fast nonlinear optical materials with refractive index changes on the order of 1, a paradigm shift for nonlinear optics.

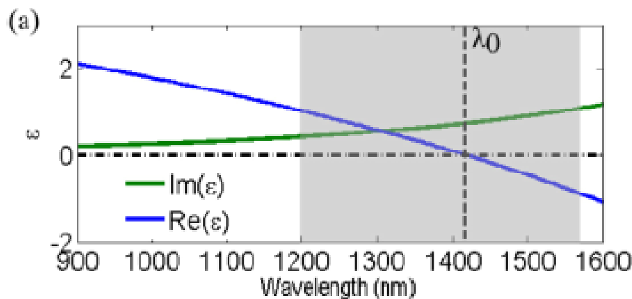

Figure 1: Real and imaginary permittivity of a thin ITO film, with the ENZ region shaded in grey.

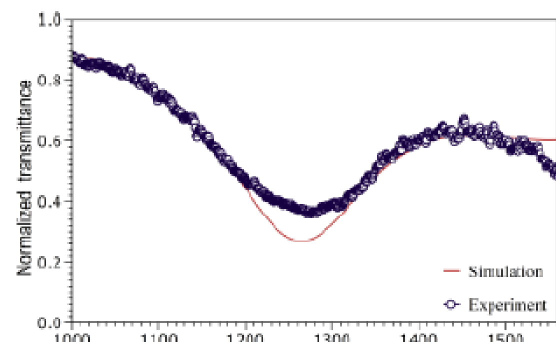

Figure 2: Transmittance of the metamaterial, showing a broad spectral response and resonance splitting.

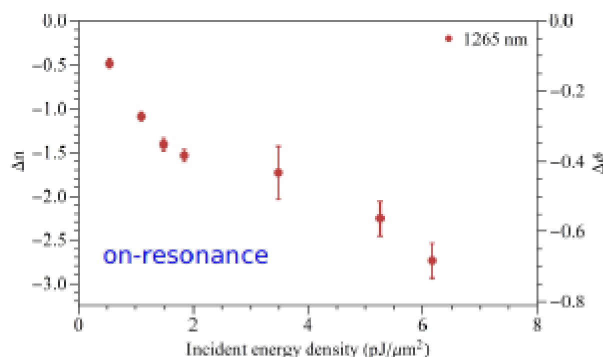

Figure 3: Nonlinear index and phase change, pumped with 1265nm light.

References: 1. N. Engheta *Science* **340**, 286 (2013). 2. M. Silveirinha & N. Engheta *Phys. Rev. Lett.* **97**, 157403 (2006). 3. M. Z. Alam et al. *Science* **352,** 795 (2016). 4. L. Caspani et al. *Phys. Rev. Lett.* **116**, 233901 (2016). 5. A. Alu et al. *Phys Rev B* **75**, 155410 (2007). 6. S. A. Schulz et al *Phys Rev A* **93**, 063846 (2016). 7. M. Z. Alam *Nature Photon* **12**, 79 (2018).

Abstracts

Session 2: Photodetectors

A18_37 Growth of Type-II InAs/GaSb superlattice

Marie Delmas[1], Yaksh Rawal[1], Baolai Liang[2], Diana Huffaker[1,2].
[1]School of Physics and Astronomy, Cardiff University, the Parade, Cardiff, CF24 3AA, UK; [2]California NanoSystem Institute, University of California, Los Angeles, CA90095, USA.

In this communication the epitaxial growth of type II superlattice (T2SL) is studied. One of the key challenges of growing good quality T2SL is to compensate the tensile strain of InAs with GaSb. We have therefore studied the shutter sequence employed at the interfaces between the InAs and GaSb layers to compensate this strain by forming an "InSb-like" interface. Two samples have been grown and consists of GaSb buffer layer grown on a p-type GaSb wafer, followed by 100 pairs of InAs/GaSb T2SL and a GaSb layer. The difference between both the samples is that one was grown using an Sb-soak after growing the InAs layer to exchange the As atoms with Sb ones.[1]. The other sample was grown using the Migration Enhanced Epitaxy (MEE) [2], which incorporates the InSb layer on either sides of GaSb layers. Photoluminescence (PL) peak observed at 77K for both the samples is in the mid-IR spectral domain – around 5µm for the Sb-soak sample and 5.5µm for the MEE one. The X-ray diffraction (XRD) data is shown in figure 1. XRD data shows a peak for the GaSb substrate and the T2SL satellite peaks. The Sb-soak sample shows promising results with good lattice matching, Δa/a of 0% (<50 arcsec) and a full width at half maxima (FWHM) for the satellite peak SL-1 equal to 56 arcsec as compared to the MEE sample which shows a lattice mismatch Δa/a of about 0.479% (~570 arcsec) with a FWHM for the satellite peak SL-1 of 73 arcsec which is slightly higher. In conclusion, Sb-soak method seems better in terms of lattice matching and for compensating strain. Following these results, a PiN photodiode structure has been grown using the Sb-soak method and fabricated using standard lithography process to understand the device performances.

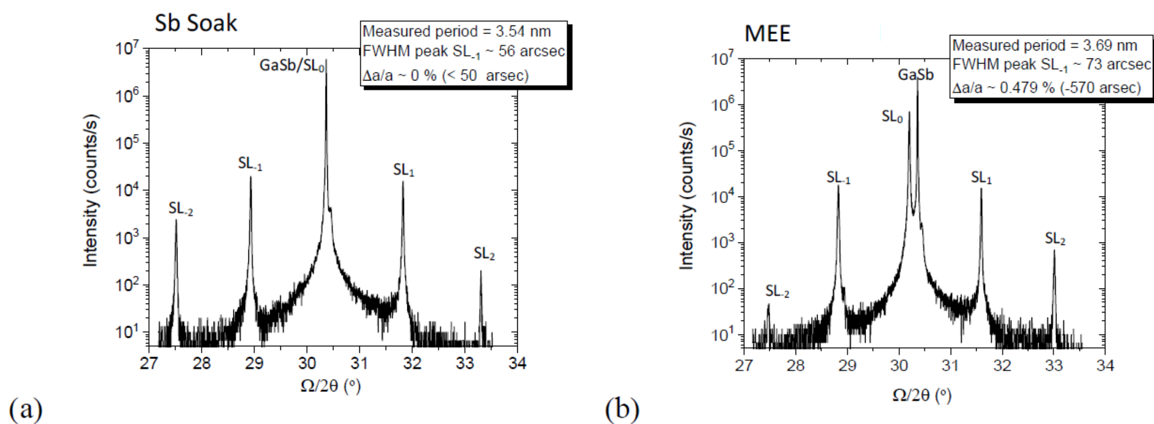

Figure 1 XRD data for (a) Sb-soak (b) MEE

References: 1) E. Plis, S. Annamalai, K. T. Posani, S. Krishna, R. A. Rupani and S. Ghosh, "Midwave Infrared Type-II InAs/ GaSb Superlattice Detectors with Mixed Interfaces," Journal of Applied Physics, Vol. 100, No. 1, 2006, Article ID: 14510. doi:10.1063/1.2214222 2) Y. Horikoshi, M. Kawashima, H. Yamaguchi: Jpn. J. Appl. Phys. 25, L 868 (1986).

A18_43 Modification of hole ionization coefficients in GaAsBi based avalanche photodiodes

X. Yi, Y. Liu, Z. Zhou, F. Harun, R. D. Richards*, C.H. Tan and J. P. R. David*. *j.p.david@sheffield.ac.uk
Advanced Detector Centre, Department of Electronic & Electrical Engineering, University of Sheffield, Sheffield, South Yorkshire, S1 3JD, UK.

Avalanche photodiodes (APDs) utilise impact ionisation to amplify optical signals at low incident photon fluxes. Impact ionisation involves an excited carrier being accelerated through a strong electric field and imparting some of its resulting energy to create further electron-hole pairs as it travels. Although the signal can be amplified by this process, the stochastic nature of the ionisation process adds some 'excess' noise. To minimise the excess noise of the APD, it is important to have very different electron and hole ionisation coefficients (α and β respectively)[1]. Unfortunately most III-V semiconductors have α approximately the same as β. Work done on GaInAsN devices with ~4% of N showed that α and β both decreased compared to GaAs but with α decreasing more rapidly [2]. This has been attributed to the change in the conduction band structure and the enhanced scattering electrons undergo with the addition of N to GaAs. It is therefore possible that the addition of Bi to GaAs would have a similar effect on β as the valence band structure would be affected in this case [3].

To investigate this, a series of p+-i-n+ and n+-i-p+ structures were grown with heavily doped GaAs cladding layers and with nominally undoped intrinsic regions of GaAsBi. Due to the strain generated by the addition of Bi to GaAs, the maximum thickness that can be grown for the 3-4% of Bi investigated is limited to thicknesses of 200nm to 800nm. Growth was undertaken on an Omicron STM-MBE reactor and circular mesa devices were fabricated by wet chemical etching. X-ray rocking curves and photoluminescence measurements showed that the Bi incorporation variation between samples was relatively small. Current-voltage measurements on the devices showed good diode characteristics with forward ideality factors of n~2. Capacitance voltage measurements showed that the background doping in the intrinsic regions was low at <1e16 cm^{-3}. Photomultiplication measurements were undertaken by shining light of different wavelengths on the top of the devices as a function of reverse bias. Due to the strain and the presence of defects and dislocations in the material, the maximum voltage that could be applied was limited by the high dark currents near breakdown. Nevertheless some degree of avalanche multiplication was observed in all the samples studies.

A preliminary analysis of the photomultiplication results suggests that α in all these samples does not differ significantly from that of GaAs, however the β appears to show a significant reduction. This suggests that a relatively large α to β ratio can be obtained by the addition of Bi to GaAs. As Bi is known to affect predominantly the valence band in GaAs via the band-anti-crossing model interaction and not affect the conduction band structure, this result is not too surprising. Considering that the addition of Bi also extends the wavelength of detection in GaAs, it is possible to envisage a low noise near infrared APD based on GaAsBi.

References: 1. R.J. McIntyre, 'Multiplication noise in uniform avalanche diodes', IEEE Trans Electron Devices, ED-13, pp. 164, 1966; 2. S.L. Tan et al., 'Experimental evaluation of impact ionization in dilute nitride GaInNAs diodes', Applied Physics Lett. 103, 102101 (2013); 3. K Alberi and O.D. Dubon, 'Valence band anti-crossing in GaAsBi', Applied Physics Lett., **91**, 051909 (2007).

A18_35 Modelling Timing Jitter in Silicon Single Photon Avalanche Diodes

J. Petticrew, S. Dimler, and J. S. Ng*. ** j.s.ng@sheffield.ac.uk*
Department of Electronic & Electrical Engineering, University of Sheffield, Sheffield, UK.

Silicon Single Photon Avalanche Diodes (SPADs), which rely on impact ionisation to produce infinitely large internal amplification, are used in a growing number of optical systems detecting light at the single photon level. These applications include Raman spectroscopy, deep space optical communications and optical tomography. Based on the Simple Monte Carlo technique, we recently developed a Si SPAD simulation model for avalanche breakdown probability and its timing statistics [1, 2]. In this work, the model is utilised to investigate the effect of SPAD design on avalanche breakdown timing statistics.
Our Si SPAD model has been extensively validated against experimental electron and hole drift velocities, impact ionisation coefficients [3], and avalanche gain statistics (avalanche gain, excess noise factor, and breakdown voltage) from Si devices. An example of the avalanche gain validation using experimental results from four Si devices [4] is shown in Fig. 1(a). Breakdown probability characteristics simulated by the model for the four Si devices are shown in Fig. 1(b). In the model, an avalanche breakdown event is recorded once the instantaneous avalanche current reaches 0.1 mA.
The model was used to simulate avalanche breakdown timing characteristics for different SPAD designs. The designs have the same width for their avalanche region (where electric field is high), but different widths for their absorption region (where electric field is low). The timing information, recorded as mean time to breakdown and timing jitter (defined as the Full-Width at Half-Maximum of the distribution of time to breakdown), is shown in Fig. 2. SPADs with wider absorption widths require more time to reach breakdown. They also show a larger variation in the time taken to reach breakdown.

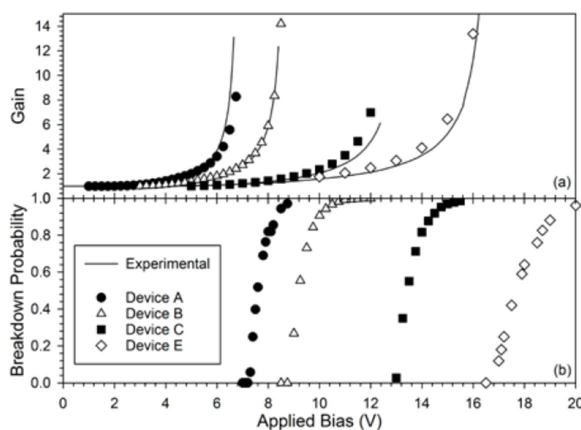

Fig. 1. Simulated (symbols) (a) avalanche gain and (b) breakdown probability versus reverse bias characteristics for four Si diodes. Experimental avalanche gain for the diodes [4] are shown as lines.

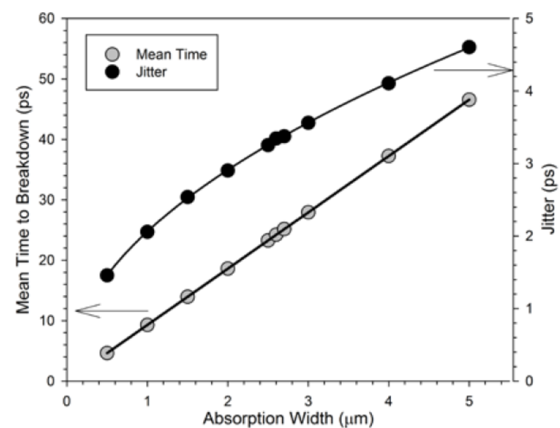

Fig. 2. Mean time to breakdown (left axis) and timing jitter (right axis) for Si SPADs with increasing absorption width.

Acknowledgements: Funding - This work was supported by the Engineering & Physical Sciences Research Council (EP/M506618/1) and by the Science and Technology Facilities Council (ST/N000145/1).

References: [1] J. D. Petticrew *et al., IEEE J. Sel. Top. Quantum Electron.*, **24**(2), 3801506, 2018; [2] J. D. Petticrew *et al.,* "Simple Monte Carlo Simulator v1.0.0", figshare, 2018. DOI:10.15131/shef.data.5683939; [3] X. Zhou *et al., J. Inst.*, **7**(08), p. 06006, 2012; [4] C. H. Tan *et al., Appl. Phys. Lett.,* **76**(26), p. 3926, 2000.

A18_32 InGaAs-InP HBT-PIN Based Optoelectronic Integrated Circuit for over 10Gb/s Optical Systems

S. G. Muttlak*, J. Sexton and M. Missous. *saad.muttlak@postgrad.manchester.ac.uk
School of Electrical and Electronic Engineering, University of Manchester, UK.

The dramatic increase in data traffic due to rapidly growing demands for ultra-high data rates for both telecom and datacom is driving sustained developments in cost effective, mass produced, optoelectronic integrated photoreceiver (OEIC) operating at 10Gb/s and beyond. Design, characterization, modeling and fabrication of Transimpedance Amplifier (TIA)-photodetector integrated circuits with attempts at widening the optical bandwidth of the OEICs is one of the key drivers of this study. Among all optical receivers, the InP/InGaAs material technology using heterojunction bipolar transistors (HBTs) has been extensively investigated. Such a system offers the capability of monolithically integrating SHBT with a PIN diode, facilitating the fabrication process and for further reduction in the parasitic elements as well as shrinking in ICs sizes and cost reduction.

The work reported here is concerned with both characterization and modeling of TIA integrated with a PIN diode for high Gb/s (> 10Gb/s) optical receivers using an InP/InGaAs HBT. To this end, both the photodiode and HBT were successfully fabricated, with the former utilizing the base and collector regions of the HBT. The measured dc responsivity and quantum efficiency of the PIN without AR coatings were 0.5 A/W and 0.45 respectively. The equivalent circuit of the diode was experimentally validated up to 40GHz using S-parameter measurements taking both depletion region capacitance and collector transit time effect into account. Due to the specific design of the InP-InGaAs epilayer structures, and considering the trade-off between high performance PIN and the heterostructure transistor, a $10\times10\mu m^2$ emitter mesa size HBT achieved an f_T and f_{max} of 54 and 57GHz respectively which are amply adequate of low cost integrated 10Gb/s optical receiver. Further minimizing in the HBT mesa area to $4\times4\mu m^2$ led to over 100 GHz cut-off frequencies. The TIA was modeled using ADS software and a transimpedance gain of 36dBΩ was obtained. Additionally, a series peaking inductor of 0.5nH was utilized to alleviate the loading effect of the photodiode's capacitance on the TIA and thereby enhancing the bandwidth of the circuit. The optimized circuit had an optical bandwidth of ~15GHz, which is theoretically adequate for up to 20 Gb/s operation. Detailed characterization and modelling of the components and OEICs and their optimization for high data rate communication systems will be presented.

A18_03 Physical Modelling of InGaAs-InAlAs APD and PIN Photodetectors for > 25Gb/s Data Rate Applications

O. S. Abdulwahid[1], Saad Muttlak[1], J. Sexton[1], I. Kostakis[2], K.W. Ian[2] and M. Missous[1].

[1]School of Electrical and Electronic Engineering, the University of Manchester, United Kingdom; [2]Integrated Compound Semiconductors, Manchester, United Kingdom.

Optical links are the most appropriate solution to accommodate society's need for high-speed communication systems. The perceived advantages of PIN and Avalanche Photodetectors (APD) make them highly preferred at the receiver front end to detect optical signals and convert them into electrical ones. Sustained development efforts for high speed photodetectors have been ongoing for many years in order to have a component that can be easily grown and fabricated and most importantly meet the increasing demand of high operating bandwidth and data rate as well as fulfilling low cost requirements for mass market adoption. III-V material systems and in particular $In_{0.52}Al_{0.48}As$ - $In_{0.53}Ga_{0.47}As$ are considered as the best technology for the 1.2 to 1.6 µm wavelength range.

This work concentrates on the optimization of three process parameters, specifically the absorption region length, light window aperture, mesa area size in order to produce PIN and APD photodetectors capable of operating at data rates in excess of 25Gb/s. The InAlAs-InGaAs APD and InGaAs PIN are grown on semi-insulating InP. Standard 10Gb/s APD (1.2µm absorber thickness) denoted as #30S and 10Gb/s PIN (2µm absorber thickness) denoted as #15S were fabricated into 30µm and 15µm window size devices respectively for modelling validation. For the characterization of the fabricated APD and PIN, a 1.55 µm laser with varying power (1 to 100 µW) was utilized to illuminate the devices and measure the resulting photo-currents and the S_{21} frequency responses. 3D physical models were built and simulated for both photodetectors using the ATLAS SILVACO tool. The modelled structures are validated by the fabricated devices in terms of DC, CV, s-parameter, and optical characteristics. SILVACO models were then created by selectively thinning down the absorption layers for the proposed high speed APD and PIN diodes (and which are denoted as #15C) to further reduce the transit time in the absorber layers. Further optimization was accomplished through scaling of the light window aperture and mesa area sizes with the aim of reducing the device capacitances. The proposed PIN photodetector (denoted as PIN #15C) has an optical 3-dB bandwidth of 35GHz at -5V bias voltage and 10µW incident light power, while the proposed APD (denoted as APD#15C) has an optical bandwidth of 21GHz and a multiplication gain of 3 at 90% V_{BR} (-21.6V) and 1µW input light power. Figure 1 (a, and b) depicts the S_{21} responses for the standard 10Gb/s and proposed > 25Gb/s PIN and APD photodetectors. The simulated data indicate that the proposed PIN and APD devices can successfully work at data rate of 40 Gb/s and 25 Gb/s respectively. The merit of using these PINs and APDs in the 25- 40Gb/s data rates applications will be discussed in details.

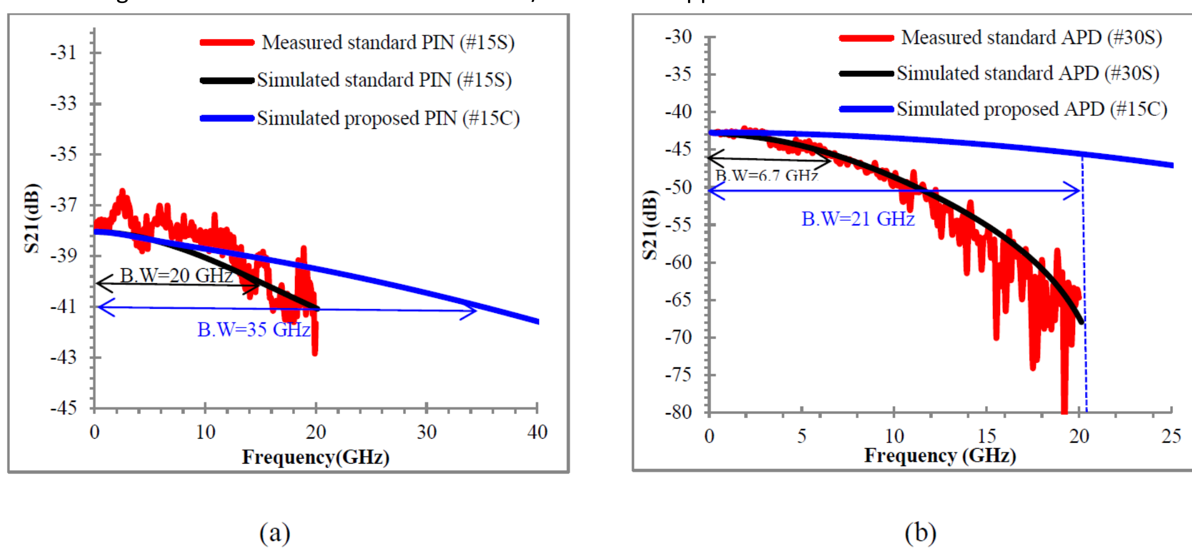

Fig 1: S_{21} response of the standard and proposed PIN and APD photodetectors

A18_02 Temperature and temporal stability of avalanche gain for $Al_{0.85}Ga_{0.15}As_{0.56}Sb_{0.44}$ avalanche photodiodes

S. Abdullah, C.H.Tan*, L. Pinel and J.S. Ng *c.h.tan@sheffield.ac.uk

Avalanche gain and breakdown voltage in semiconductors are dependent on temperature. Photonic sensing instrumentation utilising the Avalanche Photodiodes (APDs) thus requires either voltage adjustment or a temperature stabilisation circuitry to maintain a constant avalanche gain. The temperature coefficient of breakdown voltage, $C_{bd} = dV_{bd}/dT$, V_{bd} is the breakdown voltage and T is the temperature, is normally used to assess the temperature dependence of avalanche process.

For detection of infrared wavelength at 1550 nm an InGaAs absorption layer is combined with a wide bandgap avalanche layer such as InP and InAlAs. These wider bandgap materials exhibit good temperature stability when the avalanche region is small. For example, a 100 nm thick InAlAs APD gives C_{bd} of 2.5 mV/K compared to the 6 mV/K from an 130 nm thick InP APD [1]. More recently 100 nm thick $Al_{1-x}Ga_xAs_{0.56}Sb_{0.44}$ (x = 0 to 0.15) grown lattice matched to InP substrates exhibit even smaller C_{bd} values of 0.86-1.08 mV/K [2]. Therefore in this work we evaluate the temperature and temporal stability of thin 100 nm $Al_{0.85}Ga_{0.15}As_{0.56}Sb_{0.44}$ from room temperature to 80 °C.

The breakdown voltage increases linearly with temperature, exhibiting a C_{bd} = 1.60 mV/K. The avalanche gain reduces by 15% (compared to 52% for S-6045 commercial Si APD) when temperature is increased from 24 °C to 80 °C. Moreover the avalanche gain is also monitored over time when the APD is biased at again of $M = 10$. The fluctuations are within ± 0.7 % of the mean gain value at room temperature increasing to a maximum of ± 1.33 % of the mean gain value at 80 °C. The dark currents for the APDs before and after the gain measurement at high temperatures show no significant degradation.

In conclusion we demonstrated that $Al_{0.85}Ga_{0.15}As_{0.56}Sb_{0.44}$ exhibit smaller C_{bd} than InP and InAlAs. The gain reduction is smaller than that of a commercial Si APD. Our APDs also show high temporal stability at elevated temperature up to 80 °C.

Acknowledgements: S.A acknowledges the support of S. Dimler and M. Hobbs from the University of Sheffield for the LabVIEW programs. EPSRC National Epitaxy Facility at the University of Sheffield is acknowledged for wafer growth.

References: [1]L. J. J. Tan, D. S. G. Ong, J. S. Ng, C. H. Tan, S. K. Jones, Y. Qian, and J. P. R. David, "Temperature Dependence of Avalanche Breakdown in InP and InAlAs," IEEE J. Quantum Electron. 46(8), 1153–1157 (2010). [2]X. Zhou, C. H. Tan, S. Zhang, M. Moreno, S. Xie, S. Abdullah, and J. S. Ng, "Thin $Al_{1-x}Ga_xAs_{0.56}Sb_{0.44}$ Diodes with Extremely Weak Temperature Dependence of Avalanche Breakdown," R. Soc. Open Sci. 4(5), 170071 (2017).

Abstracts

Session 3: Posters

A18_06 Modelling of single-mode GaAs-based 1x2 MMI and Y-branch splitters

T. Albiladi*, D. Beggs, E. Le Boulbar Z. Li and P. M. Smowton. *AlbiladiTR@cardiff.ac.uk
School of Physics and Astronomy, Cardiff University, Queen's Building, The Parade, Cardiff, Wales, UK, CF24 3AA.

Generic photonic integration is the technology where a number of basic building blocks (BBBs), with fixed design rules, are integrated on a common planar substrate to generate multiple functionalities. To date much work has been done on substrate such as Buried Silicon Oxide (Box) but also on InP based substrates [1]. The basic building blocks (BBBs) can also be combined to build more complex optical components known as composite building blocks (CBBs) to create a library of blocks with certain functionality and known performance. This technology is preferable and reliable due to the reproducibility and yield that can be obtained from using a small number of well characterised features that still produces a vast range of possible functionality [1,2]. We are interested in the development of a GaAs based substrate and here focus on one of the key functionalities that must be achieved in such systems, that of the splitter, or when operated in reverse, the combiner. Here we describe the development and computational comparison of GaAs-based 1x2 MMI and Y-branch for this purpose.
Fig.1 shows the typical MMI and Y-branch we have modelled and in the work we will report the optimised design for a compromise of performance and manufacturability and also report that both MMIs and Y-branch have relative advantages in terms of performance, scalability, complexity and size.

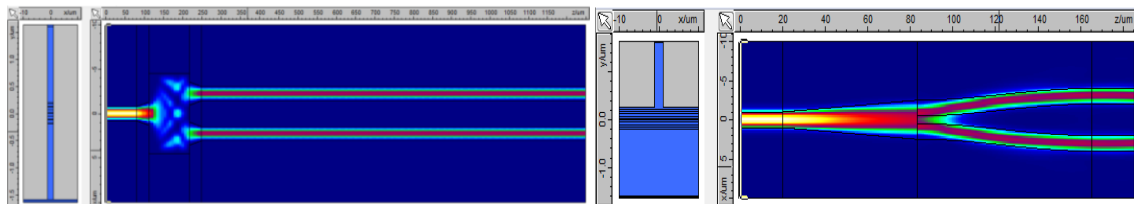

Fig. 1: deep-etched 1x2 MMI and shallow-etched Y-branch

References: [1]Smit, M. *et al.* (2014) ‘An introduction to InP-based generic integration technology’, *Semiconductor Science and Technology*. IOP Publishing, 29(8). doi: 10.1088/0268-1242/29/8/083001; [2]Lifante, G. es (2003) *Integrated Photonics: FUNDAMENTALS*. 1st edn. John Wiley & Sons Ltd.

A18_08 Optical properties of drug-resistant human osteosarcoma cells - the potential for microfluidic-based Lab-on-Chip analysis

Basmah Almagwashi[1], Marie Wiltshire[2], Rachel Errington[2], and Peter Smowton[1].
[1]School of Physics and Astronomy, Cardiff University, 5 The Parade, Cardiff, CF24 3AA, UK; [2]School of Medicine, Division of Cancer Genetics, Heath Park, Cardiff University, Cardiff, CF14 4XN, UK.

The ongoing research of Lab-on-chip (LOC) devices finds great potential in its medical applications, where minimal stress and simple set-ups are desired when handling the delicate biological samples. An integrated semiconductor microfluidic chip, where an optically active substrate containing lasers/detectors is integrated with a 3D microchannel, has recently been developed [1]. It can perform flow-cytometric measurements, such as cell counting and size-profiling, on a simple capillary-driven platform. Osteosarcoma is a bone cancer that often targets long bones of humans during their childhood or late adulthood, with a 10-year survival rate of about 55% (England, 2009-2013) [2], [3]. Challenges in the development of the drug treatment of osteosarcoma are observed due to the high heterogeneity associated with its cells [4]. When osteosarcoma cells (U-2 OS cells) are treated with ICRF-193, which inhibits the function of DNA Topoisomerase II, the cells become unable to divide during mitosis, consequently turning them into a polyploid phenotype [5]. Here we examine the forward and side scattering of these large cells, providing feedback on their viability and size based on the scatter properties and the granularity of their molecular content (DNA content and cell cycle position) using a range of standard commercial flow cytometers, with a view to understanding the potential of a semiconductor integrated microfluidic chip for analysis and incorporation of non-invasive sorting using on-chip techniques such as dielectrophoresis.

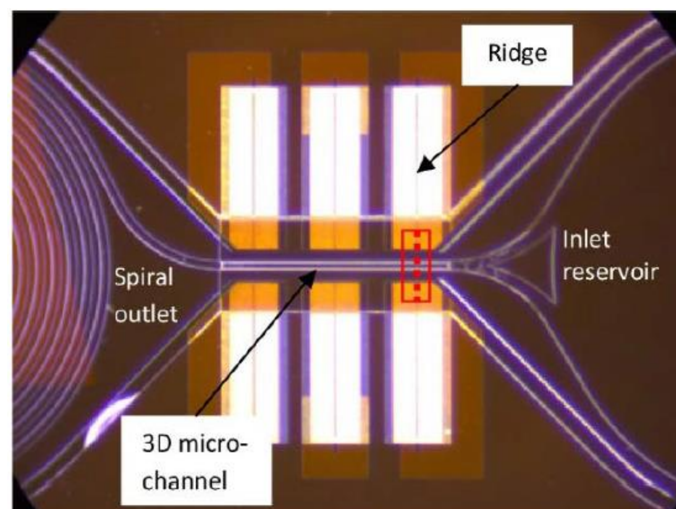

1-1: Top view of a semiconductor microfluidic chip, showing its main parts, from the right: the inlet, the main channel containing the lasers/detectors on the sides, and the outlet. Figure reproduced from [1].

References: [1] R. Thomas, A. Harrison, D. Barrow, and P. M. Smowton, 'Photonic integration platform with pump free microfluidics', Opt. Express, vol. 25, no. 20, p. 23634, Oct. 2017. [2] 'Bone sarcoma statistics', Cancer Research UK, 14-May-2015. [Online]. Available: http://www.cancerresearchuk.org/health-professional/cancer-statistics/statistics-by-cancer-type/bonesarcoma. [Accessed: 28-Jan-2018]. [3] Y.-H. Lin, B. E. Jewell, J. Gingold, L. Lu, R. Zhao, L. L. Wang, and D.-F. Lee, 'Osteosarcoma: Molecular Pathogenesis and iPSC Modeling', Trends Mol. Med., vol. 23, no. 8, pp. 737–755, Aug. 2017. [4] H. K. Brown, M. Tellez-Gabriel, and D. Heymann, 'Cancer stem cells in osteosarcoma', Cancer Lett., vol. 386, pp. 189–195, Feb. 2017. [5] P. J. Smith, N. Marquez, M. Wiltshire, S. Chappell, K. Njoh, L. Campbell, I. A. Khan, O. Silvestre, and R. J. Errington, 'Mitotic Bypass Via An Occult Cell Cycle Phase Following DNA Topoisomerase II Inhibition In p53 Functional Human Tumor Cells', Cell Cycle, vol. 6, no. 16, pp. 2071–2081, Aug. 2007.

A18_15 InP Nanowire Solar Cells with Carrier-Selective Layers

M. Fleet* and S. Mokkapati. *FleetMR@cardiff.ac.uk
School of Physics and Astronomy, North Queen's Building, Cardiff University, The Parade, Cardiff, UK, CF24 3AA.

InP nanowires show great potential for use in photovoltaic devices [1] [2] due to their light absorption and emission characteristics and low surface recombination velocity. Despite these advantages, the current efficiencies of InP nanowire solar cells remain below that of planar cells. This, in part, is due to the inability to fabricate well-defined, good quality p-n junctions as a means to separate and extract photo-generated charge carriers in nanowires. To alleviate this issue, I propose the use of carrier-selective layers and eliminate the need to make p-n homo-junctions in nanowires for photovoltaic applications.
'Carrier selective' layers are materials that have band offsets with the absorber (InP in our case) such that either electrons or holes are selectively transferred into the selective layer. The other charge carrier remains in the absorber material. **Figure 1** shows the schematic band offsets at InP-TiO_2 and InP-MoO_x interfaces. TiO_2 [3] and MoO_x act as electron and hole selective layers, respectively.

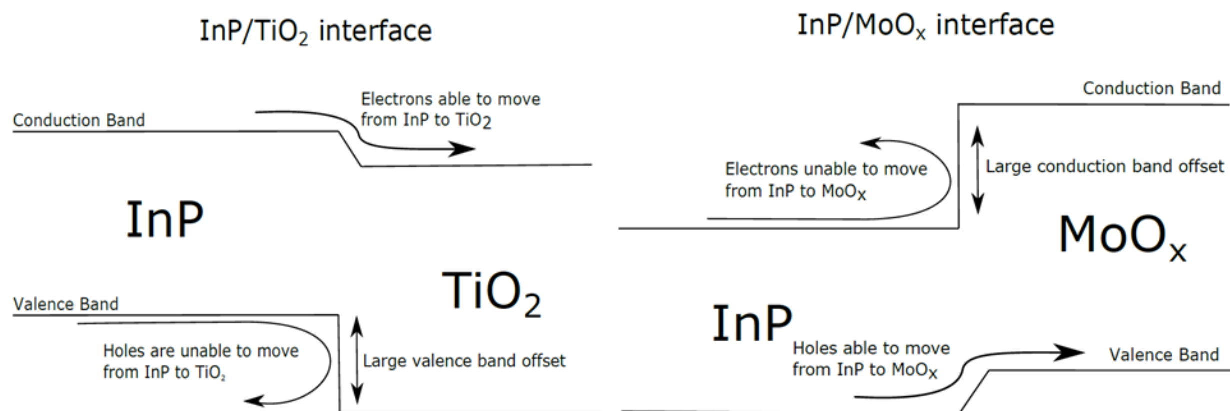

***Figure 1** Band structures of an electron-selective interface (InP/TiO2) and a hole-selective interface (InP/MoO_x)*

I aim to develop conformal deposition of TiO_2 and MoO_x on InP nanowires, and study the carrier dynamics of these structures for photovoltaic applications. Through the use of carrier-selective layers (rather than a conventional p-n junction), I aim to demonstrate high efficiency, thin, flexible nanowire solar cells. In the conference poster, I will present a comprehensive review of work done on carrier selective layers for inorganic solar cells, and present my initial results.

References: 1. Xu, Y., T. Gong, and J.N. Munday, *The generalized Shockley-Queisser limit for nanostructured solar cells.* Sci Rep, 2015. **5**: p. 13536; 2. Kayes, B.M., H.A. Atwater, and N.S. Lewis, *Comparison of the device physics principles of planar and radial p-n junction nanorod solar cells.* Journal of Applied Physics, 2005. **97**(11): p. 114302; 3. Xingtian Yin, C.B., Yongjing Lin, Kevin Chen, Mark Hettick, Maxwell Zheng, and D.K.a.A.J. Cheng-Ying Chen, *19.2% Efficient InP Heterojunction Solar Cell with Electron-Selective TiO2 Contact.* 2014.

A18_26 Computing Resonant Modes of PCSELs using the Transfer Matrix Method

G. Li, J. Sarma*, R. A. Hogg. *Visiting Researcher
School of Engineering, University of Glasgow, Glasgow, G12 8TL, UK.

Semiconductor lasers with the combination of characteristics such as large output power, single mode operation and good beam quality are very often desired. The photonic crystal surface emitting laser (PCSEL) has shown significant promise and has received much attention with the purpose of achieving devices with the desired characteristics [1]. The evaluation of the resonant modes of the structure is a primary requirement in modelling PCSELs. Plane Wave Expansion (PWE) [2], Finite Difference Time Domain (FDTD) [3], and Coupled Mode Theory (CMT) [4] have been widely used to analyse the pertinent 2-d PC structures. But these techniques are either computationally very time consuming or mathematically rather intensive. In this paper a different approach based on a Transfer-Matrix (TM) formulation applicable to piecewise constant media, in combination with a simple and fast numerical computation is used to establish the resonant modes in a rectangular geometry 2-d PC structure. The 2-d (x-z axes) PC is first considered as a piecewise-constant multilayer (say, along x but uniform along z) structure and the characteristic waves propagating along the z-axis with the corresponding wave indices are evaluated using the TM method. Then, discontinuities along the z-axis corresponding to the PC structure and the characteristic wave indices are introduced and the TM method is again used to finally obtain the resonances of the 2-d PC. This procedure provides good physical insight and is fast and well suited to efficiently incorporate the additional complexities of PCSEL modelling. Band edge (potentially lasing) resonator modes obtained by this method match extremely well with those derived by the PWE method, Fig. [1], for a large range of the filling-factor. The corresponding in-plane field distribution of band edge mode, Fig. [2], is also seen to match very satisfactorily with that obtained using the CMT [5]. The details of the method and further results will be presented at the conference.

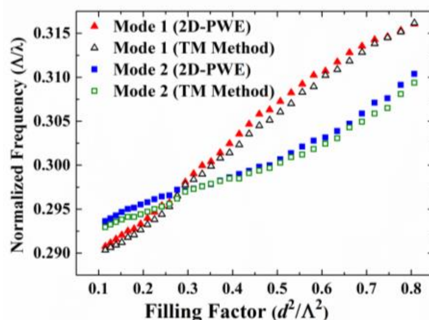

Fig 1. Band edge modes comparison of 2D-PWE and TM method where Λ is the periodicity of the structure

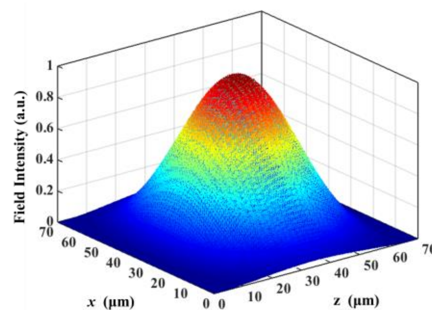

Fig 2. In-plane field distribution of band edge mode

References: [1] Hirose, Kazuyoshi. *et al.* Nature photonics 8, no. 5 (2014): 406-411; [2] Plihal, M., and A. A. Maradudin. Physical Review B 44, no. 16 (1991): 8565; [3] Ryu, Han-Youl, Masaya Notomi, and Yong-Hee Lee. Physical Review B 68, no. 4 (2003): 045209; [4] Sakai, Kyosuke, Eiji Miyai, and Susumu Noda. Applied Physics Letters 89, no. 2 (2006): 021101; [5] Liang, Y., *et al*. Optics Express, 20(14), pp.15945-15961.

A18_41 Multi-beam Laser Interference Patterning of Semiconductors

Y. R. Wang*, C. Y. Jin, and M. Hopkinson. *ywang224@sheffield.ac.uk
Department of Electronic and Electrical Engineering, University of Sheffield, Sheffield S3 7HQ, UK.

The development of new methods to pattern surfaces at the nanometer scale is of considerable importance for the future of semiconductor nanotechnology. Laser interference lithography is a cost-effective, high efficiency technique based on the interference of two or more coherent beams that can be used to create large-area periodic nanostructures on semiconductor materials1. The technique has been widely used to produce one-dimensional gratings and more recently has shown great potential for applications such as photonic crystals3 and as templates for nano optoelectronic devices4. Two-beam interference forms a parallel fringe pattern whilst multi-beam interference can form densely ordered distribution of holes or dots5. In our studies, we propose to apply four-beam laser interference in a semiconductor growth environment in order to use this as a template for production of a highly regular array of semiconductor nanostructures.
The pattern resulting from four-beam laser interference has been analysed by numerical simulations. We find the intensity distribution can be modulated by controlling the beam parameters, such as incident angle, azimuth angle and polarization direction. The results show the period of the interference pattern is inversely proportional to the incident angle, that polarization has a strong influence on the pattern symmetry/contrast and that the relative phase difference results in a shift of the pattern. An optimal dense pattern with a pitch of <200nm can be produced using an all TE polarized mode at equal large incident angles, with an incident laser wavelength at 355nm. We have also examined the thermal effect resulting from the laser-semiconductor interaction, since an understanding of the absorption of light and the resulting thermal profile is crucial for understanding the potential for in-situ nanopatterning. We have simulated the transient temperature distribution of a GaAs surface following pulsed laser irradiation using four-beam laser interference (355nm, 7ns pulses, 100mJ pulse energy). Based on the heat flow equation solved by the finite-difference time-domain method, we observe that the temperature of a GaAs surface rises rapidly after pulsed laser irradiation reaching 1200℃. A temperature difference of a few 100℃ exists between the maxima and minima which then slowly equilibrates over a timescale of ~100ns. The observed thermal transients
are expected to be compatible with surface diffusion and desorption processes which take place during semiconductor growth, providing us with a potential mechanism to create ordered nanostructures in-situ during the semiconductor growth process.

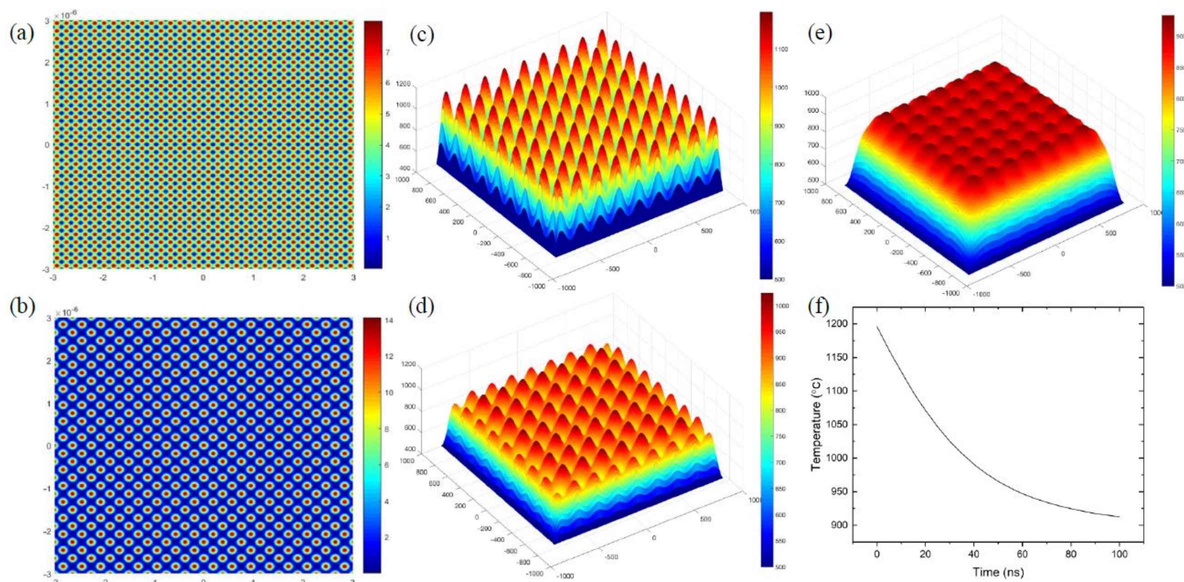

Fig. Simulated intensity distribution of four-beam interference (a) all TE polarization mode with incident angle θ = 70°; (b) all TM polarization mode with incident angle θ = 70°; Transient temperature distribution of GaAs at different time following pulsed laser irradiation (c) 0ns; (d) 30ns; (e) 70ns; (f) maximum surface temperature of GaAs versus time after pulsed laser irradiation.

Acknowledgements: Support from the EU H2020 program 'Nanostencil' and EPSRC is gratefully acknowledged.
References: [1] C. Lu, R. H. Lipson, Laser Photonics Review, 4, 568-580 (2010); [2] J. Zhang, Y. K. Verevkin and M. J. Mannini, DELILA Newsletter, 28, 3-14 (2007); [3] A. P. Zhang, R. Burzynski, Y. Yoon et al., Optics Letters, 33, 1303-1305 (2008); [4] A. Chen et al., Nanotechnology, 17, 3903–8 (2006); [5] Z. Wang, J. Zhang, Z. Ji et al., Proc. 3rd International Conference on Manufacturing Engineering, 929-936 (2008).

A18_30 Silicon mid-infrared photodetectors

M. A. Lourenço[1,2] and K. P. Homewood[1,2,3].
[1]Materials Research Institute and School of Physics and Astronomy, Queen Mary University of London, Mile End Road, E1 4NS London, UK; [2]Advanced Technology Institute, Faculty of Engineering and Physical Sciences, University of Surrey, Guildford, Surrey GU2 7XH, UK; [3]School of Materials Science & Engineering, Hubei University, Wuhan 430062, P. R. China.

We utilise a new technology - band edge modification (BEM) of rare earth (RE) optical transitions in silicon. BEM refutes previous asumptions on the interaction of REs with semiconductors and other hosts (M. A. Lourenço *et al*, Adv. Funct. Mater., 26, 1986-1994, 2016). This approach opens up a route to efficient, fully-silicon-based, optoelectronic devices across the near and mid-IR. Intrinsic RE transitions are internal to the RE and do not contribute directly to carrier conduction in the bands of the host. Consequently, this makes them of limited use for optical detectors. The band edge modified RE levels exampled here interact directly with the silicon bands and so offer the possibility of extrinsic photovoltaic or photoconductive detectors.
Silicon detectors and cameras currently completely dominate the UV, visible and very near-IR regions - however they do not work well beyond 1.1 μm, the silicon band gap. We have used ion implantation to introduce europium, ytterbium and cerium into silicon photodiodes, also formed by ion implantation. We show that BEM enables efficient silicon detectivity to be extended from 1.1 μm out to the mid-IR region. The responsivites and detectivities of these new silicon detectors offer a real challenge to existing detector materials and devices in the 2 to 6 μm range - currently dominated by more challenging, and expensive materials such as mercury cadmium telluride, indium antimonide and the arsenides. Replacing these materials with silicon would offer enormous benefits in cost, reliability and also integration with the silicon microelectronics for detection and imaging. An additional benefit is using much less toxic materials and production processes – a major concern with current technologies. Low leakage currents achievable in silicon based photodiodes mean that further development of this new mid-IR silicon technology could lead to thermoelectrically cooled or even room temperature detectors. Current commercial detectors in this area have to be cooled to liquid nitrogen temperatures (77 K) to achieve the performance needed for most applications. Higher operating temperature (HOT) detectors are an industry aim and, particularly if implemented in silicon, would be a major breakthrough.

Acknowledgements: We acknowledge the Royal Society UK for the award of the 2015 Brian Mercer Award for Innovation.

A18_12 Growth mechanisms in InAs/GaAs QDs with and without Bi surfactant

X. Y. Chen, Y. Gu*, Y. J. Ma, B. Du, J. Zhang, Y. H. Shi, W. Y. Ji, Y. G. Zhang. *ygu@mail.sim.ac.cn
State Key Laboratory of Functional Materials for Informatics, Shanghai Institute of Microsystem and Information Technology, Chinese Academy of Sciences, Shanghai 200050, China.

Self-assembled InAs quantum dots (QDs) on GaAs substrate were grown by gas source molecular beam epitaxy at different temperatures with and without exposure of bismuth (Bi) surfactant. Atomic force microscopy showed that the dot size and density were sensitive to Bi-surfactant exposure except for the growth temperature, as shown in Fig. 1. Compared with the growth without Bi exposure, the coalescence among InAs QDs was inhibited by the exposure of Bi surfactant in temperature ranges from 475 to 500 °C, leading to improved dot uniformity and a more stable InAs QD density. It was ascribed to the suppression effect of Bi surfactant on the strain-induced islanding through inhibit the indium adatom mobility on the surface kinetically during the InAs QD growth. By plotting the temperature-dependent photoluminescence (PL) integrated intensities and fitting the thermal activation energies of InAs QDs grown at 492 °C with and without Bi exposure, it was observed that the reduction of 3D island introduced more or less non-radiative recombination centers in InAs QDs though the Bi-surfactant exposure enhanced the PL intensity at growth temperature ranges from 475 to 492 °C. Nevertheless, it still showed some potential for applications of InAs QDs in nanoscale photonic and optoelectronic device areas by controlling the QD density and size using the Bi surfactant.

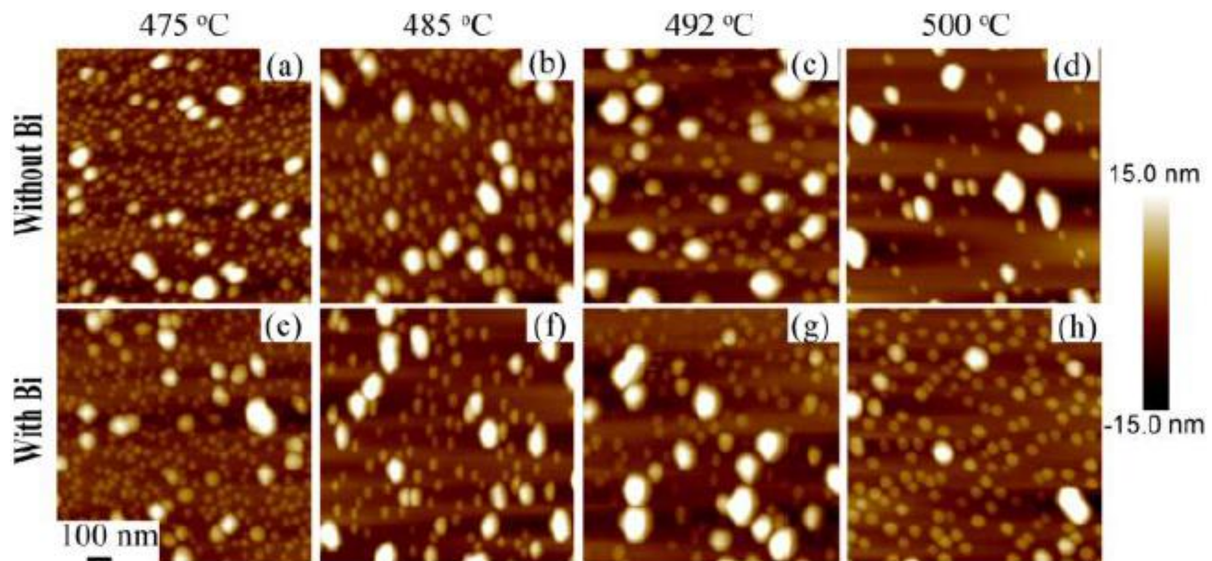

Fig. 1. AFM images of InAsQDsat different temperatures with and without Biexposure.

Abstracts

Session 4: Light Sources & Lasers I

A18_42 Simulation and Depth Profiling of Telecoms Vertical-Cavity Surface-Emitting Lasers Using Cross-Sections and X-Ray Photoelectron Spectroscopy

T. J. Wilson[1]*, P. D. Hodgson[1], A. J. Robson[1,2], J. Counsell[3] and M. Hayne[1,2]. *t.wilson6@lancaster.ac.uk

[1]Department of Physics, Lancaster University, Lancaster, LA1 4YB, UK; [2]Lancaster Material Analysis, Lancaster University, Lancaster, LA1 4YB, UK; [3]Kratos Analytical Ltd, Trafford Wharf Rd, Wharfside, Manchester, M17 1GP.

Vertical cavity surface emitting lasers (VCSELs) are taking an increasing share of the laser diode market, especially in the field of information transmission [1]. A key advantage of a VCSEL is that a full laser can be epitaxially-grown cheaply and efficiently in a single growth due to the distributed Bragg reflectors being lattice matched to the active region [2]. Whilst ubiquitous in datacoms, VSCELs have yet to significantly penetrate the telecoms market: the technological bottleneck being combining GaAs/$Al_xGa_{1-x}As$ distributed Bragg reflector (DBR) technology with an active region that emits at long wavelength.

We report a study of DBRs incorporated into a telecoms VCSEL [3]. Top-down reflectance is measured and also simulated using the transfer matrix method [4]. The VCSEL is grown using molecular-beam-epitaxy (MBE), cross-sectioned using beam-exit cross-sectional polishing, and imaged using scanning probe microscopy [5] to find the thicknesses of each layer in the device. Using these measurements, simulations of the actual and intended VCSEL structures are performed and compared with the measured top-down reflectance (Fig. 1). The simulation of the actual device is in good agreement with the measured reflectance at long wavelengths, while appearing to miss features at short wavelengths. This, and the disagreement in the cavity resonance, are believed to be due to the Al fractions in the many $Al_xGa_{1-x}As$ layers not being accurately known.

Further measurements are taken using x-ray photoelectron spectroscopy (XPS) to determine the aluminium mole fraction in the DBR layers and assess the technique's suitability for many-layer depth profiling. Aluminium percentage of the upper DBR $Al_xGa_{1-x}As$ layers is found to be 72 ± 2 % compared to the intended 60%. However, the XPS data does not currently cover the entire sample depth, and thus is not suitable for simulation. Further work is planned to expand upon these measurements as they show promising results

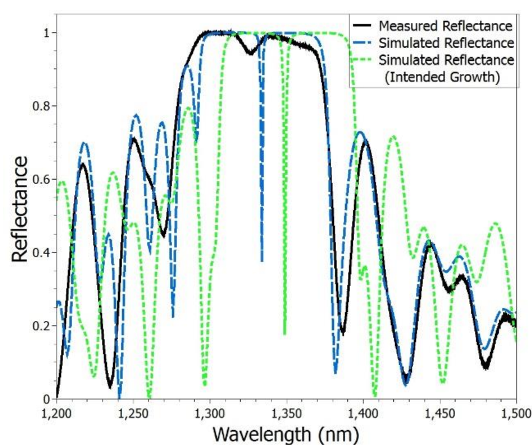

Fig. 1. Top-down reflectance vs. wavelength for a telecoms wavelength VCSEL showing measured reflectance (black), simulated reflectance from cross section results (dashed), and simulated from ideal growth (dotted)

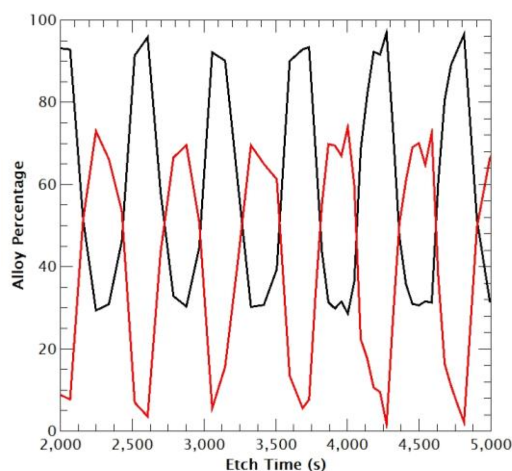

Fig. 2. A section of the upper DBR XPS depth profile showing the gallium alloy percentage (black) and the aluminium alloy percentage (red)

Acknowledgments: With thanks to Lancaster Material Analysis and Kratos Analytical, and supported by EPSRC and IQE plc.

References: [1] K. Iga, IEEE J Sel Top Quant Electron **6**, 1201 (2000); [2] M. Guden and J. Piprek, Model. Simul. Mater. Sci. Eng 4, 349 (1996); [3] P. Hodgson *et al.*, SIOE '17, Cardiff, 18th – 20th April 2017; [4] G. Burkhard, E. T. Hoke, and M. D. McGehee, Advanced Materials 22, 3293 (2010); [5] A. Robson *et al.*, ACS Applied Materials and Interfaces **5**, 3241 (2013).

A18_14 Effect of feedback phase on the stability of semiconductor nanolasers

Yuanlong Fan[1], K. Alan Shore[1], Pu Li[2,3] and Yanhua Hong[1].
[1]School of Electronic Engineering, Bangor University, Wales, LL57 1UT, United Kingdom; [2]Key Laboratory of Advanced Transducers & Intelligent Control System, Ministry of Education, Taiyuan University of Technology, Taiyuan, 030024, China; [3]Institute of Optoelectronic Engineering, College of Physics & Optoelectronics, Taiyuan University of Technology, Taiyuan, 030024, China.

In the past two decades, considerable progress in miniaturing lasers has been achieved along with the development of integrated photonic circuits and system-on-a-chip technologies where light sources are required. As part of that effort, considerable attention has been given to the design of semiconductor nanolasers (SNLs) [1] which offer ultra-small footprints and compatibility with existing photonic integrated circuits (PICs) platforms. For most applications it would be expected that SNLs can operate stably. However, as the complexity of PICs increases with the incorporation of a variety of optical components, such stable operation may be compromised due to unwanted external optical feedback (EOF) into the SNL from such PIC components.

Investigations of the stability of SNLs subject to optical feedback have been reported in [2]. However, [2] only considers cases of optical feedback where the feedback phase is fixed. In fact, the influence of feedback phase is of particular importance due to its laser-wavelength-scale sensitivity. For instance, a half-wavelength change of the external cavity length will lead to a phase change of 2π. Within such a change of phase, it has been seen in conventional semiconductor lasers that transitions between stable and unstable states can easily occur. However, in practice, it is challenging to maintain a fixed feedback phase even with use of precise phase control elements [3]. For SNLs which may be operated in photonic integrated circuits, it can be anticipated that the feedback phase will be difficult to control. Therefore, from a practical point of view, it is important to fully understand the effects of feedback phase in order that the SNL can be operated stably independently of the feedback phase.

Figure 1 shows the stability map of an SNL with respect to feedback coupling factor η and feedback phase $\phi 0$. The blue shaded region is the unstable region which is separated from the stable region by the stability limit (red in Fig. 1). From Fig. 1, it is seen that below some value of the feedback coupling factor a feedback-phase-independent stable SNL is obtained. We define this minimum feedback coupling factor as critical feedback coupling factor and denote it as ηc (shown as dashed line in Fig. 1).

Fig. 1: The stability map of an SNL when injection current is 3 *mA* and external cavity length is 15 *mm*.

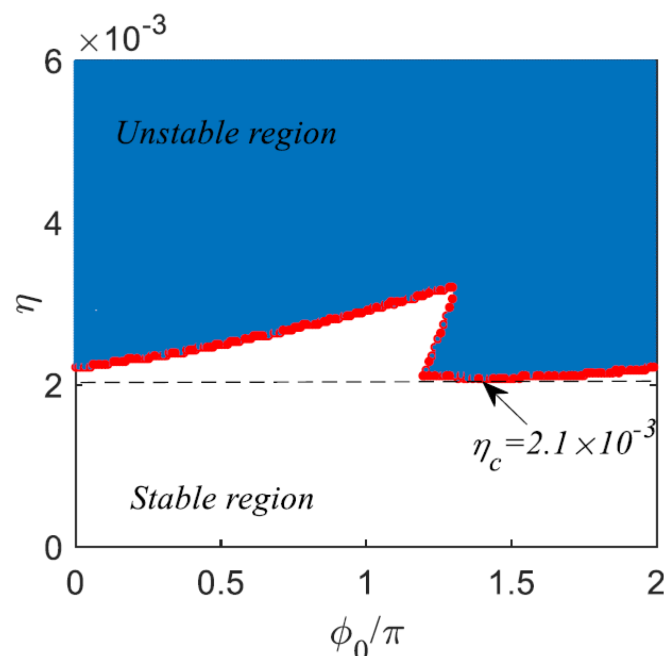

Further results will be offered to show that how ηc depends on the other two main system parameters, i.e., the injection current, and initial external cavity length, and hence to explore the opportunities for achieving stable operations of the SNL over a wider operating range.

Acknowledgement: Financial support provided by the United Kingdom Engineering and Physical Sciences Research Council (U.K. EPSRC Grant No. EP/P006027/1).

References: [1] Q. Gu and Y. Fainman, Semiconductor Nanolasers. Cambridge, U.K.: Cambridge University Press, 2017; [2] Z. A. Sattar and K. A. Shore, "External optical feedback effects in semiconductor nanolasers," IEEE J. Sel. Topics Quantum Electron., vol. 21, no. 6, pp. 1800106, Nov./Dec. 2015; [3] D. Lenstra, "Relaxation oscillation dynamics in semiconductor diode lasers with optical feedback," IEEE Photon. Technol. Lett., vol. 25, No. 6, pp. 591-593, Mar. 2013.

A18_05 Nanolaser optimization through statistical optoelectronic analysis

Juan Arturo Alanis1, Tim Burgess2, Mykhaylo Lysevych2, Dhruv Saxena2, Sudha Mokkapati3, Xiaoyan Tang1, Kun Peng2, Lan Fu2, Hark Hoe Tan2, Chennupati Jagadish2 and Patrick Parkinson1.*

**patrick.parkinson@manchester.ac.uk*
1The Photon Science Institute and School of Physics and Astronomy, University of Manchester, UK; 2Electronic Materials Engineering, The Australian National University, Canberra, Australia; 3School of Physics and Astronomy and Institute for Compound Semiconductors, Cardiff University, UK.

Due to their characteristic elongated shape and reflective end-facets, semiconductor nanowires can be used as Fabry-Perot resonators to fabricate nanolasers. As a way of studying the key elements for lasing operation in these devices, we have developed and successfully employed a large scale optical technique to study interwire functional inhomogeneity. Taking advantage of this novel method we are able to locate and optically study a large number of nanolasers by μ-Photoluminescence (Figure 1). Through a statistical comparison, different parameters such as nanowire length, material inhomogeneity, lasing wavelength etc. are correlated to identify which mechanisms contribute to low-power lasing. We discuss two applications of this approach; nanowires with multi-quantum-well GaAs/AlGaAs active region [1], and p-doped GaAs nanowires [2].

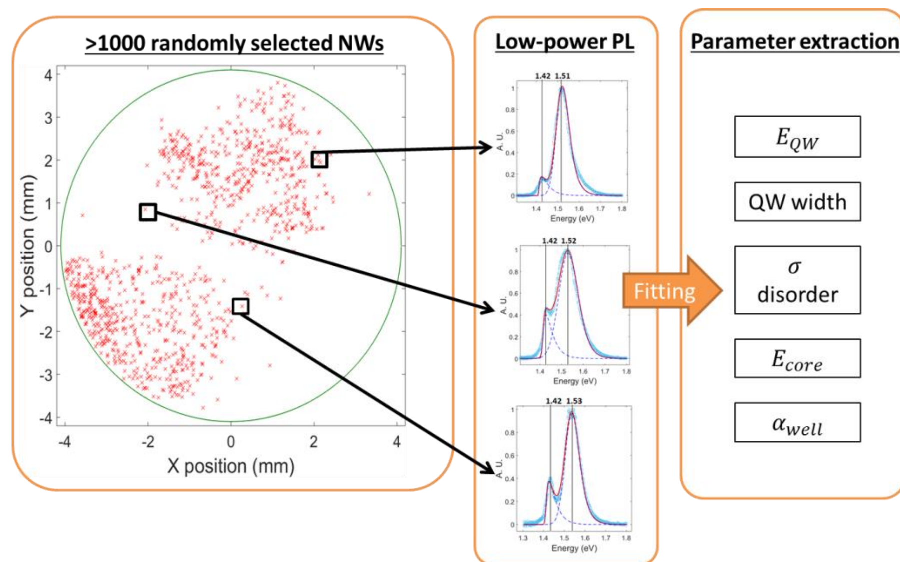

Figure 2. Large-scale spectroscopy performed on >1000 nanowires. From left to right: Scatter plot of nanowires found, three example PL spectra with their respective curve fitting and parameter extraction.

Both studies allowed us to assess the lasing yield of ~1000 nanowires and identify nanolasers operating at very low threshold. Through establishing the critical parameters, sub-populations can be simply identified with high room-temperature lasing yield (>80%). This approach is of industrial value, as well as providing identification of best operating nanolasers for the fabrication of devices for fundamental study.

References: [1] J. A. Alanis, D. Saxena, S. Mokkapati, N. Jiang, K. Peng, X. Tang, L. Fu, H. H. Tan, C. Jagadish, and P. Parkinson, *Nano Lett.*, vol. 17, no. 8, pp. 4860–4865, Jul. 2017; [2] T. Burgess, D. Saxena, S. Mokkapati, Z. Li, C. R. Hall, J. A. Davis, Y. Wang, L. M. Smith, L. Fu, P. Caroff, H. H. Tan, and C. Jagadish, *Nat. Commun.*, vol. 7, no. May, p. 11927, Jun. 2016.

A18_21 Linewidth Reduction of Photonic Microwave in Optically Injected VCSELs Using Optical Feedback

Songkun Ji[1], Chenpeng Xue[1,2], Angel Valle[4], Paul Spencer[1], Hongqiang Li[4] and Yanhua Hong[1].

[1]School of Electronic Engineering, Bangor University, Wales, LL57 1UT, UK; [2]School of Communication and Information Engineering, University of Electronic Science and Technology of China, Chengdu 611731, China; [3]Instituto de Física de Cantabria (CSIC-Univ. de Cantabria), Avda. Los Castros s/n, E39005 Santander, Spain; [4]Tianjin Key Laboratory of Optoelectronic Detection Technology and Systems, School of Electronics and Information Engineering, Tianjin Polytechnic University, Tianjin 300387, China.

The nonlinear dynamics of period-one (P1) in optically injected semiconductor lasers have attracted considerable research interests for their potential application in photonic microwave generation. Photonic microwave generation based on P1 oscillation offers many advantages, such as, widely tunable signal far from the lasers' original relaxation oscillation frequency, low cost due to all-optical configuration and nearly single sideband (SSB) spectrum. Photonic microwave generation based on P1 oscillation has been reported in DFB lasers, quantum dot lasers and vertical-cavity surface-emitting lasers (VCSELs). We have experimentally demonstrated a broad tunable microwave frequency utilizing P1 oscillation in a single-mode VCSEL in our previous work [1]. A drawback of photonic microwave generation based on P1 dynamics is the broad linewidth of a few MHz due to the fluctuations in the lasers, which affects its applications. In this paper, we exam whether optical feedback is an effective method to reduce the linewidth of the microwave generated in a single-mode VCSEL. We also experimentally and theoretically study the optical feedback phase effect on the linewidth reduction.

Fig. 1 show the power spectra the VCSEL exhibiting P1 dynamics. Fig. 1 (a) is for the configuration without optical feedback, the 3dB linewidth is measured to be 3.6 MHz. Fig. 1(b-d) show the power spectra of VCSEL with feedback. It is noted that the fundamental frequencies in Fig. 1(b-d) are about 1.5 GHz lower, which is because the injection parameters are different compared with those in Fig. 1(a). But the linewidth of the microwave under the same injection parameters as in Fig. 1(b-c), but without optical feedback, is similar to that in Fig.1(a). Fig. 1(b) is for single feedback with optimal feedback phase, we can see that the linewidth has reduced significantly to 0.453 MHz. If the second feedback is added, the linewidth is further decreased to 0.296 MHz. If we adjust the feedback phase of one feedback cavity, the linewidth starts to increase. In the worst case, it increases to 0.499 MHz. The results indicate that optical feedback can be used to reduce the linewidth of the microwave generated in a single-mode VCSEL. The linewidth reduction is also sensitive to the feedback phase.

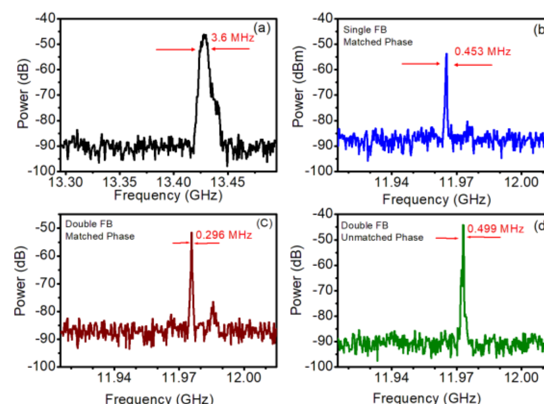

Figure 3 Power Spectra of the VCSEL

Reference: [1] S. Ji, Y. Hong, P. S. Spencer, J. Benedikt, and I. Davies, Opt. Express, vol. 25, no. 17, pp. 19863-19871, Aug. 2017.

A18_20 The effects of P-doping on 1.3µm quantum dot lasers grown on GaAs and Si substrates

L. Jarvis[1]*, S. Shutts[1], P. M. Smowton[1], M. Tang[2], J. Wu[2], and H. Liu[2]. *jarvislk@cardiff.ac.uk
[1]School of Physics and Astronomy, Cardiff University, The Parade, Cardiff, CF24 3AA; [2]Department of Electronic and Electrical Engineering, University College London, Torrington Place, WC1E 7JE.

The field of Silicon Photonics has attracted a lot of interest in recent years [1-2]. It aims to use light to process information at a rate which is much faster than that which is possible using conventional electronics. Quantum Dot lasers for use in Silicon Photonics have been grown directly on Si substrates and have excellent threshold performance, but to date only devices will relatively low cavity losses have been possible due to low gain. P-type modulation doping adds a number of holes close to the device's active region to counter inefficiencies brought about by valence band asymmetry and has been demonstrated to improve the available gain in Quantum Dot devices grown on GaAs [3].
This work examines 1.3µm InAs Quantum Dot lasers with varying levels of p-doping and cavity lengths grown on both GaAs and Si substrates to explore the potential of this approach for increasing the available gain. The lasers are made into ridge waveguide devices of 100µm width with a stripe of 50µm for those grown on GaAs and 100µm width with a stripe of 50µm for those grown on Si. To understand the resulting behaviour devices are mounted in a cryostat and characteristics recorded from 200 – 400K.

References: [1] R. Soref, *The Past, Present, and Future of Silicon Photonics*, IEEE Journal of Selected Topics in Quantum Electronics, vol. 12, no. 6, 2006; [2] A. Rickman, *The commercialization of silicon photonics,* Nature Photonics 8, 579–582, 2014; [3] P. M. Smowton and I. C. Sandall, *Gain in p-doped quantum dot lasers,* Journal of Applied Physics, 2007.

A18_07 **Resonant pulse amplification based on mode-locked semiconductor lasers**

M. A. Alloush[1*], R. H. Pilny[1], C. Brenner[1], A. Klehr[2], A. Knigge[2], G. Trankle[2], M. R. Hofmann[1].

*Mohammad.A.Alloush@rub.de

[1]Lehrstuhl fur Photonik und Terahertztechnologie, Ruhr-Universitat Bochum, Bochum, Germany; [2]Ferdinand-Braun-Institut, Leibniz Institut fur Hochstfrequenztechnik, Berlin, Germany.

Mode-locked semiconductor diode lasers are promising sources for ultrashort pulse generation. Due to the electrical pumping which allows for a compact design, they are cost-effective alternatives to traditional solid-state systems. However, due to the low peak power obtained from semiconductor lasers, a subsequent amplification is typically required to make them attractive for applications such as, material processing[1] and two-photon microscopy.[2] For standard solid-state femtosecond lasers as, e.g. Ti:Sapphire lasers, typically regenerative amplifiers are utilized to amplify the ultrashort pulses.[3] However, they have some drawbacks concerning the necessity for using Pockels cells and polarizers which are needed to inject and extract pulses. As an alternative, we present a ring semiconductor amplifier system which is seeded by ultrashort pulses for resonant amplification. We built an external cavity diode laser geometry to generate ultrashort pulses based on a hybrid mode-locking regime since the generated pulses are found to be less sensitive to vibration and temperature influences. A monolithic multi-segment diode laser is used as a light source in the operating oscillator. We operate
the oscillator at a fundamental repetition-rate (RR) of 206 MHz and it can also be driven on various harmonics of this frequency. The generated pulses are seeding a tapered amplifier (TA) inside a ring cavity. The amplified pulses are coupled back towards the TA forming a resonant setup as depicted in Fig 1(a). By matching the cavity lengths of the oscillator and ring resonator, we can obtain resonant amplified pulses. The spectrum of the amplified pulses is investigated for different pumping parameters of the TA using an optical spectrum analyzer. Furthermore, the system is characterized for the optimum seeding parameters by observing the output signal with an autocorrelator. We found that the best performance is obtained when the amplifier is seeded by pulses at the second harmonic
of the fundamental RR (412 MHz). We blocked the seeding pulses to operate the amplifier in CW regime and compared the obtained spectra for CW and amplified pulses as shown in Fig 1(b). Consequently, we ensure that most of the power is contained in the pulses upon pulsed operation. Additionally, we analyzed the single-pass amplification when the TA is seeded by the second harmonic. We obtained higher average output power from the additive amplification than from the single-pass with an approximate ratio of 5/1. In future, we will modulate the TA in order to suppress the CW signal. Thus, we ensure that most of the carriers in the TA are depleted by the injected pulses and as a result, higher peak power can be obtained.

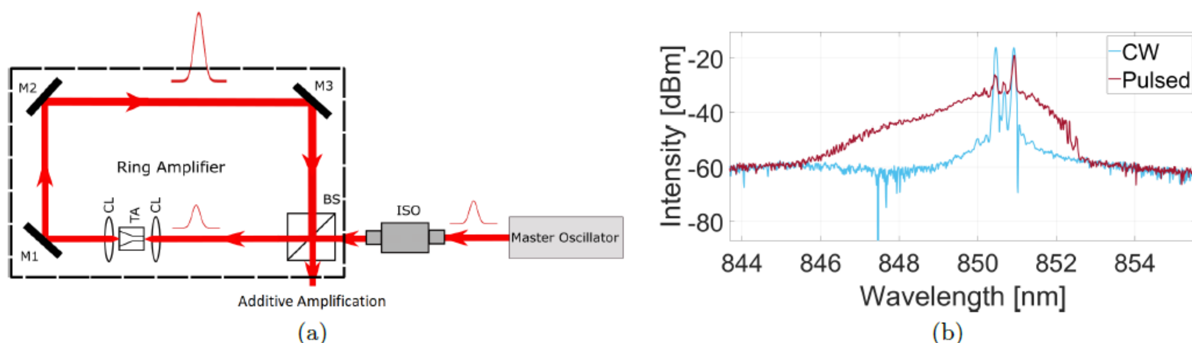

Figure 1. (a) Schematic illustration of the experimental setup. (b) Amplified Pulses and CW Spectra.

References: [1] Liu, X., Du, D., and Mourou, G., "Laser ablation and micromachining with ultrashort laser pulses," IEEE, Journal of Quantum Electronics 33(10), 1706-1716 (1997); [2] Kawakami, R., Sawada, K., Sato, A., Hibi, T., Kozawa, Y., Sato, S., Yokoyama, H., and Nemoto, T., "Visualizing hippocampal neurons with in vivo two-photon microscopy using a 1030 nm picosecond pulse laser," Scientific Reports vol. 3, pp. 1-7 (2013); [3] Wynne, K., Reid, G. D., and Hochstrasser, R. M., "Regenerative amplification of 30-fs pulses in ti: sapphire at 5 khz," Optics letters 19(12), 895-897 (1994).

A18_04 Semiconductor Quantum Well Lasers with a Temperature Insensitive Threshold Current

A. R. Adams[1]*, I. P. Marko[1], J. Mukherjee[1], S. J. Sweeney[1], A. Gocalinska[2], E. Pelucchi[2] and B. Corbett[2].

**alf.adams@surrey.ac.uk*

[1]Advanced Technology Institute and Department of Physics, University of Surrey, Guildford GU2 7XH, UK; [2]Tyndall National Inst., University of Cork, Lee Maltings, Dyke Parade, Cork, Ireland.

Quantum well lasers have been extremely successful in a wide range of applications, with optical fibre communications being of particular importance. However, in spite of their success, their performance is not ideal, for example, the threshold current of semiconductor lasers is often very sensitive to temperature. This has led to the need for thermoelectric coolers and associated control electronics to stabilize the laser temperature, however, such coolers often consume more energy than the laser they are controlling and also add to the overall heat dissipation of the system. Such coolers also tend to have far less long-term reliability than the laser diode itself. There are consequently many circumstances where it would be advantageous and far cheaper to simply compensate for temperature variations by mechanisms built into the epitaxial structure of the laser chip itself. This paper focuses on a new design and demonstration of a MQW laser structure which can overcome the intrinsic temperature sensitivity of the laser.

There are several mechanisms that may cause the threshold current (I_{th}) of semiconductor lasers to increase rapidly with increasing temperature, T. These include thermal broadening of the gain spectrum, thermally activated carrier escape, Auger recombination and inter-valence band absorption. Normally all of these processes act together to cause I_{th} to increase as T increases. However, here we present a novel design of quantum well active region [1] such that carriers released from some of the wells are fed to the other wells in such a way that these mechanisms compensate rather than augment one another.

The idea is in principle applicable to a range of materials systems, structures and operating wavelengths. However, we chose to demonstrate the effect for the first time in 1.5µm GaInAsP/InP edge emitting lasers, since these have been so extensively characterised and their parameters are relatively well known [2].

The devices were grown by MOVPE with seven 6nm wide InGaAsP quantum wells designed using computer simulation. The compressive strain in the wells was compensated overall by tensile strain in the barriers. Devices were fabricated with 50µm and 80µm wide stripe contacts so that any temperature dependent current spreading was negligible. One millimetre long devices were produced with as-cleaved facets.

The results are shown in Fig 1. Sample "A" was the first to be grown and as can be seen, it displayed a constant threshold current over a range of approximately 70K but centred at low temperature (80K~ 150K). The device lased at 1.63µm at room temperature and analysis of the emission spectra and TEM of the structure showed that the growth was far from the design.

However, the fact that a region of constant I_{th} existed indicated that the concept was a robust one. Sample "B" was the second to be grown and as can be seen the flat I_{th} region was successfully moved from low temperature and now spanned from approximately 140K to 270K. This device lased at 1.47µm at room temperature indicating that the structure was still not exactly as designed. However, the changes made between sample "A" and sample "B" were well within the limits of the variations available and therefore provides confidence that further iterations would make it possible to produce a device able to work at, for example, 1.55 µm and with a constant I_{th} at room temperature and above. This work is in progress and will be presented at the conference.

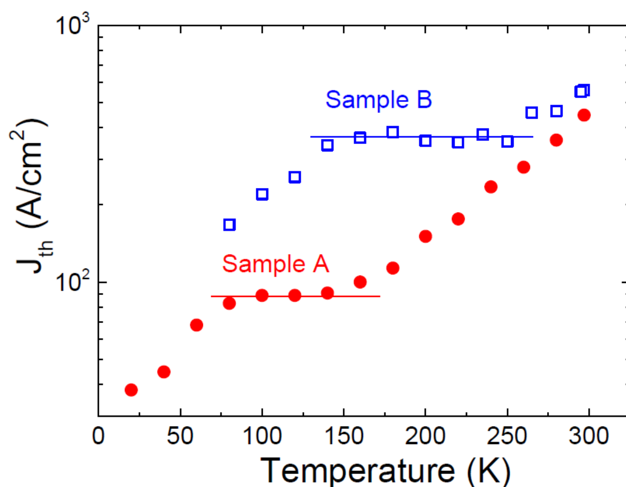

This generic design approach, which will be presented in more detail in the talk, is equally applicable to 1.3µm lasers as well as shorter wavelengths and to Mid IR devices in both edge-emitting and vertical cavity geometries.

Fig. 1. Temperature dependence of threshold current density in two InGaAsP/InP laser structures grown according to a simulated design with predicted temperature insensitive behaviour.

Acknowledgements: The authors wish to thank Dr V Stolojan for TEM studies of these structures. **References:** [1] A. R. Adams, International Patent Application WO2012/153136 (2012); [2] A. F. Phillips, S. J. Sweeney, A. R. Adams, P. J. A. Thijs, "The Temperature Dependence of 1.3- and 1.5-µm Compressively Strained InGaAs(P) MQW Semiconductor Lasers", IEEE J. Select. Topics Quant. Electr., 5, iss.3, 401 (1999).

A18_13 Effects of Auger Recombination on the Temperature and Wavelength Dependence of Type I Mid Infrared Lasers

Timothy Eales[1], Igor P. Marko[1], Barnabas A. Ikyo[1], Alf R. Adams[1], Shamsul Arafin[2], Stephan Sprengel[2], M.-C. Amann[2], Leon Shterengas[3], and Stephen J. Sweeney[1]*. *s.sweeney@surrey.ac.uk
[1]Advanced Technology Institute, University of Surrey, Guildford GU2 7XH, United Kingdom; [2]Walter Schottky Institut, Technische Universität München, Am Coulombwall 3, 85748 Garching, Germany; [3]Department of Electrical and Computer Engineering, State University of New York at Stony Brook, New York 11794, USA.

The development of lasers operating between 2-3 µm is motivated by a diversity of applications which include compact IR spectroscopy, communications and micro-surgery. The Type-I GaSb-based QW laser is the most competitive laser system in the 2-3 µm range [1]. However, the performance of type-I devices deteriorates rapidly with increasing wavelength and temperature. This operational instability is typically attributed to the non-radiative Auger recombination and carrier leakage. In this work we use temperature dependent characterisation and hydrostatic pressure techniques to investigate the efficiency limiting mechanisms in type-I GaSb lasers [2].

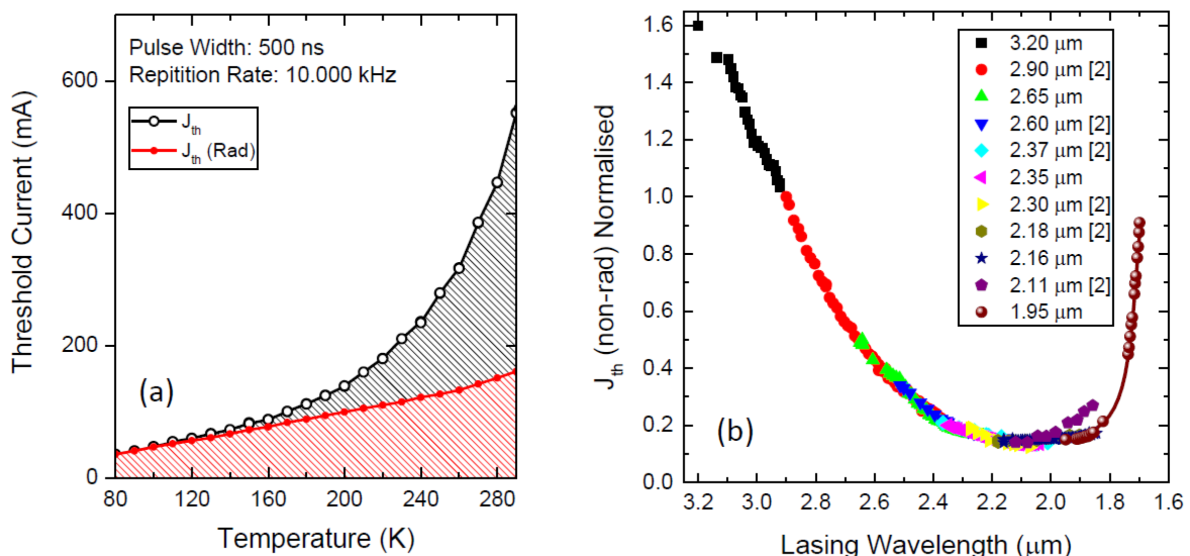

Figure 1: *a) the temperature dependence of the radiative and non-radiative components of the threshold current. b) the normalised wavelength dependence of the non-radiative threshold current.*

Temperature dependent measurements of the threshold current and spontaneous emission reveal a transitional behaviour. At low temperatures radiative recombination dominates the threshold current. Beyond a certain *break point* temperature, the non-radiative component of threshold diverges rapidly from the radiative component, accounting for the majority of threshold at room temperature [3]. To investigate the nature of the non-radiative pathways we use high hydrostatic pressure to reversibly vary the bandgap. Normalising the hydrostatic pressure data for multiple wavelength devices we show that between 1.7-3.2 µm two different Auger mechanisms operate in this wavelength regime and are the dominant recombination channels at room temperature, which will be discussed in the presentation in more detail.

References: [1] S. D. Sifferman, et al. IEEE J. Sel. Top. Quantum Electron., vol. 21, no. 6, 2015; [2] T. D. Eales, et al. IEEE J. Sel. Top. Quantum Electron., vol. 23, no. 6, 2017; [3] S. J. Sweeney, et al. IEEE Photonics Technol. Lett., vol. 10, no. 8, pp. 1076–1078, 1998.

Abstracts

Session 5: Light Sources & Lasers II

A18_33 Terahertz Generation in Nonlinear Gain Coupled Distributed Feedback Mid-Infrared Quantum Cascade Lasers

W. Oberhausen*, F. Demmerle, D. Burghart, A. Wolf, G. Boehm, H. Schmeiduch, M. C. Amann.
*wolfhard.oberhausen@wsi.tum.de
Walter Schottky Institut, Technische Universitaet Muenchen, 85748 Garching, Germany.

We present a nonlinear distributed feedback quantum cascade laser using gain coupling. The device operates at room temperature in pulsed mode. It uses a buried, doped grating layer to select two specific mid-infrared wavelengths, which are then converted to the desired THz radiation using the integrated nonlinearity. A promising approach for room temperature generation of THz radiation [1] is the use of mid-infrared (MIR) quantum cascade lasers (QCLs) with a built-in second order nonlinearity. In these devices, two simultaneously lasing MIR modes are converted to the desired THz radiation through difference frequency generation (DFG), meaning that the frequency of the emitted THz radiation is determined by the frequency spacing of the two MIR pump wavelengths. Using a gain coupled distributed feedback (DFB) grating for the selection of the MIR modes allows for simultaneous control of the THz emission frequency and the position of the MIR standing wave patterns in the cavity. This in turn can be used for surface emission of the THz radiation using an additional surface grating structure for THz extraction. Considering possible benefits of surface emission [2] compared to the Cherenkov phase matching (CPM) emission scheme [3] present a unique opportunity to improve device performance. The distributed feedback (DFB) grating is realized as two layer, higher order, buried, silicon doped GaInAs structure. Choosing both MIR pumps to be two adjacent grating orders ensures that there are no additional modes in the intermediate wavelength range, where the gain peak of the active region is located. The use of a higher order grating leads to a reduction in grating coupling strength and consequently the necessity of a high refractive index step to compensate this effect. Therefore, the first grating layer, closest to the active region, is highly doped with a carrier density of N = 5.5 · 1018 cm−3 and a thickness of 40 nm. This, in turn, significantly lowers the real part of the refractive index of GaInAs in the MIR wavelength range leading to index coupling. Therefore, a second 260 nm thick, undoped GaInAs layer is used to match the real part of the refractive index of the two-layer system to the surrounding InP wavecladding, preventing indexcoupling effects of the grating.

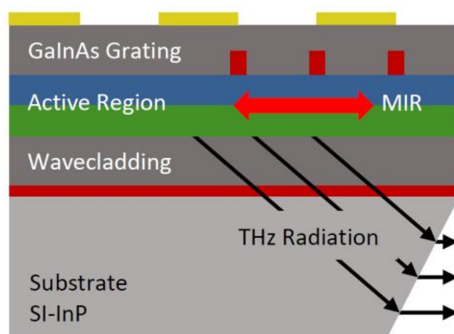

Fig. 1: Schematic of the device, illustrating the position of the DFB grating, MIR oscillation and the THz extraction path

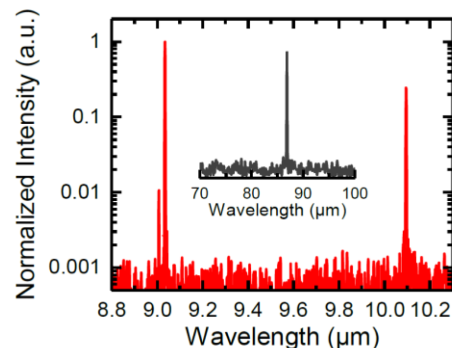

Fig. 2: Mid-infrared spectrum produced by the gain coupled device and its emitted THz spectrum (inset).

A basic schematic of the device is shown in Figure 1. The device was grown on semi-insulating InP, starting with a current extraction Layer and an InP wavecladding, followed by two stacks of the different active region designs described in [3]. On top of the active region the 300 nm thick, lattice matched, partially doped GaInAs layer is grown for the production of the grating. This layer is then structured into 370 nm broad stripes, using ebeam lithography and dry etching and subsequently overgrown with the upper InP wavecladding using MOCVD. After further processing, the substrate at the front facet was polished in order to also allow THz emission using the CPM scheme. 4. Results Figure 2 shows the spectral characterization of a gain-coupled device. The measurements were performed at room temperature in pulsed mode. The devices emitted on the designed wavelengths and their difference frequency at 3.5 THz. The additional mode in the MIR spectrum at 9.0 µm can be attributed to a higher order lateral mode. The spectra obtained through surface and top emission show the same emission wavelengths.

We have reported gain coupled nonlinear THz QCLs emitting on two MIR frequencies and their difference frequency in the THz range. A gain coupled DFB grating is used to select two MIR wavelengths and define the positions of their standing wave patterns in the laser cavity, enabling top emission through an additional surface grating 6. Acknowledgements This research was supported by the German Excellence Initiative via the Nanosystems Initiative Munich (NIM).

References: [1] M .A. Belkin, F. Capasso, A. Belyanin, D. L. Sivco, A. Y. Cho, D. C. Oakley, C. J. Vineis, G. W. Turner, Nat. Photonics 1, 288 (2007) [2] C. Pflügl, M. A. Belkin, Q. J. Wang, M. Geiser, A. Belyanin, M Fischer, A. Wittmann, J. Faist, F. Capasso, Appl. Phys. Lett. 93, 161110 (2008) [3] K. Vijayraghavan, Y. Jiang, M. Jang, A. Jiang, K. Choutagunta, A. Vizbaras, F. Demmerle, G. Boehm, M. C. Amann, M. A. Belkin, Nat. Commun. 4, 2021 (1013).

A18_10 Theory of strain-balanced In(N)AsSb/AlInAs metamorphic quantum wells for mid-infrared applications

Reza Arkani[1, 2], Christopher A. Broderick[1, 2], Eva Repiso[3], Peter J. Carrington[4], Anthony Krier[3], and Eoin P. O'Reilly[1, 2].

[1]Tyndall National Institute, Lee Maltings, Dyke Parade, Cork, T12 R5CP, Ireland; [2]Department of Physics, University College Cork, Cork, T12 YN60, Ireland; [3]Department of Physics, Lancaster University, Lancaster, LA1 4YB, United Kingdom; [4]Department of Engineering, Lancaster University, Lancaster, LA1 4YW, United Kingdom.

The growth of InAsSb quantum well (QW) structures offers the ability to achieve mid-infrared emission on an InAs substrate [1, 2]. However, there are two limitations associated with growth of InAsSb on InAs. Firstly, the presence of type-II band alignment, leads to electrons (holes) being confined in the InAs (InAsSb) layers of the structure. Secondly, the compressive strain in the InAsSb layers limits the InAsSb QW thickness and also the number of InAsSb QWs that can be grown without structural degradation.
Both issues can be overcome by growing on metamorphic buffer layers, and by introducing tensile strained InAlAs barrier layers. Such structures exhibit type-I band alignment, with large band offsets providing good carrier confinement and high optical efficiency. Furthermore, the ability to incorporate tensile strain in the AlInAs barrier layers allows for compensation of the compressive strain in the InAsSb QW layers, making it possible to achieve multi-QWs having high structural quality. In this work, we report on theoretical calculations and experimental measurements of the electronic and optical properties of such structures.
Figure 1 shows a comparison between theoretical calculations and photoluminescence (PL) measurements undertaken at low and room temperature on a series of $InAs_{1-x}Sb_x$/AlInAs QW structures grown on a relaxed $Al_{0.125}In_{0.875}As$ metamorphic buffer layer, using a GaAs substrate. In Figs. 1(a) and 1(b) we note a redshift of the measured PL peak wavelength with increasing Sb composition x, as well as an increase in the measured room temperature PL intensity. These trends are well described by the theoretical calculations shown in Figs. 1(c) and 1(d). These indicate that the measured enhancement of the room temperature PL intensity is associated primarily with the reduction of the QW valence band edge density of states, due to the increase in the compressive strain with increasing x.
Finally, we undertake a systematic theoretical analysis of metamorphic InAsSb/AlInAs QWs, identifying combinations of layer thicknesses and Sb to Al composition ratios which deliver both strain-balancing and 3.3 µm emission at room temperature. We identify and quantify the main trends in the electronic and optical properties, and on this basis propose optimised structures for the development of mid-infrared light-emitting diodes. We also briefly discuss the ability to achieve emission up to and beyond 4 µm using dilute nitride In(N)AsSb/AlInAs structures, where nitrogen incorporation allows for control over the QW strain and emission wavelength, opening up further opportunities for band structure engineering to deliver high-performance mid-infrared light emitters.

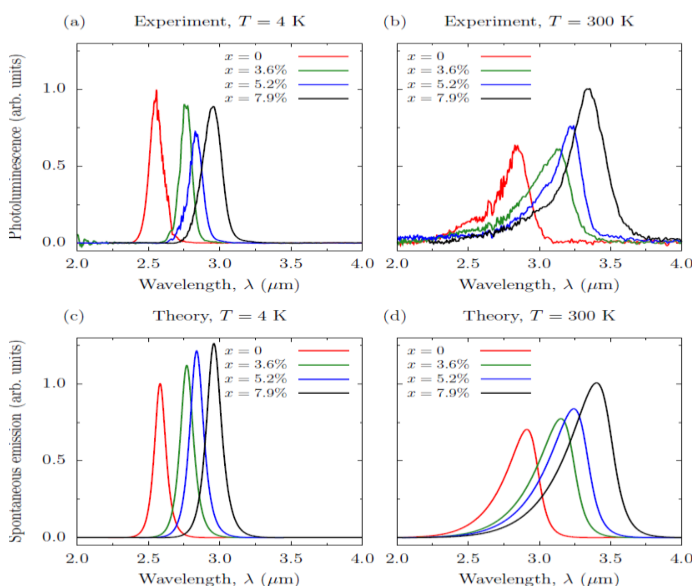

Figure 1. (a) and (b) show the measured low and room temperature photoluminescence (PL) spectra for a series of metamorphic $InAs_{1-x}Sb_x/Al_{0.125}In_{0.875}As$ QWs having Sb compositions x = 0, 3.6, 5.2 and 7.9% (denoted using red, green, blue and black lines, respectively). (c) and (d) show corresponding calculated spontaneous emission (SE) spectra for the same set of QWs, assuming an injected carrier density of 10^{15} cm^{-3}. In each case the measured PL and calculated SE spectra have been normalised to the intensity of the structure having the highest measured PL intensity at that temperature.

Acknowledgements: This work is supported by the European Commission (H2020 Marie Sklodowska-Curie Innovative Training Network "PROMIS"; project no. 641899), and by Science Foundation Ireland (SFI; project no. 15/IA/3082).

References: [1] A. Wilk et al., *Appl. Phys. Lett.* **77**, 2298 (2000); [2] P. J. Carrington et al., *Semicond. Sci. Technol.* **24**, 075001 (2009)

A18_09 Mid infrared (3-5 μm) InAsSb resonant cavity light emitting diode (RCLED)

F.A. Al-Saymari*, A.P. Craig, Y. J. Noori, Q. Lu, A.R.J. Marshall & A. Krier. *f.al-saymari@lancaster.ac.uk
Department of Physics, Lancaster University, United Kingdom.

The mid-infrared spectral range between 3-5 μm contains the fundamental absorption bands of greenhouse gases within the atmosphere, including CO and CO2. For this reason, a lot of research interest has been devoted to the realization of efficient room temperature semiconductor light emitting diodes (LEDs) and photodetectors. Enhancing the light emission from LEDs using a resonant cavity LED has been demonstrated previously by Schubert et al. [1], and has also been shown to be capable of enhancing light emission in the mid-infrared wavelength range for III-V semiconductor light emitters [2]. The device consists of a λ long cavity that contains a bulk InAsSb active region sandwiched between a bottom thirteen period Bragg mirror and a similar top five period mirror of AlGaAsSb/GaSb. The Bragg mirrors play a key role in increasing the spontaneous emission rate of the active region to levels that exceed commercially developed LED emitters within the aforementioned spectral range. Initially, the RCLED structure was designed and simulated using the transfer matrix and finite difference time domain methods. The RCLED was then realised using the molecular beam epitaxy (MBE) growth technique on a GaSb substrate and fabricated using conventional photolithography and wet etching. We report on the electroluminescence emission spectra over the temperature range 10-300 K as shown in Fig. 1. Interpretation of the resulting spectra revealed the existence of one acceptor level with an activation energy of 66 meV. Power dependence measurements were also performed at 300 K to study the characteristics of the device and its applicability as illustrated in Fig. 2. The ratio between the measured EL spectra from the RCLED and a standard non-resonant LED shows an EL enhancement factor of 10x and 100x at room and cryogenic temperatures (20 K) respectively. The difference in enhancement factors between room and cryogenic temperatures in our case is primarily related to the different spectral width at different temperatures and partially due to the shift of the emitter wavelength away from the cavity mode.

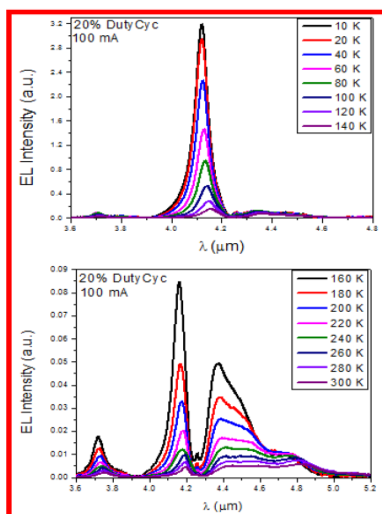

Fig. 1 The temperature dependence of EL emission from the InAsSb RCLED.

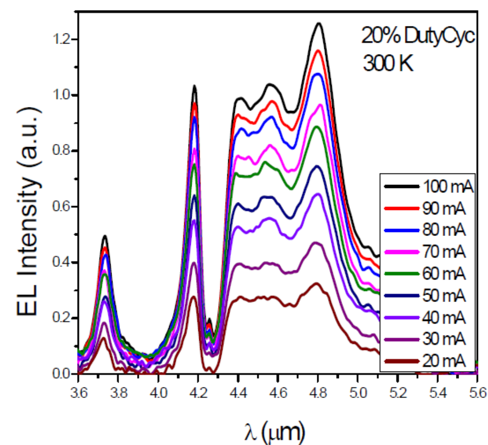

Fig. 2 The EL emission of the RCLED measured at different injection current (T=300 K).

Acknowledgments: We are grateful the Ministry of Higher Education, Iraq for providing a studentship for F.A. Al-Saymari.
References: [1] Schubert E. F., et al., "Resonant cavity light emitting diode", Appl. Phys. Lett. 60, 921 (1992). [2] Green A. M., et al., "Resonant-cavity-enhanced photodetectors and LEDs in the mid-infrared", Physica E 20, 531 (2003).

A18_18 Tamm plasmons and confined Tamm plasmons coupled to telecom wavelengths quantum dots

Edmund Harbord[1], Matthew Parker[2], Petros Androsanvitaneas[1], Andrew Young[1], Edmund Clarke[3], John Rarity[1], Ruth Oulton[1,2].

[1]Department of Electrical and Electronic Engineering, University of Bristol, Merchant Venturers Building, Woodland Road, Bristol, BS8 1UB, UK; [2]HH Wills Physics Laboratory, University of Bristol, Tyndall Avenue, Bristol, BS8 1TL, UK; [3]EPSRC National Centre for III-V Technologies, University of Sheffield, Mappin Street, Sheffield, S1 3JD, UK.

Quantum dots (QDs) – semiconductor nanostructures confined in all 3 dimensions – are attractive not only as single photons sources (SPS) but also as a gain medium for lasers. They possess close-to-unity internal quantum efficiency. However, practical applications require photonic structures to produce a high external quantum efficiency, and to shape the optical mode of the emitting light. We investigate the Tamm plasmon structure, in which light is confined vertically between a distributed Bragg reflector (DBR) and a thin metallic layer. By patterning the metal on the surface, it is possible to confine the light laterally, forming a confined Tamm plasmon (CTP). This is an ideal way of creating a confined optical state without etching into the semiconductor and forming surface states at the processed interfaces.
Our previous work [1] presented a design for telecom wavelength Tamm plasmons to couple to quantum dots. Here, we have realised these designs and measured Tamm plasmon structures coupling high areal density (2 x 10^{10} cm^{-2}) QDs that emit in the O band at room temperature. We have demonstrated Tamm plasmon emission from the coupled QD, with a 6-fold enhancement of the emission intensity. By using e-beam lithography and evaporative deposition, we also deposit size controlled disks to confine the light laterally. By Fourier microscopy of the emission, we obtain evidence for confinement of the optical mode. These results pave the way for using Tamm plasmons and QDs for telecom wavelength lasers and SPS.

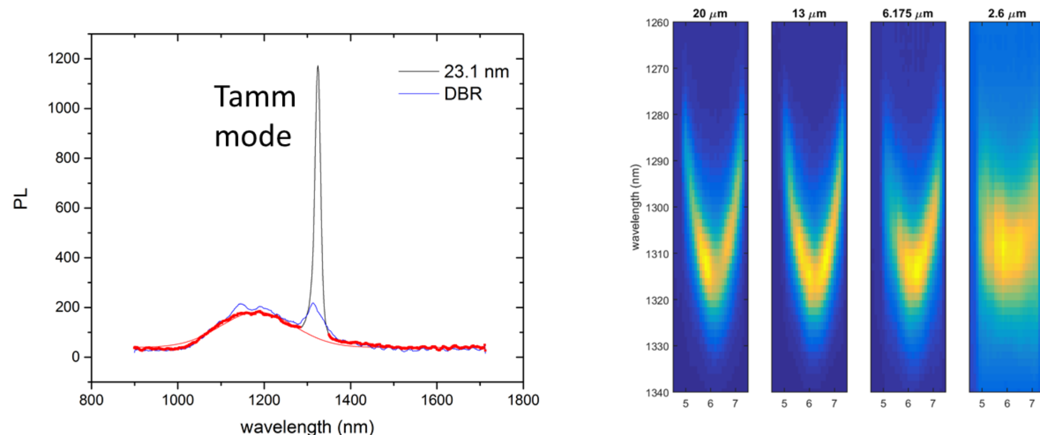

Figure: (Left) The photoluminescence spectrum of QDs in a DBR (blue) and with a thin layer of metal (black). The Tamm mode, labelled, displays a 6-fold enhancement of emission over the bare sample. (Right) Fourier microscopy on a series of progressively smaller gold disks. The blue shift, accompanied by the spectral broadening on the emission and the reduction in k-space heralds the formation of a Confined Tamm Plasmon (CTP)

Acknowledgements: This work was funded by EPSRC under project SPINSPACE (EP/M024237/1). We thank Kenneth Kennedy at the University of Sheffield for expert sample preparation.

Reference: [1] Parker et al., IET Optoelectron., 2018, Vol. 12 Iss. 1, pp. 11-14.

A18_16 The Generation of an Optical Frequency Comb using a Photonic Crystal Cavity

H. Francis*, S. Chen, C.H. Ho, K.J. Che, M. Hopkinson and C.Y. Jin. *Hfrancis1@sheffield.ac.uk
Department of Electronic and Electrical Engineering, University of Sheffield.

Optical Frequency Comb (OFC) generation plays an import role in applications such as arbitrary waveform generation, dense wavelength division multiplexing and as wideband multi-wavelength laser sources. Advances in micro-toroidal cavity resonators are at the forefront of research in OFC generation[1]. Their large Q factors, relatively compact device footprint and high efficiency have opened up new possibilities in fields such as RF Photonics, telecommunications and Metrology[2]. However, further developments to reduce noise and increase spectral coverage must be obtained before OFC generation in microcavities can be beneficial to on-chip photonic systems. To tackle these issues and decrease the complexity of device integration, a photonic crystal nanocavity is proposed here, in place of a micro-toroidal cavity.
From previous simulations in the literature[3] it is well known that by creating a flat top pulse in the time domain, multiple sidebands are produced in the frequency domain. These sidebands can then be built upon to produce an OFC. A universal method for generating a shaped carrier signal in an optical cavity-waveguide system has been implemented using coupled mode theory[4]. The carrier signal at the output waveguide of the structure shown in Fig. 1 can be shaped by optical modulation of the cavity. A high power control signal will affect the transmittance of the carrier wave across the device. By changing the temporal dynamics of the control signal, it is possible to change the carrier waves' temporal dynamics, and thus its frequency response.

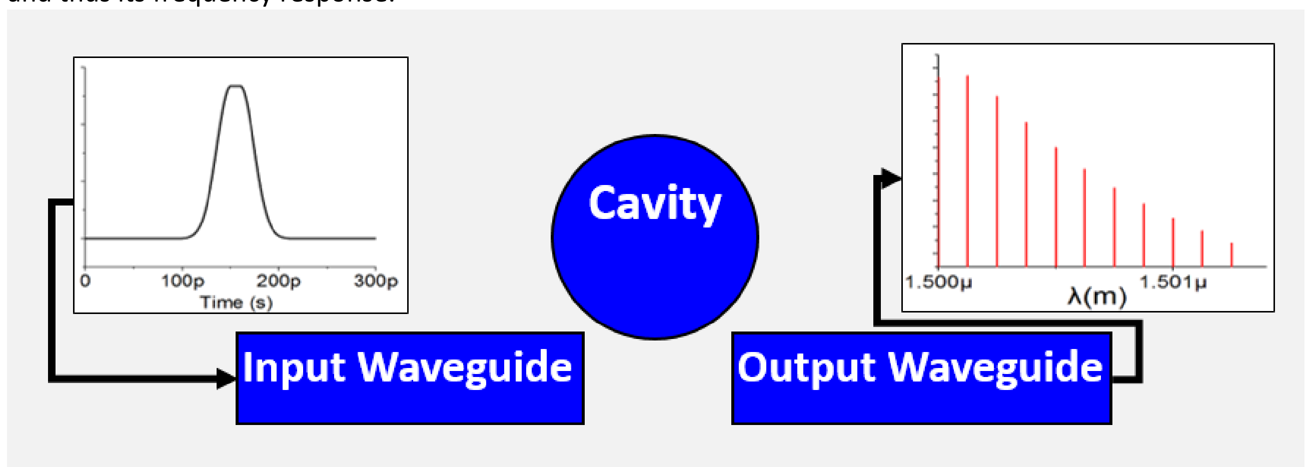

Figure 4 General schematic of device, the input is a flat topped Gaussian pulse(left inset figure), the simulated frequency response of the output signal is shown in the right inset figure

The simulations carried out in this project have shown that it is possible to manipulate the control signal input to produce a shaped carrier signal at the output using the optical modulation of the PhC cavity. The shape of the control signal needed to produce these sidebands is simplified and could be produced experimentally using readily available nonlinear fibres. Overall, it has been proved that an OFC can be produced using a nanoscale device. This has potential application in on-chip optical signal processing for telecommunications, environmental development and healthcare systems for the future.

References: 1. T.J. Kippenberg, R. Holzwarth, and S.A. Diddams, "Microresonator-Based Optical Frequency Combs" Science 332, 555–559 (2011). 2. P. J. Delfyett, S. Gee, M. T. Choi, H. Izadpanah, W. Lee, S. Ozharar, F. Quinlan, and T. Yilmaz, "Optical Frequency Combs From Semiconducor Lasers and Applications in Ultrawideband Signal Processing and Communications" Journal of Lightwave Technology 24, 2701 (2006). 3. V. Torres-Company, J. Lancis, and P. Andres, "Lossless Equalisation of Frequency Comb" Optics Letters 33, 1822-1824 (2008). 4. J. D. Joannopoulos, S. G. Johnson, J. N. Winn, and R. D. Meade, "Photonic Crystals: Modelling the Flow of Light" 2nd Edn, Pinc. Univ. Prs. (2008).

A18_25 Epitaxy of InAs/InP QD structures for single photon emitters & lasers operating at 1.5-2 µm

A.B. Krysa[1]*, J. Skiba-Szymanska[2], T. Müller[2], J. Huwer[2], M. Anderson[2,3], B. Harrison[1], R.M. Stevenson[2], D.A. Ritchie[3], A.J. Shields[2]. *a.krysa@sheffield.ac.uk

[1]*EPSRC National Epitaxy Facility, Department of Electrical and Electronic Engineering, University of Sheffield, Mappin Street, Sheffield, S1 3JD, UK;* [2]*Toshiba Research Europe Limited, 208 Science Park, Milton Road, Cambridge, CB4 0GZ, UK;* [3]*Cavendish Laboratory, University of Cambridge, JJ Thomson Avenue, Cambridge, CB3 0HE, UK.*

In this paper, we report on the first time demonstration of the epitaxial growth of an electrically driven InAs/InP quantum dot (QD) source of entangled photons operating within the telecom C-band (~1.55 µm).
Two growth regimes of self-assembled InAs quantum dots (QDs) on InP were studied: Stranski-Krastanow (SK) growth and droplet epitaxy (DE). SK growth was performed at a temperature of 500 oC. InP overgrowth was performed in two stages with a lower (~0.05 nm/s) and a higher (~0.43 nm/s) growth rates. The overgrown surface featured well-resolved atomic terraces in atomic force microscopy (AFM) scans indicating that the preferred step-flow epitaxial regime was re-established after QD growth. The alternative QD growth, DE, included formation of In droplets on the InP surface via pyrolysis of trimethylindium at 400 oC followed by InAs QD crystallization under arsine overpressure at 400-500 oC.
In the both growth regimes, low QD densities (<109 cm-2) were achieved. These allowed optical access to individual QDs without additional fabrication steps. A typical low temperature (4.2 K) QD emission spectrum represented an ensemble of narrow emission lines (Fig. 1) within the intended C-band.
1520 1530 1540 1550 1560 1570 SK InAs QDs, PL, 4.2 K Intensity, a.u. Wavelength, nm (a) 1520 1530 1540 1550 1560 1570 Intensity, a.u. Wavelength, nm DE InAs QDs, PL, 4.2 K (b) AFM studies revealed that SK QDs are elongated along [110] whereas DE QDs have essentially a round shape on the growth surface. The more symmetrical shape of DE QDs is in a good correlation with a reduced fine structure splitting measured in our optical experiments, which favours DE QDs as a source of entangled photons.
Several materials systems were considered for distributed Bragg reflectors (DBRs) with a stop-band at 1.55 µm. Earlier, we have demonstrated DBRs based on InGaAsP/InP and AlGaInAs/AlInAs [1-3]. However, the composition of the former is rather sensitive to the growth temperature, and the latter would affect the growth of InP matrix in the active region due to arsenic contamination. As a compromise, we have developed DBRs based on AlGaInAs/InP. The problem of the arsenic carry over at the As-P interface was solved and the resulting DBR surface was atomically flat.
Optical cavities incorporating InAs DE QDs for electrically driven single-photon emitters around 1.55 µm were grown [4, 5]. Using the biexciton cascade mechanism, the QD light emitting diodes produced entangled photons with a maximum fidelity of 87±4%. Entangled photon generation up to a temperature of 93 K was obtained. These results represent a considerable technological development towards practical realization of the active elements of the quantum cryptography and quantum computing devices compatible with the conventional fiber optic communication systems.
Laser diode structures based on high density (~1010 cm-2) SK QDs operating at ~1.7-1.8 µm were also fabricated.

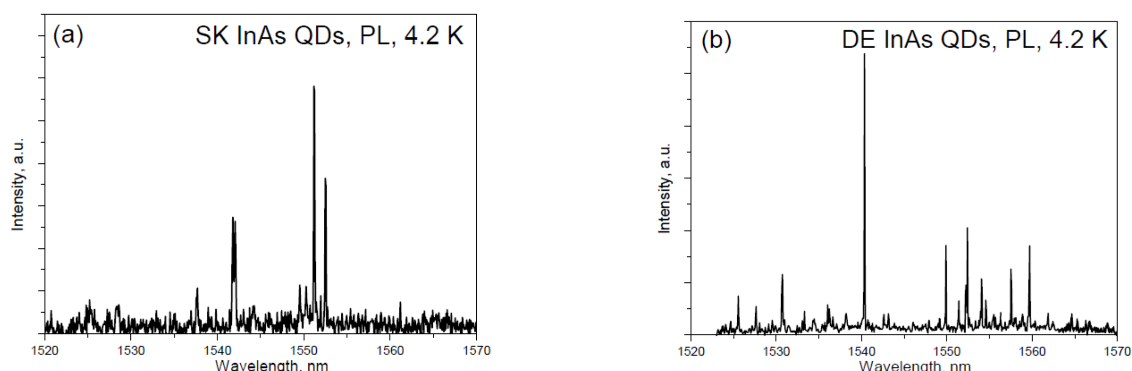

Fig. 1. PL spectra of SK (a) and DE (b) InAs QDs at 4.2 K

References: [1] C.-P. Liu *et al*, "Design, fabrication and characterisation of normal-incidence 1.56-µm multiple-quantum-well asymmetric Fabry-Perot modulators for passive picocells", IEICE Transactions on Electronics **E86-C**, 1281 (2003); [2] M. Pantouvaki *et al*, "10-Gb/s All-optical 2R regeneration using an MQW Fabry-Pérot Saturable absorber and a nonlinear fiber", IEEE Photonics Technology Letters **16**, 617 (2004); [3] C.-H. Chuang *et al*., "IEEE 802.11a data over fiber transmission using electromagnetic bandgap photonic antenna with integrated asymmetric Fabry-Pérot modulator/detector", Journal of Lightwave Technology **26**, 2671 (2008); [4] J. Skiba-Szymanska *et al*, "Universal growth scheme for quantum dots with low fine-structure splitting at various emission wavelengths", Physical Review Applied **8**, 014013 (2017); [5] T. Müller *et al*, "A quantum light emitting diode for the standard telecom window around 1550 nm", https://arxiv.org/abs/1710.03639, accepted for publication in Nature Communications.

Abstracts

Session 6: Interaction Strategies & Approaches

A18_29 CORNERSTONE: Silicon photonics device prototyping capability

C. G. Littlejohns[1], S. Stankovic[1], D. T. Tran[1], X. Yan[1], H. Du[1], G. Sharp[2], M. Sorel[2], R. Webb[3], J. England[3], H. M. H. Chong[1], F. Y. Gardes[1], D. J. Thomson[1], G. Z. Mashanovich[1], G. T. Reed[1].

Contact: cornerstone@soton.ac.uk, website: www.cornerstone.sotonfab.co.uk

[1]Optoelectronics Research Centre, University of Southampton, Southampton, SO17 1BJ, UK; [2]University of Glasgow, Glasgow, G12 8LP, UK; [3]Ion Beam Centre, University of Surrey, Guildford, GU2 7XH, UK.

The field of silicon photonics [1] has expanded rapidly over the past decade. This has led to a degree of standardisation in the commercial foundries that are available for Universities and fab-less companies. Whilst this is advantageous in terms of yield, repeatability etc., it is not conducive for researchers to develop new and novel devices for future systems. CORNERSTONE offers researchers a flexible device prototyping capability that can support photonics research in UK, and beyond.

The CORNERSTONE project (Capability for OptoelectRoNics, mEtamateRialS, nanoTechnOlogy, aNd sEnsing) is an EPSRC funded project between University of Southampton, University of Glasgow and University of Surrey.

The project is based on deep-ultraviolet (DUV) photolithography equipment, installed at the University of Southampton, centred around a 248 nm scanner, the first of its kind in a UK university. Utilising this tool, CORNERSTONE will offer a multi-project wafer (MPW) service on several silicon-on-insulator (SOI) platforms (220 nm, 340 nm & 500 nm) for both passive and active silicon photonic devices.

The foundry service is free of charge to UK universities, until completion of the project in September 2019. To date, there have been 3 completed passive calls, with both a passive call and an active call currently under fabrication, and a call for passive device designs on the 220 nm SOI platform presently live.

This talk will give an overview of the CORNERSTONE project, present some of its early data, and summarise future calls.

References: 1. D. J. Thomson, C. G. Littlejohns, S. Stankovic, M. Nedeljkovic, and S. A. Reynolds, Wiley Encyclopedia of Electrical and Electronics Engineering: Silicon photonics, 2015.

A18_39 Investigation of the Expansion in InP layer bonded to Si and its Effects on the Performance of the Photonic Crystal Lasers with the Buried Heterostructure

A. Sakanas*, Y. Yu, E. Semenova, L. Ottaviano, H. K. Sahoo, J. Mørk, and K. Yvind. *ausa@fotonik.dtu.dk
DTU Fotonik, Technical University of Denmark, Ørsteds Plads 345A, 2800 Kongens Lyngby, Denmark.

Integration of III-V materials on silicon platform is an actively sought approach to realize efficient and low energy consumption on-chip light sources for optical interconnects in data processing and communications applications. While high-quality epitaxial growth with low defect-density is very challenging due to large lattice mismatch and different crystal structures of III-V and Si materials, the significant progress of wafer bonding technology makes it a convenient alternative for the large-scale semiconductor materials integration. Typically, wafers are bonded together either by using an intermediate adhesive layer, or directly. In general, the first method relaxes constrains on the required surface smoothness and cleanliness to achieve high bonding yield. On the other hand, the direct wafer bonding is preferred from the device point of view, as the lack of intermediate adhesive layer offers better control of the coupling between the bonded layers. Additional difficulty in the III-V to Si integration is the difference in the thermal expansion coefficients of the materials. It causes the build-up of stress in the bonded layers during the high-temperature processing steps, and can result in the formation of dislocations if the thermal strain exceeds the critical value [1, 2].

We have developed a platform, where 250 nm InP as the III-V layer on Si/SiO2 substrate is used for fabrication of photonic crystal on-chip lasers with the buried heterostructure for the emission in 1550 nm wavelength range. The buried heterostructure separates the active material region, with layer(s) of either quantum wells or quantum dots in which the laser cavity is formed by the photonic crystal pattern, from the passive material region. This helps to avoid absorption losses and surface recombination outside the cavity. Evidently, large overlap between the active region and the high-*Q* cavity is necessary for the optimal laser performance. However, achieving the necessary overlap is challenging not only due to the required high-level alignment precision, but also because of possible expansion in the bonded device layer caused by the aforementioned differences in the thermal expansion coefficients.

In order to estimate the expansion of the bonded wafers locally, and its consequences for the alignment accuracy during the device fabrication, we have devised the following experiment. We defined a pattern of crosses with the electron beam (E-beam) lithography, transferred the pattern to the InP device layer using the dry etching, and then used E-beam as metrological SEM to estimate the changes in position for each cross after the pattern transfer.

Two different bonding approaches were taken to replicate the conditions during the fabrication of real devices. In case of the adhesive BCB (Benzocyclobutene)-based bonding, the crosses were first transferred to the InP wafer, which was then bonded to Si/SiO2 in the wafer bonder at 250°C, and finally the crosses were opened from the other side by removing the InP substrate and the etch-stop layer (the equivalent of the double-sided processing). The metrological measurements show significant non-uniform distortion in the bonded InP layer observed as changes in the positions of crosses. It explains the substantial misalignment that appears between the buried heterostructure and the photonic crystal cavity in the fabricated laser, and its detrimental effect for the device performance. In case of the direct bonding approach, a thin ALD Al2O3 layer was deposited on both InP and Si/SiO2 wafers before placing them on top of each other for pre-bonding [3]. The wafers were then thermally annealed in the wafer bonder at 300°C, and after the removal of InP substrate and the etch-stop layer the transfer of crosses was performed on already bonded sample (the equivalent of the single-sided processing). Additional high-temperature annealing at 650°C was used in between metrological measurements to examine the influence of the regrowth steps during the real device fabrication on the wafer expansion. The results agree with the alignment observed in the laser fabricated on the directly bonded wafer, and indicate the possibility to readily increase the accuracy further.

In conclusion, the successful integration of high-performance and efficiency InP photonic crystal lasers with the buried heterostructure on Si platform relies both on the high-precision alignment and the level of control of the expansion in the device layer of the bonded wafer. Careful consideration of these elements and successive planning of the fabrication process flow is necessary in order to achieve the optimal device performance.

References: [1] D. Pasquariello et al., "Crystalline Defects in InP-to-Silicon Direct Wafer Bonding", Jpn. J. Appl. Phys. **40**, 4837 (2001); [2] T. Fujii et al., "Epitaxial growth of InP to bury directly bonded thin active layer on SiO2/Si substrate for fabricating distributed feedback lasers on silicon", IET Optoelectron. **9(4)**, 151 (2015); [3] H. K. Sahoo et al., "Low temperature bonding of heterogeneous materials using Al2O3 as an intermediate layer", J. Vac. Sci. Technol. B **36(1)**, 011202 (2018).

A18_01 Suspended Nanocrystalline Diamond-on-Air Waveguide Platform for Chip-Scale Infrared Photonics

A. R. Abdou[1], P. Panduranga[1], J. Richter[2], O. A. Williams[3], J. Witzens[2], and M. P. Nezhad[1].
[1]School of Electronic Engineering, Bangor University, LL57 1UT, United Kingdom; [2]Institute of Integrated Photonics, RWTH Aachen University, Sommerfeldstrasse 24, D-52074, Aachen, Germany; [3]School of Physics and Astronomy, Cardiff University, Queen's Buildings, The Parade, Cardiff, CF24 3AA, United Kingdom.

Integrated photonic chip technology has developed into a mature technology, with silicon and III-V semiconductor platforms operating within the telecommunications spectral window comprising the bulk of work in this area. Expanding this work into other parts of the optical spectrum requires new materials and architectures, mainly due to the absorption bands of the aforesaid materials. In particular, the use of the silicon-on-insulator platform at middle and long infrared wavelengths is limited by the spectral transmission windows of both the buried oxide cladding and semiconductor device layers. Diamond is a wide bandgap semiconductor with a much larger optical transmission window compared to silicon and silicon dioxide and is therefore an excellent candidate for photonic chips operating in the UV, visible and infrared spectral regions. Due to its high refractive index (2.39), it allows for the fabrication of sub-micron optical waveguides for compact integrated photonic chips. Recently many instances of photonic integrated circuits have been demonstrated using bonded and thinned single crystal diamond layers. While the optical quality of such single crystal diamond thin films is very good, the bond and transfer process adds an additional layer of complexity to the fabrication process. In addition, the cost of single crystal diamond is currently prohibitively high, particularly for covering large chip areas. As an alternative, polycrystalline diamond thin films can be readily grown on a variety of large area substrates (such as silicon and silicon dioxide wafers) by seeding the substrate surface with diamond nanoparticles. Polycrystalline diamond films with nanoscale grain sizes (nanocrystalline diamond (NCD)) inherit a great deal of the optical, mechanical and thermal properties of single crystal diamond and can be used in place of single crystal diamond thin films in numerous applications. However, examples of NCD-based photonic chips in the literature are much fewer compared to the single crystal case and are all limited to NCD grown on oxide, in order to achieve vertical confinement. While this is perfectly acceptable for operation in the visible and near IR, it prohibits operation at longer wavelengths due to absorption in the silica cladding, even though the transmission window of the diamond film itself covers a large swath of the mid- and far infrared. To address this issue, here we report, for the first time, air-clad suspended nanocrystalline diamond waveguides fabricated using NCD thin films directly grown on silicon substrates. This architecture not only creates the necessary vertical and lateral confinement needed to create a guided mode, it also offers a pathway for complete utilisation of the optical transmission window of diamond. We will present the architecture and associated waveguide simulations and design steps, followed by details of the fabrication process and optical measurement results at 1550nm. Current measurements indicate average waveguide losses of 5 db/mm , which we ascribe to be mainly due to scattering from the grain boundaries in the NCD film. Future steps for reducing this loss and expanding to longer wavelengths will be discussed.

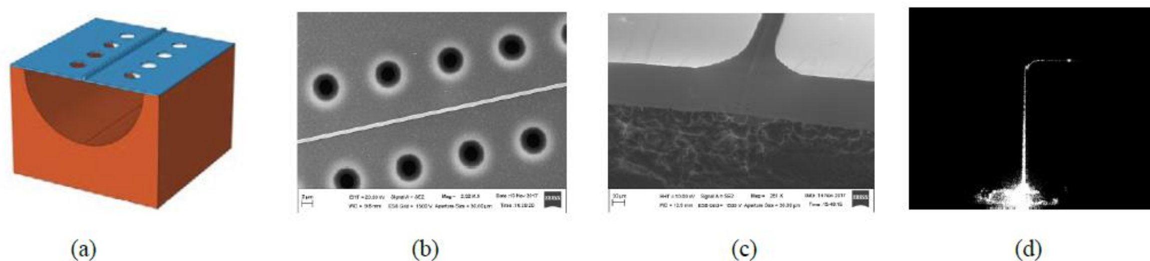

Fig. 1. (a) Architecture of suspended NCD film with Si substrate. (b) Top view SEM of undercut NCD film and waveguide. (c) Edge view of NCD tapered waveguide. (d) Top view infrared image of single mode NCD waveguide carrying 1550nm light.

A18_17 Multiplexed Integrated Source in III-V Materials

Geraint Gough[1], Daryl M Beggs[2], Jorge Barreto[1].

[1]*Centre for NSQI, University of Bristol, Tyndall Avenue, Avon, Bristol, BS8 1FD, UK;* [2]*School of Physics and Astronomy, Cardiff University, 5 The Parade, Cardiff, CF24 3AA, UK.*

Designs and fabrications procedures have been created for high contrast waveguides in gallium phosphide (GaP) and gallium nitride (GaN). These designs will be used to create fast (<10ps) and low-loss (<-60dB) switches with the intention of creating an integrated multiplexed SPS.

III-V materials have shown to be a promising alternative to silicon possessing a $\chi^{(2)}$ electro-optic effect and large bandgaps. These attributes allow essentially lossless, fast active switches and high efficiency photon sources essential for a multiplexed source. GaP and GaN have bandgaps of 2.26eV and 3.2eV respectively, with large Pockel's coefficients, GaP r_{41} = -0.97 pm/V, GaN r_{33} = 8.94 pm/V, making them viable candidates for high efficiency multiplexed sources.

Single photon sources have many applications in quantum computing, sensing, quantum cryptography and communications. Current integrated heralded single photon sources use spontaneous parametric down-conversion (SPDC) or spontaneous four wave mixing (SFWM). These are probabilistic processes but if multiplexed together then the probability of a heralded single photon event increases. These systems main components are the sources and the switch.

Silicon has been the material of choice for integrated photonics due to the processes developed by the silicon industry for creating high quality, precision circuit boards. Multiplex sources in silicon take advantage of non-linear $\chi^{(3)}$ Kerr effects such as spontaneous four wave mixing (SFWM) and free carrier dispersion (FCD), for single photon sources and active switching. However, silicon has a bandgap of 1.2 eV, which means at communications wavelengths, 1550nm, parasitic nonlinear effects, such as two photon absorption (TPA) and free carrier absorption (FCA), limit the efficiency of these devices.

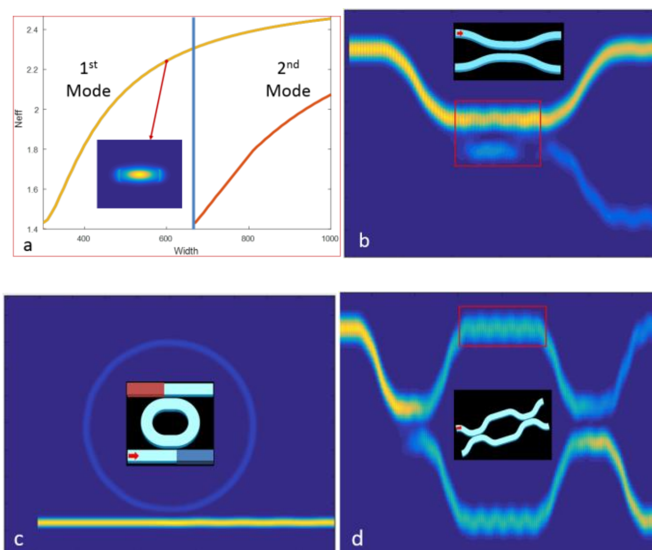

a). Mode calculation for single mode region, b). Simulation of directional coupler switch, c).Simulation of ring resonator switch, d). Simulation of Mach-Zehnder Interferometer switch

A18_24 III-V Nanowire Heterostructures on Silicon-on-Insulator for Silicon Photonics Applications

Hyunseok Kim, Ting-Yuan Chang, Wook-Jae Lee, and Diana L. Huffaker.

Integration of III-V semiconductors on silicon and silicon-on-insulator (SOI) platforms has been of great interest in silicon photonics. Here, we present monolithic integration of III-V semiconductor nanowires (NWs) on SOI platforms by catalyst-free selective-area epitaxy (SAE) using MOCVD. The proposed method could be an enabling technology for monolithic nano-LEDs, nanolasers and nanophotodetectors compatible with silicon photonic platforms, since the nanoscale footprint enables the defect-free growth on lattice-mismatched substrates without the need of Au catalysts that contaminate silicon. In this presentation, we will discuss full details of the InGaAs NWs from seeding through heterostructure, doping and passivation which yield 100 % vertical growth and excellent uniform dimensions. Advancing from NW growth on planar SOI layers, the growth of NW arrays on 3D structured SOI substrates with 1D/2D gratings, waveguides, and couplers are also demonstrated, which represents a way toward practical NW-based optical links. Lastly, we present NW-based p-i-n heterostructures on SOI platforms, which are comprised of axial p-GaAs / i-InGaAs NWs grown on n-Si layers of SOI substrates and passivated in-situ by InGaP shells. High-Q cavities with efficient 3D diffusion barriers are formed by growing the heterostructures with the NW height taller than 2200 nm. This provides an ideal structure for electrically injected bottom-up photonic crystal lasers on silicon photonic platforms.

A18_44 Hybrid polymer-based Er-doped waveguide amplifiers

Marcin Ziarko[1], Nikos Bamiedakis[1], Eric Kumi-Barimah[2], Gin Jose[2], Richard Penty[1], Ian H. White[1].
[1]*Centre for Photonic Systems, Department of Engineering, University of Cambridge, 9 JJ Thomson Ave, Cambridge CB3 0FA, UK;*
[2]*Institute for Materials Research, School of Chemical and Process Engineering, University of Leeds, Leeds LS2 9JT, UK.*

Compact Erbium-doped photonic devices are sought after for light generation and amplification within photonic integrated circuits. Different waveguide technologies are currently being investigated in order to create such components. In this work, we investigate the formation of Erbium-doped waveguide amplifiers (EDWAs) using new polymer materials and a novel deposition process, namely siloxanes (Dow Corning WG-2020) materials [1] and ultrafast laser plasma implantation (ULPI) [2]. Siloxanes are sufficiently low-cost, and exhibit the essential properties such as high temperature processability and operation for direct integration on printed circuits boards (PCBs) [3], while ULPI has been demonstrated to produce extremely high dopant concentrations with values of 1.63 × 1021 cm−3 recently reported in Er-doped silica layers [4]. The combination of these two technologies can therefore provide compact EDWAs that could be directly integrated onto PCBs. Here, we present simulation studies on the achievable performance of such devices and report initial photoluminescence (PL) measurements from Er-doped samples. Erbium-Ytterbium (Er-Yb) co-doping is used to combine C-band emission with efficient 976-nm-pump absorption. Simulation work is carried out to investigate the ratio of the two rare-earth ions that offers optimised gain performance for these siloxane-based EDWAs (Figure 1). The results indicate that a 4x4-μm channel amplifier with 4:1 Er-Yb ratio could achieve internal gain of up to 8 dB/cm. In experimental work, different concentrations of rare-earth ions have been implanted in samples with either silica glass or polymer layers. The initial measurements carried out on 1.1-cm-long polymer waveguides spin-coated on glass implanted with 6.7 x 1020 cm-3 ions demonstrate photoluminescence emission with FWHM of 17.8 nm (Figure 2). Detailed results on the simulation work and initial measurements will be presented at the conference.

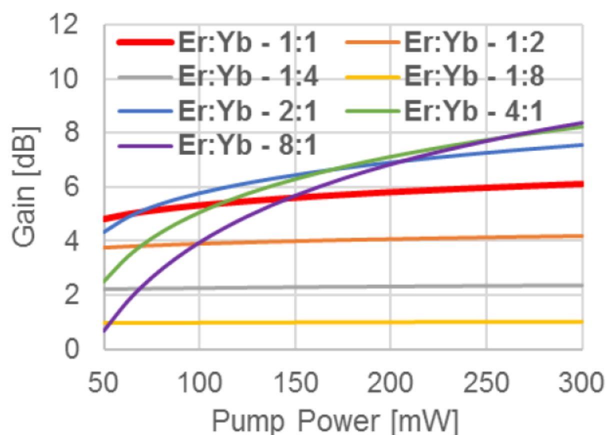

Figure 1. EDWA gain simulations for various Er:Yb ratios

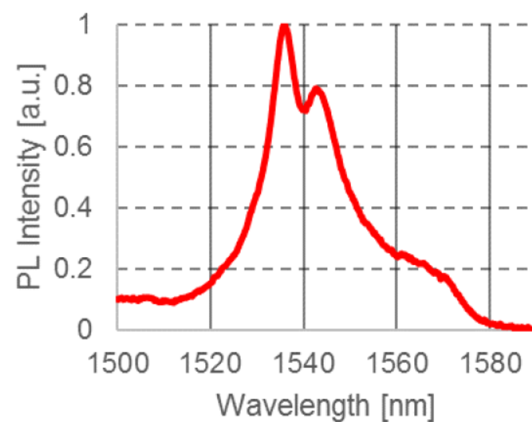

Figure 2. Averaged photoluminescence signal from polymer waveguides on Er-Yb doped glass

References: [1] Swatowski et al., "Flexible, stable, and easily processable optical silicones for low loss polymer waveguides," in Proceedings of SPIE, San Francisco, 2013. [2] Chandrappan et al., "Target dependent femtosecond laser plasma implantation dynamics in enabling silica for high density erbium doping," Scientific Reports, vol. 5, 2015. [3] Bamiedakis et al., "Cost-Effective Multimode Polymer Waveguides for High-Speed On-Board Optical Interconnects," IEEE Journal of Quantum Electronics, vol. 45, no. 4, pp. 415-424, 2009. [4] Chandrappan et al., "Doping silica beyond limits with laser plasma for active photonic materials," Optical Materials Express, vol. 5, no. 12, 2015.

A18_34 Electrical Control of Critical Coupling in Graphene Chiral Metamaterials

Sang Soon Oh[1], Teun-Teun Kim[2], Hyeon-Don Kim[3], Hyun Sung Park[3], Ortwin Hess[4], Bumki Min[3], Shuang Zhang[5].

[1]School of Physics and Astronomy, Cardiff University, Cardiff CF24 3AA, United Kingdom; [2]Center for Integrated Nanostructure Physics, Institute for Basic Science, Suwon 16419, Republic of Korea; [3]Department of Mechanical Engineering, Korea Advanced Institute of Science and Technology, Daejeon 34141, Republic of Korea; [4]Blackett Laboratory, Department of Physics, Imperial College London, South Kensington Campus, London SW7 2AZ, UK; [5]School of Physics and Astronomy, University of Birmingham, Birmingham B15 2TT, UK.

In modern technology, active control of polarization of electromagnetic waves is extremely important. Despite the recent advances in artificial materials [1,2], most active polarization control schemes rely on optical stimuli that requires complex optical setups. Recently, we experimentally demonstrated that the polarization state of terahertz wave beams can be modulated electrically using graphene [3]. Combining a chiral metamaterial with a gated single-layer sheet of graphene, we showed that transmission of a terahertz wave with one circular polarization can be electrically controlled without affecting that of the other circular polarization, achieving large intensity modulation depths (>99%) with a low gate voltage. Interestingly, this effective control of polarization is made possible by the full accessibility of three coupling regimes, that is, underdamped, critically damped, and overdamped regimes.

In this presentation, using an analytical expression of transmission coefficients for a graphene chiral metamaterial derived using the coupled mode theory [4], I will show how the damping in the system plays a role in varying the coupling regimes. Here, the transmission coefficients for right-handed circular polarization can be written as a sum of two Lorentzian terms and one constant term because there are three coupling channels between the incident and transmitted waves, that is, two via the resonance modes and one for direct coupling. The analytical expression provides us with a clear explanation on how to access critical coupling with the change of the gate voltage of graphene in the chiral metamaterials. The use of analytical expressions is not limited to graphene chiral metamaterial but can be extended to any chiral two-port system with two resonances that shows intrinsic and radiation damping.

References: [1] S. Zhang, J. Zhou, Y.-S. Park, J. Rho, R. Singh, S. Nam, A. K. Azad, H.-T. Chen, X. Yin, A. J. Taylor, X. Zhang, Nat. Commun. 3, 942 (2012); [2] T.-T. Kim, S. S. Oh, H.-S. Park, R. Zhao, S.-H. Kim, W. Choi, B. Min, O. Hess, Sci. Rep. 4, 5864 (2014); [3] T.-T. Kim, S. S. Oh, H. Kim, H. S. Park, O. Hess, B. Min, and S. Zhang. Science Advances 3, e1701377 (2017); [4] S. Fan, W. Suh, J. D. Joannopoulos. J. Opt. Soc. Am. A 20, 569–572 (2003).

Abstracts

Session 8: Materials Development I

A18_28 Novel Few-layer $MoS_{2(1-x)}Se_{2x}$ Phototransistors

Xiao Li[1], Hao Xu[1]*, Wei Liu[1, 2], Juntong Zhu[3], Guifu Zou[3], Jiang Wu[1], Huiyun Liu[1]. *hao.xu.15@ucl.ac.uk

[1]Department of Electronic and Electrical Engineering, University College London, Torrington Place, London WC1E 7JE, UK; [2]London Centre for Nanotechnology, University College London, London WC1H 0AH, UK; [3]College of Physics, Optoelectronics and Energy and Collaborative Innovation Centre of Suzhou Nano Science and Technology, Soochow University, Suzhou 215006, China.

Two-dimensional (2D) layered materials of transition metal dichalcogenides (TMDs), such as MoS_2, WSe_2, $MoSe_2$, *etc*., have attracted considerable attention due to their promising applications in electronics and optoelectronics[1]. Compared with the binary TMDs, little effort was devoted to the ternary ones. Here, we report the fabrication of back-gate phototransistors based on the novel few-layer $MoS_{2(1-x)}Se_{2x}$ nanosheets, which were synthesised by efficient and cost-effective precursor assisted deposition (PAD) approach. In Figure 1, the typical scanning electron microscope (SEM) morphology shows the obtained ternary alloys are triangular nanosheets with the edge length of 10 – 90 µm. In the Raman spectrum of $MoS_{2(1-x)}Se_{2x}$ nanosheet (the red curve shown in Figure 2), both the Raman-active modes of Mo-Se and Mo-S were resolved clearly, revealing the co-existence of Mo-Se and Mo-S bonds within the same triangular domain. The phototransistors based on atomically thin $MoS_{2(1-x)}Se_{2x}$ on SiO_2/Si substrates exhibit pronounced wavelength selectivity as illuminated by monochromatic lights (see Figure 3). A responsivity of 63 mA/W was achieved from the devices under 532 nm light illumination at the bias of 1 V.

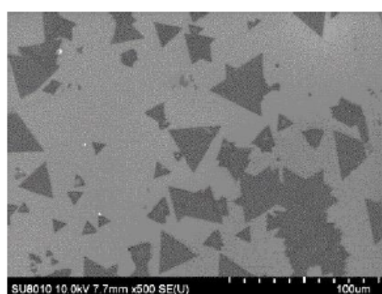

Figure 1. SEM image.

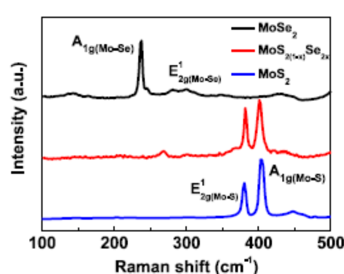

Figure 2. Raman spectra.

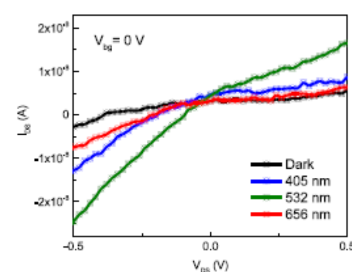

Figure 3. Photocurrent curves.

Reference: [1] J. Pu, K. Funahashi, C. Chen, *et al.*, *Adv. Mater*. **2016**, DOI: 10.1002/adma.201503872.

A18_36 Restraining Effect of Film Thickness on the Behavior of Amplified Spontaneous Emission from Methylammonium Lead Iodide Perovskite

Saif Qaid[1], M. Naziruddin Khan[2], Abdulaziz Alqasem[1], Mahmoud Hezam[2], Abdullah Aldwayyan[1,2].
[1]Photonics Lab., Physics and Astronomy Department, King Saud University, Riyadh, Saudi Arabia; [2]King Abdullah Institute for Nanotechnology, King Saud University, Riyadh, Saudi Arabia.

Summary: We report amplified spontaneous emission (ASE) behavior from methylammonium lead iodide (CH3NH3PbI3) perovskite films of different thicknesses. The ASE threshold carrier density noticeably decreased with thickness, indicating the existence of different traps with perovskite films of smaller thicknesses. We attribute this behavior to the presence of surface states, whose origins can result from different practical fabrication steps with samples of small thicknesses. Our work warns that while decreasing the film thickness is of practical importance to reduce the ASE threshold pump current, in electrically-driven LEDs for example, the solution-processing of perovskites, newly re-discovered for their potential photonic & photovoltaic applications, can be a restraining factor.
Exp. High quality Methylammonium Lead Iodide Perovskite CH3NH3PbI3 films were prepared using a single-step spin-coating deposition. The deposition solution consists of methylammonium iodide (CH3NH3I) and lead iodide (PbI2) precursors dissolved in a mixed solvent of DMF:DMSO having a 1:1 volume ratio. The total weight of the two precursors, i.e. CH3NH3I and PbI2, was used as a tuning factor for the concentration of the deposition film, and thus the resulting film thickness. Weight concentrations of 10%, 20%, 30% and 40% produced film thicknesses of 80 nm, 230 nm, 500 nm and 650 nm respectively. The film deposition process was engineered as to produce very low ASE threshold energies (< 5 μJ/cm2) over a wide range of film thicknesses. The films were excited with 70 picosecond pluses of variable power having excitation wavelength of 532 nm. The excited carrier density in the films (nth) was estimated using the linear absorbance spectra of the films, their measured thicknesses and the energies of the incident laser pulses.
Figures 1 and 2 show the static characteristics thickness dependence of both ASE threshold pump energy and ASE threshold carrier density respectively. The ASE threshold pump energy increases with film thickness from 2.35 μJ/cm2 to 3.65 μJ/cm2 when the thickness is increased from 80 nm to 650 nm. The thickness dependence of ASE threshold carrier density is also depicted in **Figure 3**. Interestingly, the ASE threshold carrier density decreases from 7.73×10^{18} cm^{-3} to 3.29×10^{18} cm^{-3} when the film thickness is increased from 80 nm to 650 nm. This might be explained by the surface defects, which increases as the thickness decreases. At higher thicknesses, the percentage of surface defects to the whole film volume will be lower, which is reflected [not shown] by a higher quantum efficiency of the film as well. Additionally, the deposition of perovskite films with homogenous and complete coverage becomes more critical for thinner films, which results in other possible origins of surface defects (e.g. deposition of islands rather than compact films [not]). When the film thickness is increased, the ASE threshold is subsequently decreased until saturation is reached at the 650 nm film, beyond which the ASE behavior is mainly dominated by the bulk properties of the grown films.
Band gap renormalization (BGR) is also studied in this work, **Fig.4**, and observed as a systematic red-shift of the ASE emission with increasing pump energy. BGR leads to a red shift of the band edge as a result of exchange and correlation effects. BGR can be estimated using the formula:

$$\Delta E = 2\gamma n^{\frac{1}{3}}$$

Where $\Delta \boldsymbol{E}$ is the renormalization value of the bandgap at high carrier densities, $\boldsymbol{\gamma}$ is the bandgap renormalization (BGR) coefficient, and $\boldsymbol{n}$ is the carrier density. The redshift in the emission peak with increasing pump power can be used to estimate BGR under respective pump powers. As mentioned above, the surface traps at small thicknesses result in reduced efficiency of radiative recombination, which result in higher ASE threshold carrier density and reduced quantum efficiency. Therefore, it does not reflect the intrinsic properties of the Perovskite because the surface effect is high due to the surface traps. Therefore, the thick sample at 650 nm (40% concentration) is the closest sample that represent the red intrinsic properties of Perovskite.
The BGR coefficient is evaluated for the 650 nm sample to be ~ 6.3 x 10-8 eV.cm. Due to the 3D and cavity-free structure of present sample and the relatively big laser spot size of ~ 2mm, different scattering and other gain losses can likely result in a gain clamping condition.

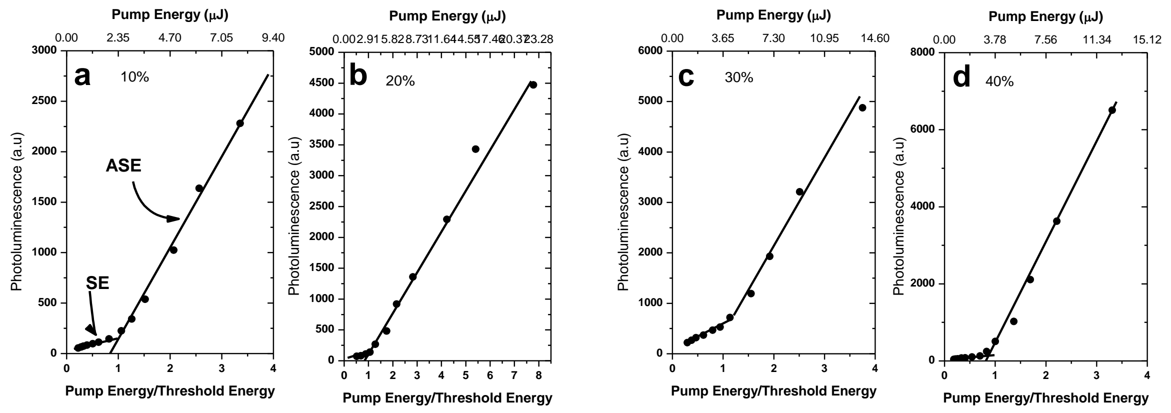

Fig.1.

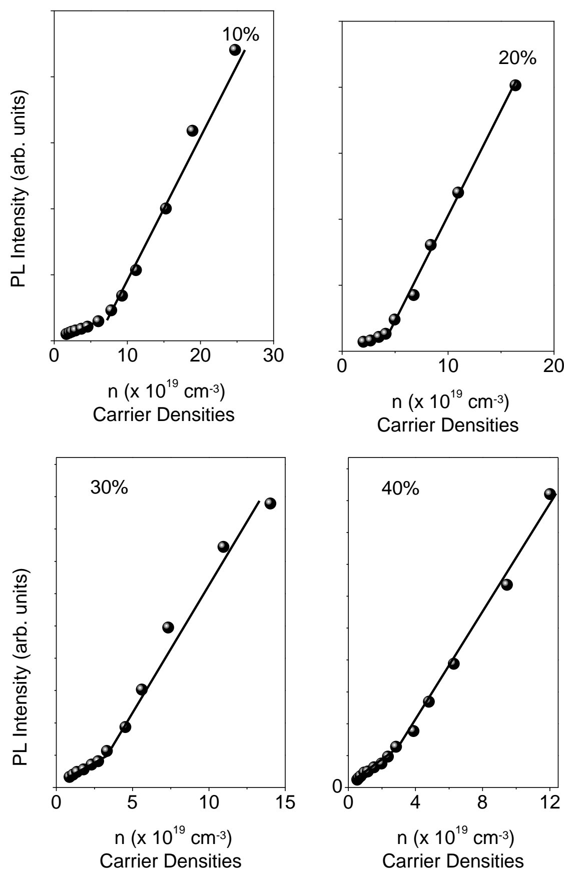

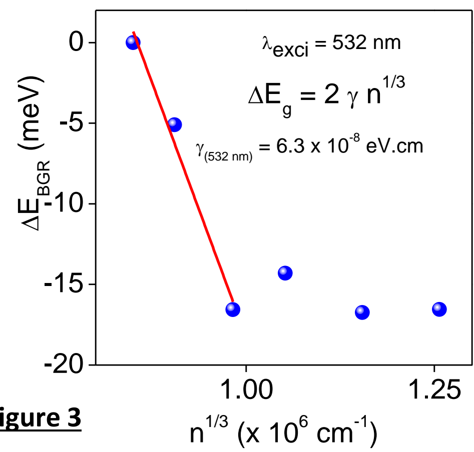

Figure 3

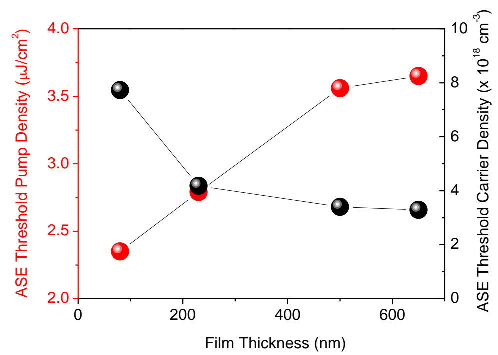

Figure 4

Fig.2.

A18_27 Low threading dislocation density GaAs growth on CMOS-compatible Si (001) by MOCVD for integration of quantum dot lasers

Qiang Li*, Zhao Yan, Kei May Lau. *qli@connect.ust.hk
Department of Electronic and Computer Engineering, Hong Kong University of Science and Technology, Clear Water Bay, Kowloon, Hong Kong.

Epitaxial growth of III-V quantum dot lasers on silicon (Si) has recently attracted tremendous interest for fulfilling the last "missing piece" in photonic integrated circuits on Si. In spite of the three-dimensional (3D) carrier confinement of quantum dots and the resultant much forgiving nature of quantum dot lasers to crystal defects, reducing threading dislocation density (TDD) in the mismatch heteroepitaxy remains critical for low threshold lasing and sufficient operating lifetime. Moreover, most of previous work has been focused on using offcut silicon substrates to remove antiphase-domains, which gives rise to additional compatibility issues in the migration to silicon CMOS foundries. Here, we present MOCVD growth of low threading dislocation density GaAs on on-axis (001) Si patterned with nano-V-grooves. By initiating selective growth on (111) Si facets inside the V-grooves, we are able to bypass challenges associated with antiphase-domains, producing a specially engineered virtual substrate, GaAson-V-grooved-Si (GoVS) templates. The GoVS templates are accomplished in a two-step MOCVD growth process. Regular array of GaAs nanoridges was formed first on SiO2 masked (001) Si, followed by the removal of the SiO2 and coalescence of the nanoridges into a planar thin film. Transmission electron microscopy (TEM) analysis revealed a stress-relaxing GaAs layer in the form of stack faults approximately a few nm thick at the GaAs/Si interface. These stacking faults were geometrically confined by leveraging the aspect ratio trapping technique. The initial GoVS templates showed at least three-fold reduction in TDD when compared to the growth on planar Si wafers. By inserting AlGaAs/GaAs or InGaAs/GaAs superlattices, we achieved smooth surface in GoVS with AFM measurement showing excellent room-mean-square roughness below 1 nm across a scan area of 10 × 10 µm2. The dependency of TDD on buffer thickness has been investigated. Various characterization techniques, including x-ray diffraction, planview TEM and electron channelling contrast imaging (ECCI), were used to inspect the crystalline quality. Thermal cycle annealing and the insertion of InGaAs/GaAs strained layer superlattices (SLS) were implemented to push the TDD into the low 107 cm-2 range. The high quality GaAs-on-V-grooved-Si templates offer a promising platform for integrating lasers, modulators and photodetectors for all-epitaxial photonic integrated circuits.

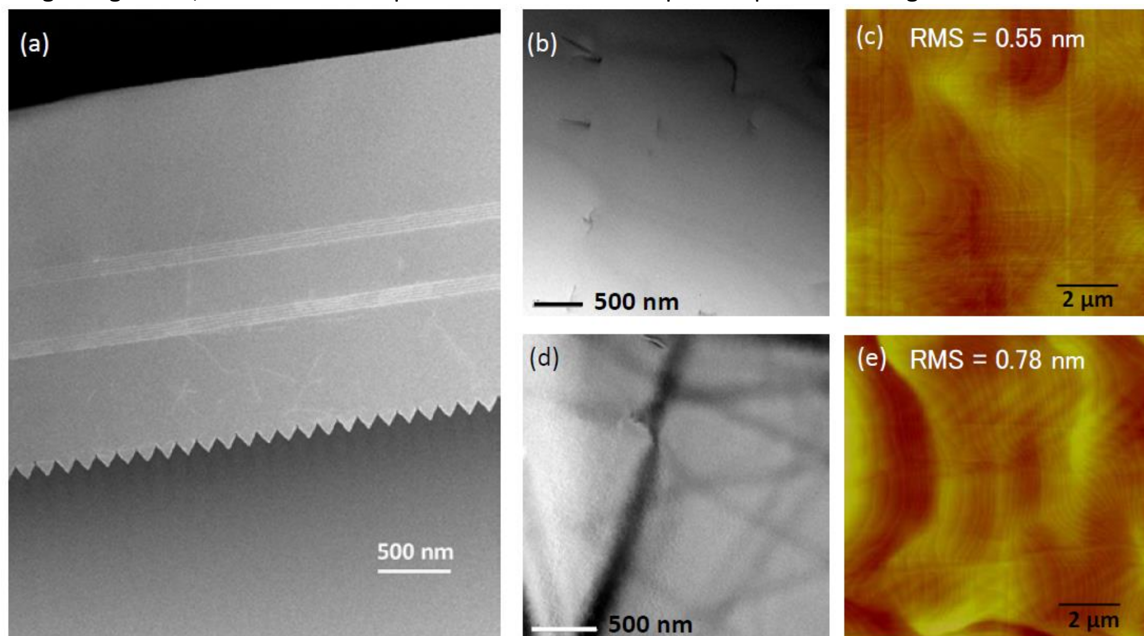

Figure 1. (a) A cross-sectional STEM image of the GoVS template with InGaAs/GaAs SLS; (b) Plan-view TEM image of GoVS with AlGaAs/GaAs SLS; (c) AFM image of GoVS with AlGaAs/GaAs SLS; (d) Plan-view TEM image of GoVS with InGaAs/GaAs SLS; (e) AFM image of GoVS with InGaAs/GaAs SLS.

A18_22 Investigation of strain and morphology of non-polar GaN overgrown on different patterned templates

L. Jiu, Y. Gong, and T. Wang.
Department of Electronic and Electrical Engineering, University of Sheffield, United Kingdom.

There is a significantly increasing demand on III-nitride based power electronics due to their intrinsic properties of high breakdown voltage and high saturation electron velocity. So far, AlGaN/GaN-based high electron mobility transistors (HEMTs) are developed mainly based on c-plane GaN where a large sheet carrier density is produced as a result of spontaneous and piezoelectric polarisations. As a consequence, such polarisations generally lead to a depletion-mode transistor, while it is ideal to have an enhancement-mode GaN device in practical applications due to safety requirements. Similar to GaAs based HEMTs, the growth of an AlGaN/GaN heterostructure with a modulation doping along a non-polar direction provides a simple but promising solution, where the polarisations are eliminated and thus the sheet carrier density can be tuned simply through optimising the doping level in the AlGaN layer. However, the crystal quality of current non-polar GaN grown on either sapphire or silicon is far from satisfactory. Typically, non-polar GaN grown on sapphire without any extra processes exhibits a high density of defects (a dislocation density of above 1010/cm2 and a stacking fault density of above 106/cm). Therefore, it is crucial to develop a new method for the growth of non-polar GaN on sapphire or silicon. In order to address this issue, we have developed a simple and effective approach for the overgrowth of (11-20) non-polar GaN on regularly arrayed micro-rods on sapphire, leading to greatly improved crystal quality. In this work, we present a comparative study of crystal morphology and strain relaxation of overgrown (11-20) non-polar GaN based on two different types of patterned template on sapphire. Our results indicate that our overgrown non-polar GaN on our regularly micro-rods exhibits isotropic strain distribution as a result of anisotropic strain relaxation during the overgrowth process, while the as-grown non-polar GaN on sapphire and the overgrown GaN on standard stripe patterned templates exhibit strong anisotropic strain. The evolution of the surface morphology and the crystal quality of our overgrown non-polar GaN on the micro-rods will be presented as well.

The evolution of the crystal quality and the strain relaxation of the overgrown layers on our regularly arrayed micro-rods has been studied by using X-ray diffraction (XRD). The surface morphology has been examined by scanning electron microscopy (SEM) in order to observe the whole coalescing process. XRD rocking curve measurements show the final overgrown layer with a smooth surface exhibits 277 and 388 arcsec full widths at half maximum (FWHM) along the (0001) and the (1-100) direction, respectively, having approached its c-plane counterpart with a similar thickness on sapphire. Figure 1 shows the plane-view SEM image of our regularly arrayed micro-rods and the cross-sectional SEM image of the overgrown non-polar GaN layer and the evolution of strain as a function of overgrowth time. It has been found that the strain in the overgrown GaN on our micro-rods is isotropic, while the strain in both the as-grown GaN and the overgrown GaN on stripe patterned templates shows strong anisotropy. For the overgrown GaN on our regularly arrayed micro-rods, the typical strain is $\varepsilon_{zz}=-1.580\times10^{-3}$ along [0001] and $\varepsilon_{yy}=-1.610\times10^{-3}$ along [1-100], which is isotropic. In contrast, the as-grown GaN on sapphire exhibits a typical strain of $\varepsilon_{zz}=-1.012\times10^{-3}$ along [0001] and $\varepsilon_{yy}=2.823\times10^{-3}$ along [1-100], and the overgrown GaN on the stripe patterned templates shows a reduced anisotropy with a typical strain of $\varepsilon_{zz}=-0.799\times10^{-3}$ and $\varepsilon_{yy}=1.781\times10^{-3}$.

In conclusion, the isotropic properties of our overgrown (11-20) non-polar GaN on our regularly arrayed micro-rods on sapphire will significantly benefit any device structures grown on its top.

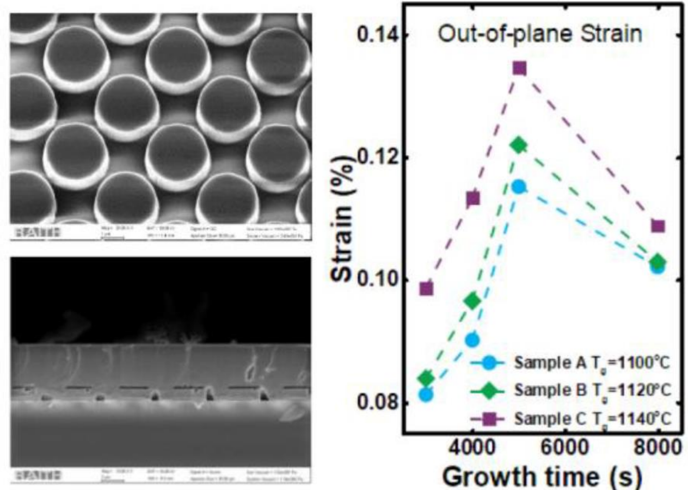

A18_23 Measurement of the transport parameters of AlGaInAs for use in Quantum Well Laser Structures

Christopher Kemp[1]*, Igor Marko[1], Ian Lealman[2], Graham Berry[2], Michael Robertson[2], Steven K. Clowes[1] and Stephen J. Sweeney[1]. * c.kemp@surrey.ac.uk

[1]Advanced Technology Institute and Department of Physics, University of Surrey, Guildford, Surrey GU2 7XH, United Kingdom;
[2]Huawei Technologies R&D (UK), Adastral Park, Martlesham Heath, Martlesham, Ipswich, Suffolk, IP5 3RE, United Kingdom.

AlGaInAs is a popular alloy choice for QW laser structures in the 1.3-1.55µm wavelength range, which are essential for use in data- and tele-communications. This is due to the range of band gaps and band offsets that can be achieved on an InP substrate. In order to improve the design and performance of such lasers (e.g. temperature stability, output power and efficiency, modulation bandwidth, etc.) it is important to have well-developed parameters for the basic material properties. Of these, the charge transport parameters are key in terms of developing lasers that operate at high modulation rates. Empirical measurements of these parameters for AlGaInAs are sparse in current literature with a high degree of variation in the values used for modelling. Praseuth et al. have studied unintentionally n-doped $(Al_{0.48}In_{0.52}As)_z(Ga_{0.47}In_{0.53}As)_{1-z}$ with a carrier concentration of $0.1\text{-}1\text{x}10^{15}$ cm^{-3} reporting an electron mobility varying by over an order of magnitude from 1,000 to 10,000 $cm^2V^{-1}s^{-1}$ over the z = 0 to 1 composition range[1].

In this study, we have grown a series of samples to measure the electron and hole mobilities in thin layers of $Al_{0.15}Ga_{0.17}In_{0.68}As$ used in 1.3 µm laser designs with a doping concentration of $3\text{x}10^{18}cm^{-3}$, which is used to determine mobility of the major type of carriers. The mobility is measured through the Hall Effect and using magnetoresistance at high magnetic fields. The former method measures the Voltage across a Hall bar caused by carriers deflected in the magnetic field. The latter method utilizes a set of concentric Corbino ring contacts and involves measuring the resistance between a pair of contacts, which will increase under a magnetic field due to deflected carriers forming a current perpendicular to the contacts, travelling around the circles. Initial studies indicate that the electron mobilities as shown in Fig. 1 are comparable to values in the literature, with hole mobilities being low, as suggested by previous modelling work[1, 2]. The temperature dependence of the charge carrier density and mobility were also measured over a wide temperature range in order to explore the role of the various scattering processes that influence charge transport in these alloys, as shall be discussed at the conference.

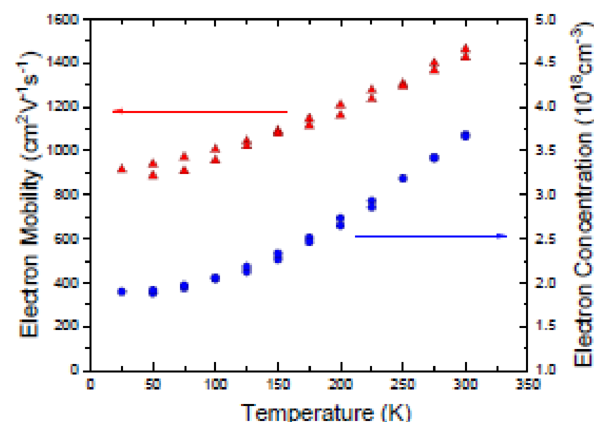

Figure 1. Measured carrier mobility and concentration for an n-doped sample using the Magnetoresistance method over a wide temperature range.

References: 1. Praseuth, J. P., et al. Growth and characterization of AlGaInAs lattice matched to InP grown by molecular-beam epitaxy. *J. Appl. Phys.* **63,** 400–403 (1988); 2. Piprek, J., et al. What Limits the Maximum Output Power of Long-Wavelength AlGaInAs / InP Laser Diodes? *IEEE J. Quantum Electron.* **38,** 1253–1259 (2002).

A18_11 InAs/GaAs Quantum Dot Solar Cells with QDs in Base Region

S. Chan* [1], D. Kim[1], M. Tang[1], J. Wu[1], and H. Liu[1] *steven.chan.12@ucl.ac.uk
[1] *Department of Electronic and Electrical Engineering, University College London, Torrington Place, London WC1E 7JE, United Kingdom.*

Intermediate band solar cell has a maximum theoretical efficiency of 63.2% calculated by Luque and Martí in 1997, and since then, intensive studies have been put unto this topic. Recent studies have shown that Si-doping and growing quantum dots in different regions e.g. base region have positive impacts on solar cell performance. Sablon *et al*. demonstrated that doping the quantum dots with Si could realise built-in field which enhanced sub-bandgap absorption and hence resulted in huge improvement in current density. However, doping the QDs within the active region inevitably reduces the material quality and thus results in voltage loss due to Shockley-Read-Hall recombination. Zhou *et al*. reported successful growth of QDs in emitter, intrinsic and base regions and the results showed that QDs in base region had good efficiency despite of a low Fill Factor.
In this work, we demonstrate molecular beam epitaxial growth of quantum dot in intrinsic, deep and shallow base regions and further investigated the device performance. The photoluminescence, short circuit current density, open circuit voltage, and external quantum efficiency results are presented and compared with a GaAs reference cell. Quantum dots in the base region are unintentionally doped with Si and the defect states are passivated at deeper region. The EQE spectra shows that solar cells with quantum dots in deeper base region have less influence from the wetting layers and still contribute to current. Hence, EQE measurements agree with J-V curves that QDs in deep region have the best performance with minor decrease in J_{sc} and V_{oc}.

Figures

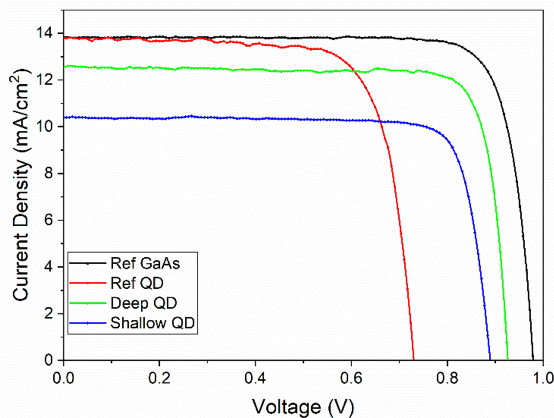

Fig. 1 Current density versus voltage characteristics for QDSCs under 1-sun (AM1.5G) illumination.

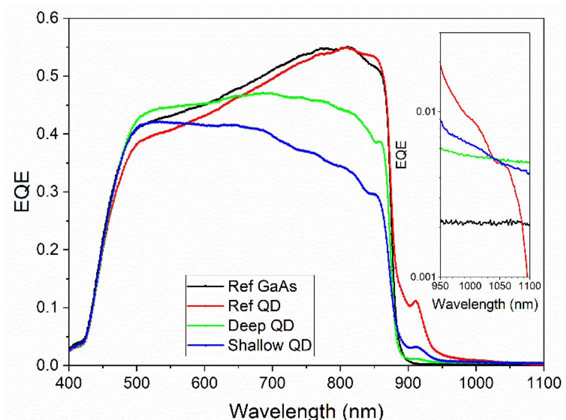

Fig. 2 External quantum efficiency spectra for QDSCs.

A18_45 Efficiency Enhancement of Plasmonic Solar Cells

Riyadh Mansoor
Faculty of Engineering, ALMuthanna University, Iraq

Solar cells are a solution to the increased demand for environmentally friendly energy sources. A solar cell is a device that use the photovoltaic effect to convert sunlight photon energy into electricity. Photovoltaic power has the potential to meet the growing needs of expanding population, since the amount of radiation striking the earth's surface is 1.76 X 10^5 terawatts (TW) and current world usage is estimated at 15 TW [1]. However, the cost of photovoltaic modules still high compared to other renewable energy sources. Reducing the per Watt cost is the driving force behind the proposing of the second generation of solar cells (thin film solar cells). Thin film SCs focus on reducing the thickness to the range of 1-2 μm as well as improving the energy production. But, reducing the thickness affects the trapping of light inside the SC, resulting in low light absorption and reduced conversion efficiency. A new generation of SC being researched with the aim of improving the efficiency of thin film SCs by exploiting the plasmonic effect.
Plasmonic effect exists mainly in metals where electrons are weakly bound to the atom and free to roam. It is either localized or propagating surface plasmon [2]. For plasmonic SCs, localized surface plasmon (LSP) is exploited to improve the scattering and hence increasing the light trapping of desired frequency. A typical dipoles or multipole oscillation of electron occurs in noble metal nanoparticles excited at their localized surface plasmon resonance (LSPR), as shown in Figure 1-A. A Plasmonic light trapping technique based on metal nanoparticle is presented and simulated in this work with the aim to improve the conversion efficiency of solar cell.
Here, CST simulation software is used to simulate a thin film solar cell with spherical nanoparticles as shown in Figure 1-B. Silver and gold nanoparticles with different radii are simulated with the aim to improve the extinction cross section. The thickness of the thin Si absorber layer is assumed to be 2 μm and spherical nanoparticles with a range of optimized size are placed on the front surface of Si layer. A unit cell boundary conditions are used in the lateral direction to mimic the ordered array of nanoparticles, while an open add space is used in the incident direction of solar irradiance (Zmax) and Electric Et=0 for Zmin. In this work, the extinction ratio is measured within a frequency range of 370-850 THz via finite element method (FEM) numerical simulation method. The scattering and absorption cross sections are shown in Figure 1-C for a 50 nm radius silver spherical nanoparticle. Simulation result shows that the photon absorption enhancement is dominated due to the scattering and near field enhancement effect of Ag nanoparticle. Optimizing the nanoparticle size and the thin film thickness leads to design of a plasmonic SC with enhanced efficiency.

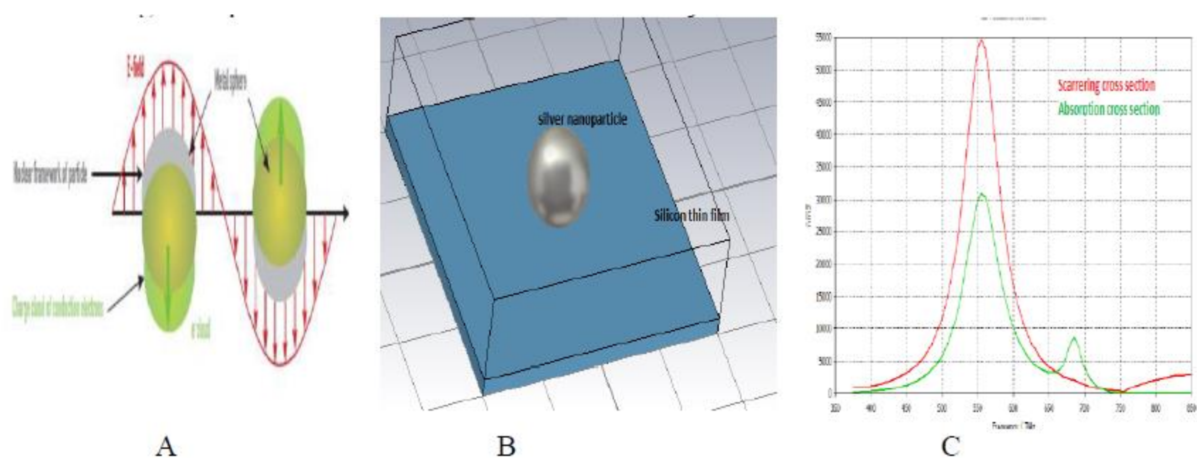

Figure 1 A. The generation of surface plasmons on nanosphere B. CST model of silicon thin film C. simulation results.

References: [1] N. S. Lewis, "Powering the planet," *MRS Bull,* vol. 32, *(10),* pp. 808-820, 2007; [2] J. D. Winans *et al*, "Plasmonic effects in ultrathin amorphous silicon solar cells: performance improvements with Ag nanoparticles on the front, the back, and both," *Optics Express,* vol. 23, *(3),* pp. A92-A105, 2015.

Abstracts

Session 9: Materials Development II

A18_19 GaAsBi MQW device performance at solar concentrator temperatures

F Harun, R D Richards*, A Ray, and J P R David. *R.Richards@Sheffield.ac.uk
University of Sheffield, Sheffield, South Yorkshire, S1 3JD, UK.

Recent work[1] has shown the potential of GaAsBi as an alternative to InGaAs in multiple quantum well (MQW) multi-junction photovoltaics. The advantage of using bismuth is that it causes a very rapid reduction in the band gap, allowing simple GaAsBi/GaAs devices to absorb across the same spectral region as far more sophisticated InGaAs based devices[2]. Two main drawbacks were identified with the GaAsBi based devices: a slow onset of absorption, which reduces the $V_{OC}.I_{SC}$ product; and a relatively low internal quantum efficiency. The former point can be addressed through improvements in the GaAsBi growth technique; the latter appears to be due to carrier trapping in the deep valence band QWs.
Carrier trapping has previously been observed in InGaAsN/GaAs MQW devices[3], where the large conduction band offset due to N incorporation prevents electrons from rapidly escaping the QWs. Bi, on the other hand, induces a large valence band shift in GaAs, trapping holes in the QWs. The trapped holes screen the inbuilt electric field and reduce the depletion width — and quantum efficiency — of the device. While this has been shown to be an issue at low temperatures, the GaAsBi based MQW technology is intended for use in high-efficiency concentrator photovoltaics, which can experience operating temperatures of up to 100 °C.
Illuminated IV measurements of a 20 QW device — under the AM1.5 spectrum and a GaAs filter to simulate multi-junction operation — show that the open circuit voltage drops by 78 % and the short circuit current increases by 59 % as the temperature of the device is increased from room temperature to 120 °C. This is accompanied by a drop in the fill factor from 53 % to 30 %. The implications of these results for the photovoltaic applicability of GaAsBi is discussed.

References: [1]Richards, R. D. *et al. Solar Energy Materials and Solar Cells* **172**, 238-243, doi:https://doi.org/10.1016/j.solmat.2017.07.029 (2017); [2]Toprasertpong, K. *et al. Progress in Photovoltaics: Research and Applications* **24**, 533-542, doi:10.1002/pip.2585 (2016); [3]Khalil, H. M., Royall, B., Mazzucato, S. & Balkan, N. *Nanoscale Research Letters* **7**, 539, doi:10.1186/1556-276x-7-539 (2012).

A18_31 Strain-Compensated $GaAs_{1-y}P_y/GaAs_{1-x}Bi_x$ Quantum Wells for Laser and Solar Cell Application

Luke J. Mawst[1]*, Honghyuk Kim[1], Kangho Kim[2], Jaejin Lee[2], Thomas F. Kuech[3]. *ljmawst@wisc.edu
[1]*Department of Electrical and Computer Engineering, University of Wisconsin-Madison, Madison, WI 53706; Department of Electronic Engineering, Ajou University, Republic of Korea;* [3]*Department of Chemical and Biological Engineering, University of Wisconsin-Madison, Madison, WI 53706.*

The $GaAs_{1-x}Bi_x$ alloy system is under development as a novel narrow band gap material for a variety of applications to microelectronic and optoelectronic devices. While several groups have demonstrated light emitting devices, laser threshold current densities remain high compared with conventional active region materials, such as strained-layer InGaAs quantum wells (QW), emitting in this wavelength region. Furthermore, there are only a few reports of solar cells employing $GaAs_{1-x}Bi_x$ base region. The critical thickness of $GaAs_{1-x}Bi_x$ system is thicker than that of $In_yGa_{1-y}As$ by an order of magnitude, with at the same time a smaller transition energy. This implies that the $GaAs_{1-x}Bi_x$ QW system has the advantage over the more conventional strained $In_yGa_{1-y}As$ QW system in that much thicker $GaAs_{1-x}Bi_x$ layers can be employed without encountering strain relaxation, which can, in turn, allow for an enhanced solar cell spectral response by minimizing quantum size effects. Prior studies on $GaAs_{0.956}Bi_{0.044}/GaAs$ MQW structures have shown that partial strain relaxation occurs for 40-period structures, indicating strain compensation schemes are required for implementing $GaAs_{1-x}Bi_x$ MQWs with sufficient total thickness in the base region of solar cells [1]. $In_yGa_{1-y}As$ MQWs with a large number of periods can be constructed by employing strain compensation utilizing tensile- strained $GaAs_{1-z}P_z$ barriers, although the strain relaxation limitations on the thickness and InAs mole fraction of the $In_yGa_{1-y}As$ QWs constrain the bandgap energy to ~1.23eV [2]. Here we report on the MOVPE-grown single junction solar cells employing 30- and 50-period $GaAs_{1-x}Bi_x$ /$GaAs_{1-z}P_z$ MQW structures in the base region as an alternative to $In_yGa_{1-y}As$ MQW based or InGaAsN based solar cells.

Two different types of single-junction solar cells (SJSC) depending the MQW period (30 period and 50 period $GaAs_{0.965}Bi_{0.035}/GaAs_{0.75}P_{0.25}$) were grown. X-ray (224) reciprocal space mapping indicates that the structures are fully strained. Both SJSC devices exhibit an extended spectral response up to 1050nm (1.18 eV), due to the absorption from the GaAsBi/GaAsP MQW base region. This measured absorption edge from the SJSC devices is in a good agreement with the measured PL peak position (1016nm). The EQE spectral response of the 50-period MQW device is higher for wavelengths longer than the GaAs absorption edge (870nm), implying that the use of a larger number of MQW periods can enhance the photocurrent of the device. InGaAs/GaAsBi type-II QWs are also under investigation to further reduce the transition energies accessible for device structures. Our preliminary studies have demonstrated PL emission wavelengths of 1140nm (1.088eV) from these type-II QWs.

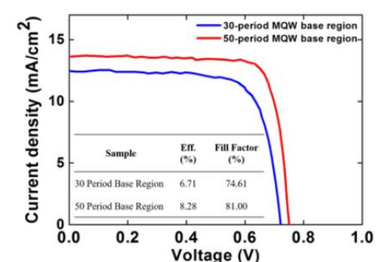

Sample	Eff. (%)	Fill Factor (%)
30 Period Base Region	6.71	74.61
50 Period Base Region	8.28	81.00

Fig. 1. Photocurrent-voltage properties of the SJSC devices employing 30-period and 50-period $GaAs_{0.965}Bi_{0.035}/GaAs_{0.75}P_{0.25}$ MQW

References: 1. Richards R. D. et al, Semicond. Sci. Technol. 30. 094013 (2015); 2. Fujii, H. et al, *Progress in Photovoltaics: Research and Applications*, *22*(7), pp.784-795.

A18_40 Uniquely designed micro-striped GaN-on-Si as a highly energy efficient photoelectrode

Z. A. Syed# Y. Hou#, X. Yu, S. Shen, M. Athanasiou, J. Bai and T. Wang*. *t.wang@sheffield.ac.uk

#contributed equally to the work

Department of Electronic and Electrical Engineering, University of Sheffield, Sheffield, S1 3JD.

An increasing demand on energy primarily relies on fossil fuels globally, leading to an upsurge in carbon emissions and thus ultimately contributing heavily to the world pollution and global climate change. Solar photoelectrolysis of water has been regarded as a promising approach towards the conversion of solar power into renewable and storable energy in the form of hydrogen. A combination of GaN and silicon would be a very promising approach to achieve high efficiency, as GaN and silicon cover a wide spectral region as a result of their bandgaps (one in the ultraviolet region and another one in the infrared region). Consequently, GaN grown on Si substrates is also expected to be a very promising way forward. A standard approach is the growth of GaN on silicon by using metal organic chemical vapour deposition (MOCVD) technique. A typical approach for the MOCVD growth of GaN on silicon substrates is primarily first growth of AlN and then GaN. The fundamental reason for utilising an initial AlN layer is to stop so-called Ga melt-back issue, as Ga metal will have a strong reaction with silicon at a high temperature required for GaN growth. AlN is typically semi-insulating, and AlN exhibits a large bandgap of 6.2eV. As a result, AlN will stop any photocurrent flowing between GaN and silicon, and thus it is impossible to take the merits from both GaN and silicon for solar powered hydrogen generation. In this work, we present a unique designed photoelectrode fabricated from GaN micro-stripes grown on a patterned Si substrate using MOCVD. In this approach, weak Ga-melt back has been observed, leading to the formation of a GaN/silicon interface. Figure 1 shows the photocurrent density of our photoelectrode as a function of applied bias, exhibiting an unprecedentedly high photocurrent density of 11 mA/cm2 under one sun illumination (i.e., AM1.5) and a H2 generation rate of 2.67 ml·cm-2·h-1. This represents 30~100 times higher compared to the values reported so far on any GaN-on-sapphire counterparts. We have also performed photocurrent measurements by aligning different long-pass filters with the cut-off wavelengths ranging from 280 nm to 1000 nm. Our device exhibits a high photocurrent density of above 1 mA·cm-2 at photon energies even below its bandgap of 3.4 eV and under low bias, indicating a contribution from silicon. Furthermore, two reference devices have been fabricated for comparative study, one photoelectrode fabricated from a planar GaN on silicon without any Ga melt-back, and another photoelectrode fabricated from a sample with heavy Ga meltback. For these two devices, we have observed a very low photocurrent density of less than 1 mA/cm2 under identical conditions. For the former, it is clear that the AlN layer stop photocurrent flowing from GaN to silicon. For the latter, as a result of strong Ga meltback, an interface between GaN and silicon cannot be formed. However, we must highlight that our high performance device shows a short lifetime in an acid solution. The fundamental reasons are under investigation. One of the possible reasons may be that the acid may destroy the interface between GaN and Silicon as a result of oxidation processes.

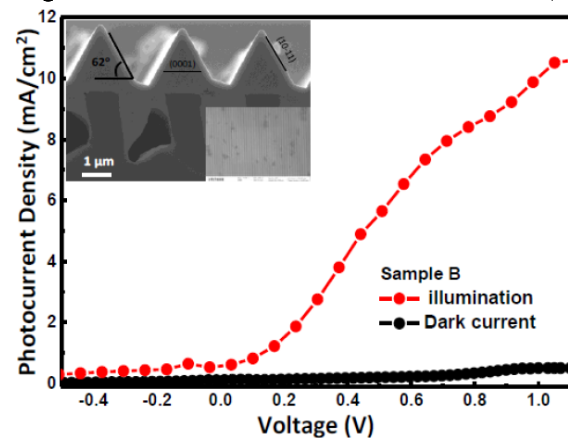

Fig 1: Photocurrent as a function of the applied bias under dark and illuminated conditions, exhibiting a record high photocurrent density of 11mA/cm^2 at 1 V bias upon an illumination of 100 mW/cm^2 (1 Sun). Inset: Cross-sectional (scale bar = 1μm) and plane-view SEM (scale bar = 2μm) images of our GaN micro-stripes

A18_38 1305nm $MoTe_2$-on-Silicon Light Source

Lewis Reeves*, Yue Wang[1], Juntao Li[2], Thomas F. Krauss[1]. *lewis.reeves@york.ac.uk

[1]*University of York, York, UK;* [2]*School of Physics, Sun Yat-Sen University, Guangzhou, 510275, China.*

Silicon photonics offers substantial reductions in operating energy and improvements in the performance of data communication systems. While many essential silicon photonics components have already been demonstrated with excellent performance, such as extremely low-loss waveguides, ultra-fast modulators, and high bandwidth detectors, a silicon light source that can be easily incorporated into the standard fabrication process has remained the missing piece in the jigsaw. Recent advances in the development of atomically thin layers of semiconducting transition metal dichalogenides (TMDs) [1], with direct bandgaps in the near-infrared region, have opened up new possibilities for addressing this need.

Here, we present a unique silicon light source that employs atomically thin layers of molybdenum ditelluride ($MoTe_2$) as a gain material on a L3 photonic crystal nanocavity resonator, fabricated in silicon-on-insulator [2]. This 2D-on-silicon geometry offers the promise of an integrated low-cost electrically pumped nanoscale silicon light source, thereby adding an essential building block to the silicon photonics platform.

To determine the performance of this light source, we pump the sample with a 785 nm CW laser at room temperature and observe light emission at 1305 nm. The emission power as a function of pump power is plotted in Fig. 1a. At low pump intensity, we observe an emission peak with a linewidth of 0.520 nm FWHM, as shown in Fig. 1(b-c). Once the pump power is increased above 35 µW, the peak narrows down to below 0.495 nm. Optical microscope and SEM images of the device is shown in Fig.1(d-e). While the device appears to operate as a laser and fulfills the generally accepted conditions for lasing, we will discuss alternative explanations for its behavior.

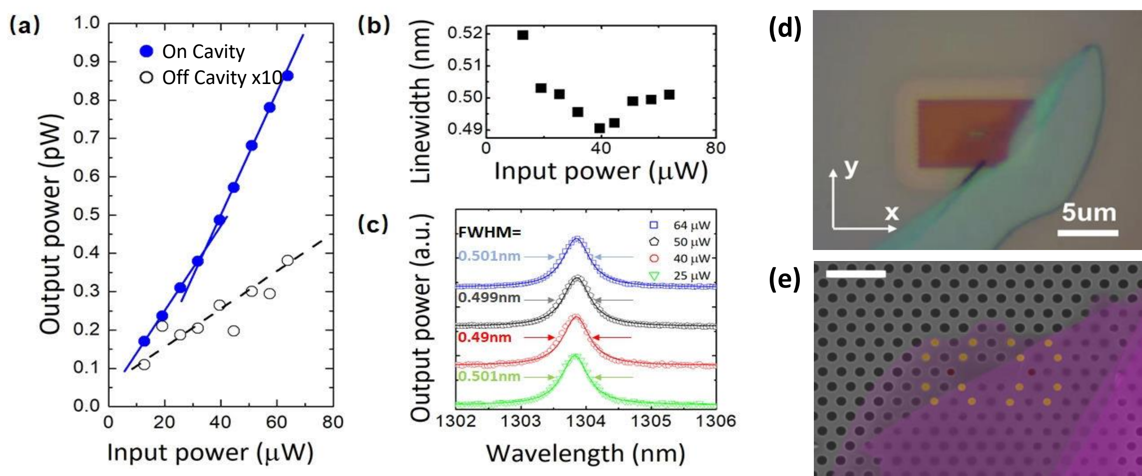

Fig. 1. **Light output and linewidth.** (a) The emission power of the fundamental cavity mode (blue dots) and PL emission at the same wavelength (black circles) as a function of pump power incident on the sample surface. (b) The linewidth of the emission at 1305 nm as a function of the pump power. (c) The fundamental mode output spectra (dots) and the corresponding Lorentzian fits (solid curves) for different pump powers. **$MoTe_2$ on silicon photonic crystal cavity**. (d) An optical microscope and (e) a false- colored SEM image of the few-layer $MoTe_2$ on silicon PhC cavity.

References: [1] Kin Fai Mak and Jie Shan, Nature Photonics 10, 216–226 (2016); [2] Hanlin Fang, Jin Liu, Hongji Li, Lidan Zhou, Lin Liu, Juntao Li, Xuehua Wang, Thomas F. Krauss, Yue Wang, arXiv:1710.01591v1 (2017).

IET Optoelectronics Special Issue
Semiconductor Integrated Optoelectronics
Call for papers

A special issue of IET Optoelectronics is to be published in conjunction with the Semiconductor Lasers and Integrated Optoelectronics Conference held in Cardiff in March 2018. Extended versions of conference talks and other original papers are invited in the field of semiconductor optoelectronics including:

- Growth and fabrication
- Mid infra-red semiconductor optoelectronics
- Semiconductor micro-cavity and photonic band gap effects
- Semiconductor lasers and optical sources
- Organic semiconductor LEDs and lasers
- Semiconductor based THz sources, sensors and detectors
- Theory and simulation of semiconductor optoelectronic devices
- Optical detectors, modulators, amplifiers and switches
- Solar cells / photovoltaic devices
- All-optical and optoelectronic integrated circuits.

Prospective papers should be submitted electronically as instructed in the IET Author Guide, available at:

http://digital-library.theiet.org/journals/author-guide

Submission deadline: Friday 27th April 2018.

Dr Sudha Mokkapati
Guest Editor
MokkapatiS@cardiff.ac.uk